



UNIVERSITY OF ROME
"TOR VERGATA"

FACULTY OF ENGINEERING

DOCTORATE IN
Sensorial and Learning Systems Engineering

XXII Cycle

Chemical Sensors Based on Image Detectors

Francesca Dini

A.A. 2009/2010

Tutor: Prof. Corrado Di Natale

Coordinator: Prof. Corrado Di Natale



UNIVERSITÀ DI ROMA
"TOR VERGATA"

FACOLTÀ DI INGEGNERIA

DOTTORATO IN
Sistemi sensoriali e di apprendimento

XXII Ciclo

Chemical Sensors Based on Image Detectors

Francesca Dini

A.A. 2009/2010

Tutor: Prof. Corrado Di Natale

Coordinatore: Prof. Corrado Di Natale

To my parents...
for being with me in my choices

Index

Introduction	5
Chapter 1: General Aspects of Chemical Imaging	11
1.1 Introduction.....	11
1.2 Absorption and Emission Spectroscopy.....	12
1.2.1 Electronic Spectra of Molecules.....	16
1.2.2 Beer-Lambert Law	17
1.3 Spectrophotometers.....	19
1.4 Colour acquisition devices	21
1.4.1 The eye	22
1.4.2 Colorimeters	24
1.4.3 Scanners	24
1.4.4 Digital Colour Cameras.....	25
1.4.5 Device Colour Space	31
1.5 Optical Chemical Sensors	33
1.5.1 Reagent-Mediated Optical Sensors	35
1.5.2 Fibre Optic Chemical Sensors	37
1.5.3 Optical Chemical Noses	38
1.6 Computer Screen Photo-Assisted Technique.....	40
1.6.1 Computer Screens.....	41
1.6.2 CSPT Measurements	43
1.6.3 CSPT Model.....	47
1.6.4 Applications	50

1.6.5	Optical Interrogation of Sensing Layer	52
	References	57
Chapter 2:	Sensing Materials - Porphyrins and Polymers	61
2.1	Introduction.....	61
2.2	General aspects of porphyrins.....	62
2.2.1	Spectral features	64
2.2.2	Metallo-porphyrin spectra	65
2.3	Porphyrin aggregates.....	71
2.4	Applications in chemical sensors.....	74
2.4.1	Application in optical chemical sensors	76
2.5	Polymers.....	79
2.5.1	Sorption and diffusion in polymers	80
2.5.2	Polymers for optical sensors.....	82
	References	86
Chapter 3:	Chemical Sensitivity of Porphyrin Nano-Aggregates ...	90
3.1	Introduction.....	90
3.2	Porphyrin-Based Nanostructures	92
3.2.1	Porphyrin Nanoparticles.....	93
3.2.2	Porphyrin Nanosheets.....	94
3.2.3	Porphyrin Nanorods and Nanorings	95
3.2.4	Porphyrin Nanowires and Nanofibers	96
3.2.5	Porphyrin Nanotubes.....	97
3.3	Self-Assembled Porphyrin Nanotubes	98

3.4	Experimental	101
3.5	Results	105
3.5.1	Optical properties	105
3.5.2	Chemical Sensitivity in Liquid Solution	106
3.5.3	Chemical Sensitivity in Gaseous Phase	111
3.6	Conclusions	118
	References	119

Chapter 4: Polymer Matrix Effect on Sensitivity and Selectivity .122

4.1	Introduction	122
4.2	Choice of polymers	126
4.3	Experimental	129
4.4	Results and discussion	134
4.4.1	Preliminary studies on the polymeric matrices	134
4.4.2	Array of polymeric matrices for VOCs discrimination	139
4.5	Conclusions	148
	References	149

Chapter 5: A bio-mimetic Approach to Volatile Detection152

5.1	Introduction	152
5.2	Chromatographic principles	154
5.3	Chromatographic principles in biological olfaction	158
5.4	Spatio-temporal patterns in artificial sensors	162
5.4.1	Artificial olfactory mucosa	165
5.5	Mono-dimensional separation geometry	166
5.5.1	Experimental	167

5.5.2	Results	168
5.6	Bi-dimensional separation layer.....	169
5.6.1	Experimental	170
5.6.2	Results	172
5.6.3	Discussion	184
5.7	Conclusions.....	186
	References	189
Chapter 6: Artificial Olfaction Platform.....		193
6.1	Introduction.....	193
6.2	Experimental	196
6.3	Results.....	200
6.3.1	Considerations on spectral features	200
6.3.2	Artificial olfactory bulb definition	203
6.3.3	Background removal	206
6.3.4	Artificial sensors signals	210
6.4	Conclusions.....	211
	References	213
Chapter 7: Conclusions.....		215
	List of Publications.....	218
	Acknowledgments.....	222

Introduction

Natural olfaction has been a continuous source of inspiration for the development of gas sensors. Nonetheless, few progresses were made since the original intuition about the similitude between an array of partially selective chemical sensors and the natural olfactory receptors. Some attempts were done in the past to cover the gap between natural and artificial systems and electronic nose is still considered, as defined by Gardner and Bartlett, a combination of *an array of non selective sensors and a pattern recognition algorithm*. Important issues of natural olfaction such as the large number of olfactory neurons, the convergence of receptors on a glomerular layer, and the active role of the olfactory mucosa are not yet embodied in artificial systems.

The development of electronic noses privileged the use of “electronic-ready” sensors, such as chemo-resistances (conducting polymers or metal oxides), and resonant sensors (quartz crystal microbalances or surface acoustic wave devices). These sensors are easily implemented in electronic circuits, nonetheless, resonant sensors are affected by a large non selectivity and only a limited number of materials change their conductivity upon chemical interactions. Straightforward techniques for chemical sensing are those based on the

modification of optical properties such as absorbance and luminescence. Indeed chemistry can synthesize a large variety of efficient molecular recognition systems that adequately transduce the adsorption events into a change of optical properties. Among the devices available to measure the optical features, image detectors, such as digital cameras, allow the simultaneous measurement of optical properties of large ensembles of individual sensors, providing a tool to develop sensing systems where the similitude between nature and technology may be enhanced.

This thesis describes an approach to improve the detection capabilities of image sensors. The development of novel strategies for optical sensors can concentrate either on the introduction of innovative technologies or in the use of new sensing materials. Herein, the attention was focused on the study and optimization of the characteristics of sensing layers. The structure of this thesis is schematically illustrated in the flow chart in Figure I.

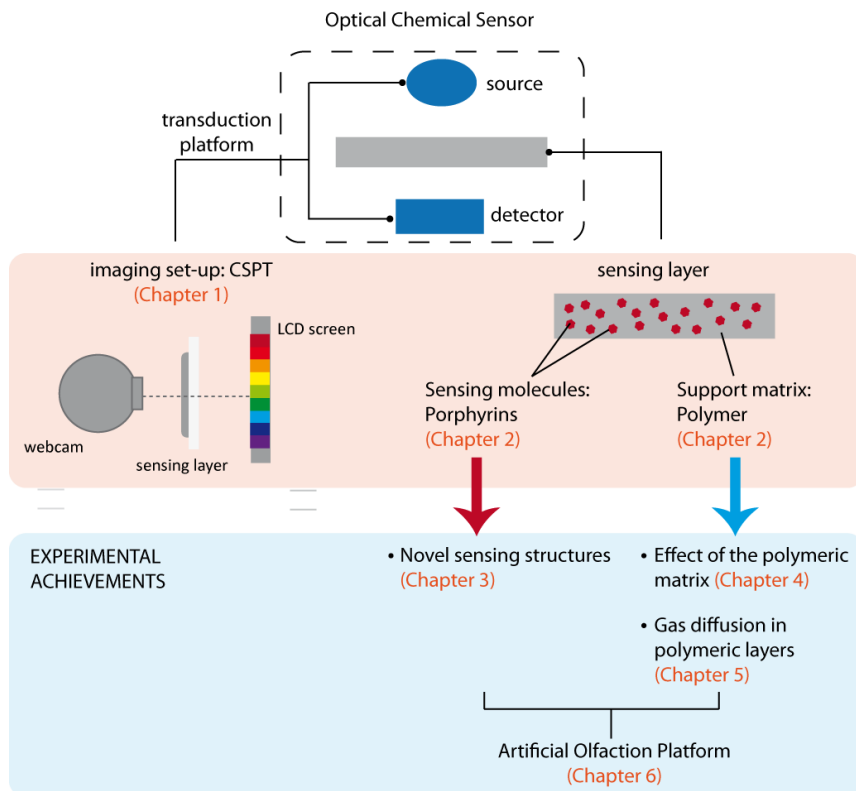


Figure I. Flow chart of this thesis.

A generic chemical sensor consists of a layer of chemical interactive material (CIM) and of a transducer that transforms the variations in CIM properties into a readable signal, usually of electric type. Different transduction chains may be conceived, and in the field of optical chemical sensors, image detectors are promising to develop innovative sensor systems. Among those, the Computer Screen Photo-Assisted

Technique (CSPT) is an optical transduction platform constituted of ubiquitous computer peripherals that was already demonstrated for opto-chemical sensing. CSPT detection is based on an image sensor that allows to simultaneously address and measure signals from individual units up to several thousands (Chapter 1).

The sensing layer in optical chemical sensors usually consists of an optically responsive molecule dispersed in an inert and gas permeable polymeric support. The sensing molecule is responsible for the detection of analytes through changes in its absorption spectrum. A suitable choice is represented by molecules from the porphyrins family that, thanks to their π - π^* transitions, undergo a strong variation after the interaction with various analytes. The polymeric matrix, on the other hand, reduces the optical density and favours gas diffusion, allowing a more efficient exposure of the sensing molecule to analyte molecules. Several polymers are suitable to this scope, and the selection of the proper one determines the overall characteristics of the resulting optical sensor (Chapter 2).

The design of sensor materials is a cornerstone for the development process of sensors. The sensing layer is crucial for the accomplishment of sensor requirements such as sensitivity, selectivity, stability and reversibility. Both the standard components of a sensing layer were dealt with to control sensing features such as sensitivity and selectivity.

Usually sensing molecules are provided with selected features through a modification of their chemical structure. Recently, progresses

in supra-molecular chemistry offered a further methodology for the development of materials, even if seldom their peculiar sensitive properties find an application as sensors. Here, nano-structured arrangements were investigated to enhance the performances of sensing molecules. A tubular self assembled formation of two different porphyrins was studied demonstrating an enhancement of performances with respect to the individual units (Chapter 3).

The effect of matrices made of different polymers to disperse a single indicator was also investigated. An array of several polymers containing the same dye was demonstrated to discriminate among a variety of vapours, revealing that the different partitioning of the matrices contributes to the analytes recognition (Chapter 4).

The behaviour of gas through a polymeric phase is a fundamental pillar in analytical chemistry. Here the diffusion of vapours in uniformly distributed layers of porphyrin-functionalized polymers was studied. A targeted feature extraction allowed to gather information from spatio-temporal data pattern, demonstrating the ability of our platform to separate and detect volatile compounds introducing the olfactory mucosa properties in an artificial sensor system. This bio-mimetic approach is then wished to prompt the development of novel principles to be incorporated in optical sensors (Chapter 5).

Finally, all the findings described in this thesis were combined in order to design an artificial olfaction platform characterized by a large

sensor array, the convergence into a glomerular layer and the emergence of a spatio-temporal response pattern (Chapter 6).

Chapter 1: General Aspects of Chemical Imaging

1.1 Introduction

In optical sensors a reagent recognizes the analyte and converts the information into changes of optical properties, such as absorbance, reflectance or fluorescence. In the most conventional arrangement the sample is irradiated with a monochromatic radiation and the magnitude of the interaction is evaluated from the attenuation of the original radiation or by observing the secondary radiation emitted from the sample. An optical chemical sensor is constituted of a membrane that contains sensing molecules, an exciting beam of light and an optoelectronic interface that provide a readable signal¹ (Figure 1.1).

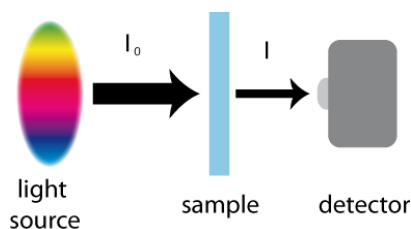


Figure 1.1. Scheme of the transduction cascade of an optical chemical sensor

In this chapter, an introduction will be given concerning spectroscopic properties of molecules and the principles of absorption and emission spectroscopy. A brief overview of optical chemical sensors will follow and, within it the principles of operation of the Computer Screen Photo-Assisted Technique (CSPT) will be described.

1.2 Absorption and Emission Spectroscopy

The interaction of electromagnetic radiation with matter occurs over a broad range of frequencies and in a highly specific fashion. The study of these interactions concerns the domain of spectroscopy that provides information on atoms and molecules structure.

The spectrum of electromagnetic radiation is arbitrarily divided into several regions (Figure 1.2). The typical spacing between electronic energy levels is roughly 2-10 eV, corresponding to photon energies in the visible and ultraviolet (UV) region. Whereas spacing between vibrational energy levels corresponds to photon energies in the infrared region, and spacing between rotational energy levels corresponds to photon energies in the microwave region.

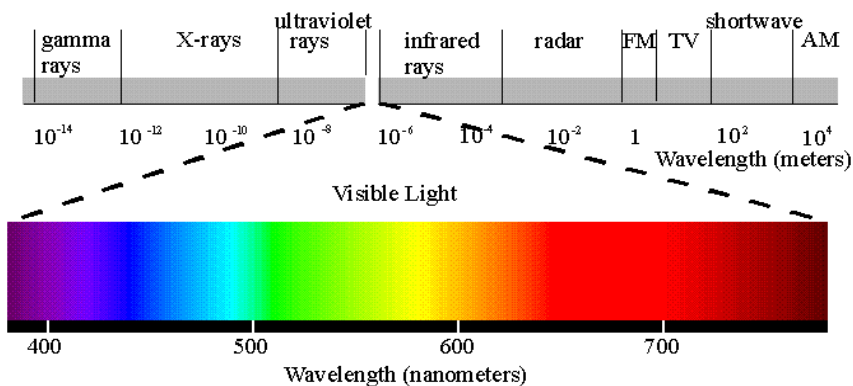


Figure 1.2. Regions of the electromagnetic spectrum, with the range of visible frequencies magnified.

According to the Planck-Einstein relation, the energy of a photon is:

$$E = h\nu = h \frac{c}{\lambda} \quad (1.1)$$

where h is Planck's constant, ν is the frequency of the radiation, c is the speed of propagation of electromagnetic radiation and λ is the wavelength.

When light, either visible or ultraviolet, is absorbed by valence electrons these are promoted from their normal states to higher energy states, called excited states. The atom or molecule makes thus a transition between levels whose difference in energy is equal to the energy of the absorbed photon.

Valence electrons are found in three types of electron orbitals. Single, or σ , bonding orbitals, double or triple (π bonding orbitals), and non-bonding orbitals (lone pair electrons). The σ bonding orbitals tend

to be lower in energy than π bonding orbitals, which in turn are lower in energy than non-bonding orbitals. When electromagnetic radiation of the matching frequency is absorbed, a transition occurs from one of these orbitals to an empty orbital. Usually most of the absorptions involve transition to antibonding orbitals such as $\text{as} \rightarrow \pi^*$, $\text{n} \rightarrow \sigma^*$ and $\text{n} \rightarrow \pi^*$ (Figure 1.3).

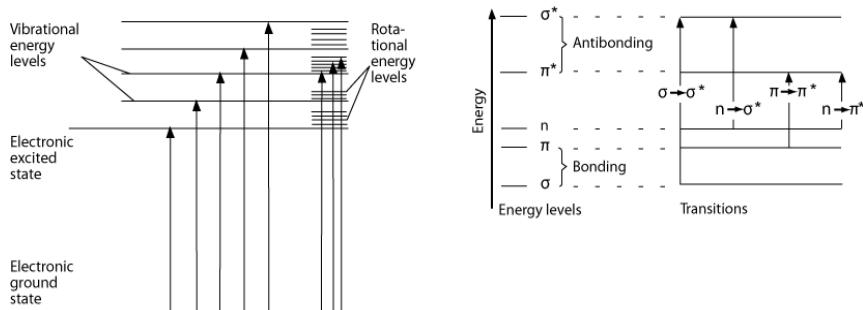


Figure 1.3. Electronic states and transitions.

UV-Visible spectroscopy deals with the study of the interaction between photons and matter as a function of wavelength in the visible region of the electromagnetic spectrum. There are two principal types of optical spectroscopy. In absorption spectroscopy the attenuation of an incident beam due to absorption is observed, while in emission spectroscopy emitted radiation from excited atoms or molecules is measured. In fluorescence spectroscopy the photons are re-emitted at longer wavelengths, while in absorption spectroscopy the energy that is transferred to the chemical compound is lost by non-radiative means, such as transfer of energy as heat. The intensity of absorption for a

given transition depends on three main factors: the intensity of the radiation, the inherent probability that the transition will take place, and the number of molecules in the upper and lower states (i.e. the "population" of the state).

The classical way to observe emission or absorption spectra is to disperse the radiation, which means separate the different wavelengths from each other. A triangular prism of transparent material or a diffraction grating can be used to this purpose. Absorbance is usually measured with spectrophotometers that will be discussed in section 1.3. In spectrophotometers, the light is dispersed and collimated into a beam of nearly parallel rays, so that only a narrow band of wavelengths passes through the sample at one time. A detector determines the intensity of transmitted radiation.

A quantity that is commonly plotted to represent an absorption spectrum is the transmittance, $T(\lambda)$, defined as follows:

$$T(\lambda) = \frac{I(\lambda)}{I_0(\lambda)} \quad (1.2)$$

where $I(\lambda)$ is the intensity after the light beam passes through the cell and $I_0(\lambda)$ is the incident intensity. Complementarily, the absorbance is defined as follows:

$$A(\lambda) = -\log T(\lambda) = \frac{I_0(\lambda)}{I(\lambda)} \quad (1.3)$$

1.2.1 Electronic Spectra of Molecules

Atoms have absorption lines at wavelengths corresponding to the differences between the energy levels of the atomic orbitals. For the hydrogen atom, selection rules establish the conservation of angular momentum in the atom-radiation system. Thus, a hydrogen atom in an *s* subshell can make a transition only to a *p* subshell, while an atom in a *p* subshell state can make a transition to an *s* subshell or to a *d* subshell. In multielectron atoms, the general rule is that the spin must not change ($\Delta S=0$), hence transitions between singlet and triplet states are forbidden, even if they do occur with low probabilities.

Transitions of a diatomic molecule from one electronic state to another are characterized by rotational and vibrational transitions that take place simultaneously with the electronic transitions. Each electronic transition produces a number of bands, with one band for each vibrational transition and with the lines of each band corresponding to different rotational transitions. Measurement and interpretation of such an electronic band spectrum can yield not only the energy differences between electronic levels, but also between vibrational and rotational levels. Selection rules forbid transitions that change the value of the spin *S*. Since these rules are approximate, forbidden transitions between triplet ($S = 1$) states and singlet ($S = 0$) states do occur, but with low probabilities and corresponding low intensities compared with singlet-singlet transitions. An electronic transition corresponding to the transition of a single electron from one orbital to another can be

characterized by specifying the initial orbital and the final orbital. For example, if the electron makes a transition from a π bonding orbital to a π antibonding orbital, the transition is called $\pi \rightarrow \pi^*$ transition. If the electron goes from a nonbonding orbital to π antibonding orbital, the transition is said to be an $n \rightarrow \pi^*$ transition.

As far as polyatomic molecules are concerned, since there are several normal modes in any polyatomic molecule, the simultaneous electronic, vibrational, and rotational transitions can give very complicated spectra. The selection rules for electronic transitions are more complicated than in atoms and diatomic molecules. In many cases a whole class of compounds will exhibit similar spectral lines that can be attributed to a functional group or other group of atoms within a molecule. Such a group that exhibits a characteristic absorption is usually called a chromophore².

1.2.2 Beer-Lambert Law

Absorption spectroscopy can be used to measure the concentration of absorbing molecules. Figure 1.4 shows a drawing of a cell containing absorbing molecules at concentration c and with a beam of light passing through it in the x direction. Considering a thin slab of unit area within the cell, lying between x and $x+dx$, the volume of the slab is dx times unit area, so the amount of absorbing substance in this portion of the slab equals $C \cdot dx$ times unit area. Let the intensity of light in the small range of wavelengths $d\lambda$ be denoted by $I(\lambda, x) d\lambda$. This intensity depends

on x because of absorption phenomena that make the light become less intense the farther it travels into the cell. The amount of light absorbed in the layer per unit time is proportional to the initial intensity of light and to the amount of absorbing substance, so that the change in I from one side of the thin layer to the other is given by:

$$-dI = k(\lambda)ICdx \quad (1.4)$$

The proportionality factor k is a function of wavelength and it does not depend on molecules concentration. It is different from zero only for wavelengths such that the photon energy equals the energy difference between a significantly occupied molecular energy level and a higher level.

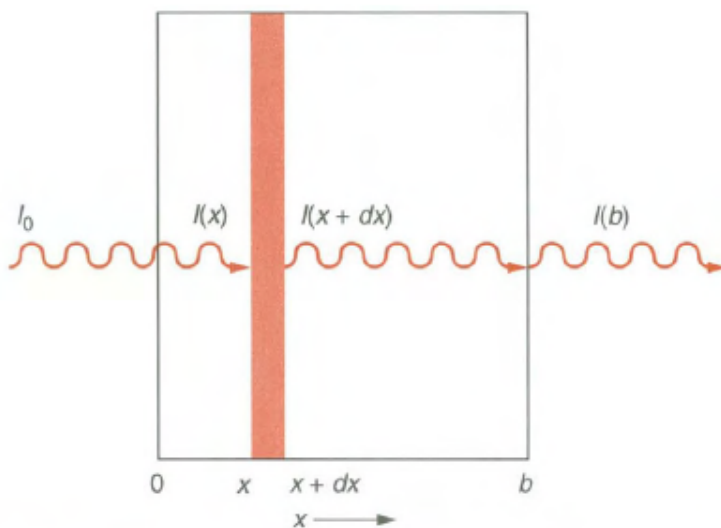


Figure 1.4. Absorption of light in a thin layer. According to Beer-Lambert law, it is proportional to the absorptivity and to the thickness of the layer.

Equation 1.4 is a differential equation that can be solved for the intensity of light as a function of position. It is solved by a definite integration, letting $x = 0$ be the front of the cell and $x = d$ be the back of the cell. Assuming that the concentration is uniform, it yields:

$$A = \ln \left(\frac{I(\lambda, 0)}{I(\lambda, d)} \right) = \varepsilon(\lambda)cd \quad (1.5)$$

Equation 1.5 is known as Beer-Lambert law, where $\varepsilon(\lambda)$ is the absorptivity (also called the extinction coefficient). The absorptivity depends on the wavelength of light as well as on the absorbing substance and on the media. The Beer-Lambert law is well obeyed by many substances at low concentrations. Deviations occur at higher concentrations, corresponding to an absorptivity that depends on concentration. These deviations can be caused by specific chemical effects such as association of the molecules of the substance, which provides one way to study molecular association.

1.3 Spectrophotometers

A spectrophotometer is a device for measuring the spectral reflectance or absorbance of an object. In spectrophotometers the light is dispersed by a monochromator, a prism or a grating, collimated into a beam of nearly parallel rays, and then it is passed through a cell containing the sample. A photocell or other detector determines the

intensity of transmitted radiation. The radiation cannot be dispersed so completely that a single wavelength is separately presented to the sample. A spectral line with a very narrow inherent width appears to have a larger line width due to the limitations of the instrument. The difference in wavelength of the most closely spaced narrow spectral lines that can be resolved determines the resolution of the instrument.

In a single-beam instrument, the cell containing the sample substance and a "blank" cell not containing this substance are placed alternately in the beam. In a double-beam instrument, the beam is divided and passed simultaneously through the sample cell and the blank cell. In a diode-array instrument, a number of detectors in different locations are used, and the entire spectrum is taken at one time. The instrument measures reflectance as the ratio of two measurements, as shown schematically in Figure 1.5. The light source is contained within the spectrophotometer and is used to illuminate both a standard sample with known reflectance, and the test object.

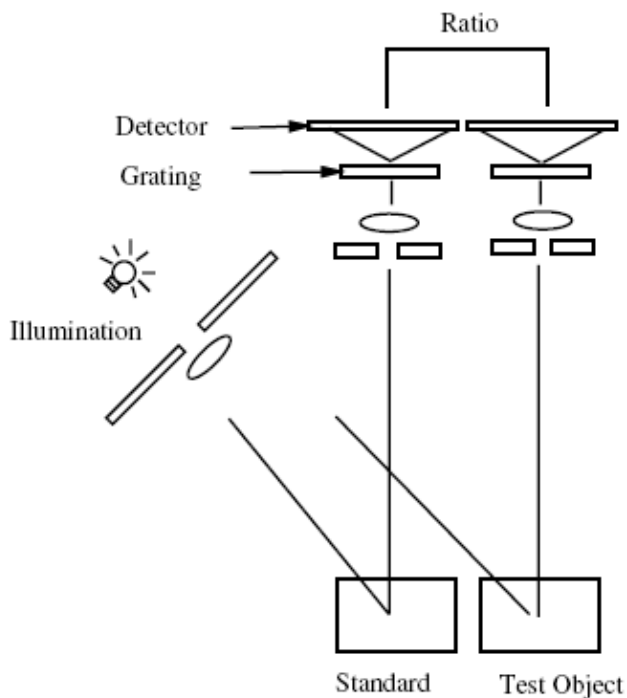


Figure 1.5. Basic scheme of a dual-beam spectrophotometer

1.4 Colour acquisition devices

Colour measurement instruments are used primarily for determining the colour characteristics of objects. Systems for recording colour information include both colour measurement instrumentation useful for large uniform regions and colour image capture devices designed to capture spatially varying colour information. They include both spectral

measuring devices such as spectroradiometers or spectrophotometers and filter-based instruments that directly measure colorimetry. The correct colour measurement for a particular application depends on several factors including the cost of the instrument, the desired accuracy, and the particular optical access. Colour image capture devices include conventional and digital colour cameras, which record colour information from a scene of real world objects, and colour scanners, which record colour information of a bi-dimensional object such as a printed colour image, slide, or negative. The next paragraphs deal a brief overview of colour acquisition devices, starting with the description of the vision system in humans.

1.4.1 The eye

In the human eye, the incident light is focused by the cornea and the eye's lens to form an image of the object onto the retina located at the back of the eyeball. Photoreceptors within the retinal membrane are responsible for sensing the image and creating the neural signals that breed the sense of sight. In the human retina there are two kinds of photoreceptors: rods and cones. The rods are extremely sensitive to light and primarily useful for vision under very low light levels, termed as scotopic vision. In scotopic vision, only shades of gray can be perceived, colours are not distinguished and it is primarily used in the darkness. Under typical light levels, the rods become saturated and do not contribute to vision, while the less-sensitive cones are active. This is

referred to as photopic vision. The cones are responsible for colour vision, and in human retina there are three different types of cones, with photosensitive pigments that differ in their spectral absorption characteristics and, consequently, in their spectral sensitivities. The three types of cones have their peak of sensitivity in different regions of the visible spectrum (Figure 1.6). Under a fixed set of viewing conditions, the response of these cones can be accurately modelled by a linear system defined by the spectral sensitivities of the cones. To a first order of approximation, under similar conditions of adaptation, the sensation of colour may be specified by the responses of the cones.

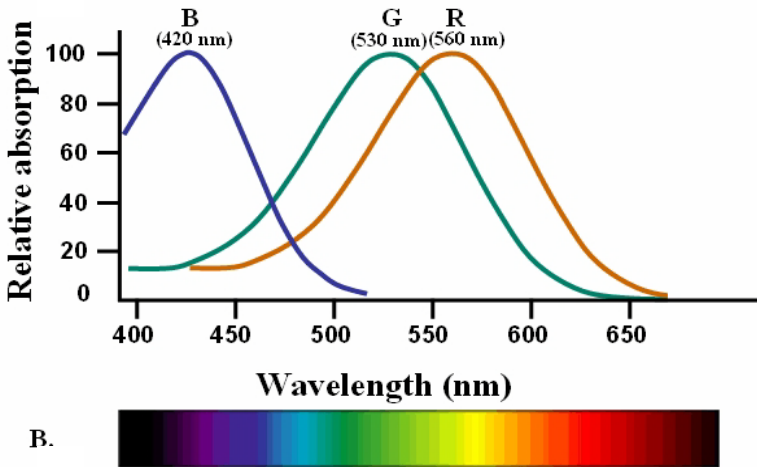


Figure 1.6. Human eye pigment absorbance spectra.

In normal human observers, the spectral sensitivities of the three cones are linearly independent. Furthermore, the differences between

the spectral sensitivities of cone are relatively small. If a standardized set of cone responses is defined, colour may be specified using the three-vector, known as a tristimulus vector³.

1.4.2 Colorimeters

A colorimeter measures colour tristimuli and reports these as colour values in the related colour spaces. Some colorimeters have an internal light source for the measure of reflective objects, whereas others measure only self-luminous or externally illuminated samples. Most colorimeters are small, hand-held devices with no moving parts and a single light detector. They achieve their spectral separation by means of colour filters placed before the detector or with spectrally separated light sources used for illumination. Colorimeters are less expensive than spectrophotometers but they do not provide the same detailed spectral information.

1.4.3 Scanners

Scanners are usually designed to reproduce images on paper or transparencies and include their own sources of illumination. Because the objects are stationary, these devices do not need to capture the entire image in a single exposure. Typically flatbed moving stage scanners use a single sensor per channel which is scanned across the image to provide spatial sampling. The single sensor makes the characterization of the

device easier and more precise, and also allows the use of more expensive and accurate sensors. For desktop scanners, speed is of greater importance, and they usually employ an array of three linear CCD sensors with red, green, and blue colour filters. The linear sensors extend across one dimension of the scanned image. This allows three filtered channels of the image along a line to be acquired simultaneously. To sample the entire image, the linear array is moved optically or mechanically across the other dimension of the image. In another variation of these devices, three different lamps are used in conjunction with a single linear CCD array to obtain a three-band image from three successive measurements⁴.

1.4.4 Digital Colour Cameras

Digital colour cameras capture colour images of the real world by transmitting the image through a number of colour filters having different spectral transmittances and sampling the resulting coloured images using electronic sensors.

The core of a digital camera is a sensor array that converts light into electrical signals. There are many different image sensor architectures used in digital cameras, and the most common choice is the Charge Coupled Device (CCD). A CCD photo-detector consists of a two-dimensional array of cells, each having metal-insulator-semiconductor capacitors, usually of the form of metal-oxide-silicon (MOS). The photocapacitors are arranged as parallel, vertical charge-coupled device

shift registers. The device is based on the photoelectric effect: when the silicon is hit by photons, some electrons are excited to the conduction band and accumulate in the wells. These electrons are collected in the MOS capacitors and after a certain exposure time, the charge build-up is measured. Each MOS capacitor functions as a small well in which the released electrons are trapped. Because the number of electrons collected is proportional to the incident illumination level, the sensor has a linear response curve. This means that the digital code value representing each pixel from the A/D converter, corresponding to each photosite on the CCD, is linearly related to the number of electrons collected by the photosite. In very bright areas of an image, the number of electrons generated in a particular photodetector may exceed the charge capacity of the potential well. These excess electrons must be eliminated, or they will migrate to nearby wells, causing blooming effects. Image sensors used in digital cameras normally include an anti-blooming overflow drain to direct the excess charge into the sensor substrate and prevent it from spilling into neighbouring cells. Nevertheless, setting the proper camera exposure level is critical, as overexposure will clip the image highlights. Underexposures can be corrected by digitally adjusting the code values of the final image, but this will consequently increase the noise.

In the readout phase, an appropriate voltage applied to a cell deepens its potential well, causing electrons from an adjacent cell to be transferred into it. This phenomenon is used to sequentially read all the

pixels by moving them in an ordered fashion. The charge collected by the photocapacitors is shifted into an opaque serial, horizontal CCD register at the bottom of the array and then serially transferred to an output amplifier. The amplifier converts the charge into a voltage, which is in turn transformed by an AD-converter, enabling it to be processed by a computer.

The full-frame CCDs used in most professional digital cameras have cell sizes ranging from about $6 \times 6 \mu\text{m}$ up to $16 \times 16 \mu\text{m}$. A larger cell size provides higher dynamic range and lower noise, enabling the camera to operate at a higher ISO speed. However, the larger cell size also makes the sensor physically larger and more costly, and the camera lens is likewise more bulky and expensive. Most consumer megapixel cameras use an interline (IL) sensor architecture. The size of each cell is typically between $2.5 \times 2.5 \mu\text{m}$ and $5 \times 5 \mu\text{m}$, so the sensor size is very small as compared to the size of the previous sensors.

Silicon semiconductors have an inherent sensitivity to light in the visible and the near-infrared regions of the spectrum. The quantum efficiency of a typical photodiode used in a CCD is shown in Figure 1.7. The spectral response decreases above 500 nm because of the vertical overflow drain used to provide antiblooming protection. The long-wavelength photons penetrate deeper into the silicon before they are absorbed; therefore, the free electrons have a higher probability of migrating to the antiblooming drain rather than to the potential well of the photodiode, as compared to shorter wavelength photons.

Nevertheless, the CCD has significant sensitivity in the near-infrared region. Therefore, colour digital cameras normally use an IR blocking filter to prevent problems caused by IR light⁵.

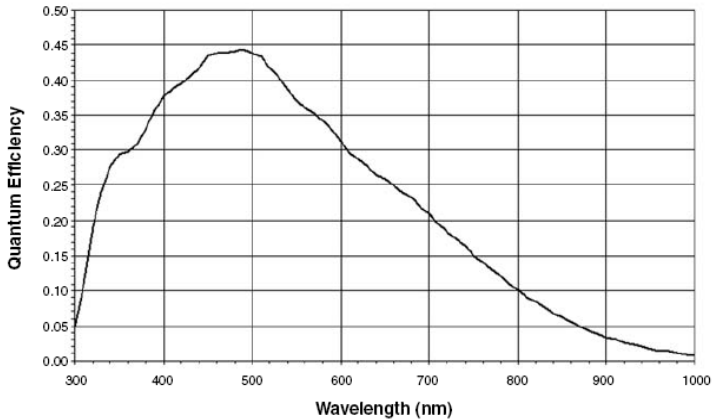


Figure 1.7. Quantum efficiency of a typical photodiode.

These image sensors are sensitive only to the luminance part of the colour and can produce only gray scale images, so that each pixel is represented with 8 bit intensity levels. However, to obtain a 24 bit colour resolution, different schemes may be used to achieve the spatial sampling and colour filtering operations concurrently. A possible arrangement uses three CCD arrays with red, green, and blue colour filters, respectively. This is adopted in sophisticated image detection systems where the light is split towards three identical CCD that measures the intensity in separated bands, and a real 24 bit resolution is obtained by the linear superposition of acquired matrix. In such an

arrangement, precise mechanical and optical alignment is necessary to maintain correspondence between the images from the different channels.

A more cost effective configuration is adopted for web cameras and for the majority of CCD-based devices, consisting in a colour filter mosaic of red, green and blue filters that is overlaid on the CCD array during the semiconductor processing steps. This is called Bayer filter⁶. The three filters are arranged in a repetitive bi-dimensional pattern with 50% of the elements covered by green filters and the other 50% equally covered by red and blue areas, as showed in Figure 1.8.

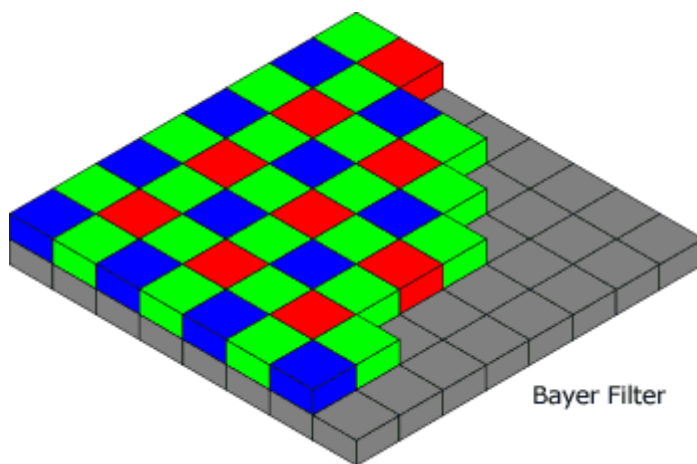


Figure 1.8. Patterning of red, green and blue colours in a Bayer filter.

The predominance of green filters is needed to improve the perceived sharpness of the image because the human eye is more sensitive to high spatial frequency in luminance than in chrominance, and luminance is

composed primarily of green light. On the contrary, the red and blue photo-sensors represent the chrominance-sensitive elements. The polychromatic intensity colour of each pixel is gleaned with several types of interpolation from neighbour pixel values (demosaicing algorithms). Among the variety of possible algorithms, the most diffuse are the bilinear interpolation, the constant hue-based interpolation, the median-based interpolation, and the gradient based interpolation⁷. Unfortunately, due to compression routines compatible with USB standard, with standard web cameras it is usually not possible to deal with the raw Bayer image.

Figure 1.9 shows the quantum efficiency of a typical CCD sensor overlaid with an RGB colour filter array, cascaded with a typical camera lens and IR blocking filter. This colour sensitivity will be compensated for by the camera's digital image processing, to produce a standard colour response. Each camera can have a slightly different response because of the manufacturing tolerances of the sensor and filters.

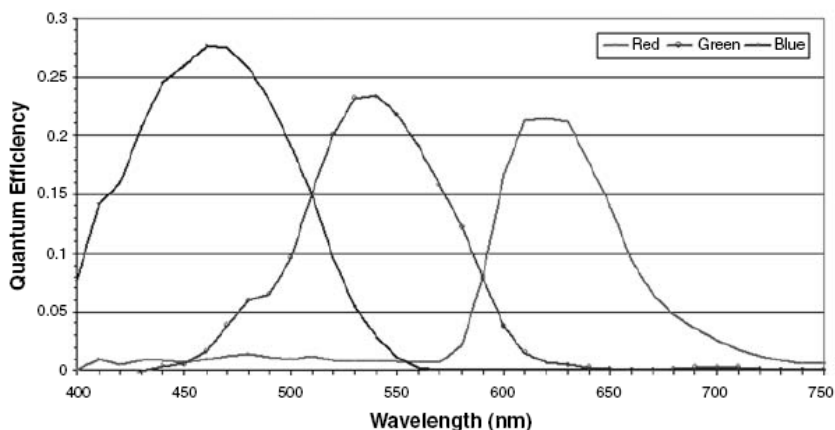


Figure 1.9. Red, green and blue channel transmittances of a generic camera.

Recently, a novel camera design has been developed that avoids the problems of both colour filter arrays and of multiple images by using a single sensor and effectively layering the red, green, and blue filters by using the spectral selectivity of light penetration in silicon⁸.

1.4.5 Device Colour Space

The measurements from colour recording devices and the control values for colour output devices are the colour representations of recorded images or the images to be reproduced, respectively. Thus, typically we identify RGB colour spaces for scanners, cameras, and other input devices, and CMY/CMYK colour spaces for colour printers. Most of these colour spaces are not standard and cannot be directly used for the meaningful archival of image data. However, if these device

spaces are related to the standard colour spaces in a clear unambiguous way, these can also be potentially used for the exchange of colour information. An advantage of such a scheme is that no transformations of the image data are required for display if the data are specified in the native colour space of the device. Because a large fraction of digital images are primarily targeted for display on CRT or LCD monitors, the RGB colour space has been proposed for use based on these devices. The RGB colour space is basically a gamma-corrected additive space that uses red, green and blue as primaries. It can determine any colour contained in the triangle defined by these primary colours. In addition, the RGB standard includes provisions for specifying the viewing conditions, such as white-point chromaticities, image surround, and flare. The RGB space is tied to the characteristics of common computer displays and it is limited in some respects. In particular, there are colours in the cyan and bright yellow regions that can be produced on common printers but lie outside the range of colours that are can be encoded in RGB. Recently, extensions to the space to remedy some of its limitations with regard to gamut have been proposed. Standardized CMYK spaces have also been defined in the graphic arts industry to allow colour data to be supplied to printing press operators in a form that can be unambiguously interpreted.

1.5 Optical Chemical Sensors

Optical chemical sensors employ optical transduction techniques to yield analyte information. The most widely used techniques used in optical chemical sensors are absorption and luminescence spectroscopy, but sensors based on other optical parameters, such as refractive index and reflectivity, have also been developed. Recent developments in the field have been driven by such factors as the availability of low-cost, miniature optoelectronic light sources and detectors, the need for multianalyte array-based sensors particularly in the area of bio-sensing, advances in micro-fluidics and imaging technology, and the trend toward sensor networks. In the case of luminescence-based sensors, direct intensity detection has been replaced in many applications by lifetime-based sensing, often using sophisticated phase-based techniques.

Chemical and biochemical sensing until recently was limited to single-point measurements and to the analysis of a single, homogeneous, and statistically mixed sample. However, there are numerous applications where the two-dimensional distribution of a chemical or physical parameter is of interest. Optical imaging methods can image areas that are, in principle, not limited in terms of area and even chemical imaging of the whole globe is not beyond feasibility. Fluorescence imaging is a widespread method that is applied to scan large areas for fluorescent species such as polycyclic aromatic hydrocarbons, chlorophylls and algae.

In general, optical chemical sensors may be categorized under the headings of direct sensors and reagent-mediated sensors. In a direct optical sensor, the analyte is detected directly via some intrinsic optical property. Many gas sensors measure the intrinsic optical absorption using a variety of techniques including Fourier Transform Infrared Spectroscopy (FTIR) or correlation spectroscopy. Usually the detection occurs in the infrared region of the spectrum since the fundamental vibrational transition take place in the near and mid-IR, spanning wavelengths from 1 to 10 μm . IR spectroscopy is the most widely used direct optical sensing technique, especially for gases such as CO, CO₂, NO₂, NH₃ and CH₄.

In reagent-mediated sensing systems, a change in the optical response of an intermediate agent, usually an analyte-sensitive dye molecule, is used to monitor analyte concentration. This technique is particularly useful in case the analyte neither has an intrinsic luminescence nor can be rendered luminescent with the help of labels or probes, as happens for oxygen, pH, CO₂, or ammonia¹.

Among the variety of sensing platform, the optical fibre is arguably the most exploited one in the development of optical chemical sensors⁹. Whereas electronic components such as CCD chips, CMOS devices, and high-density integrated circuits provide the ability to deal with high density sensing arrays and to collect enormous amounts of data on short time scales¹⁰. Recently lots of research is also exploring new techniques based on broadly diffuse and common sensing interfaces, co-opting the

optical capabilities of devices originally conceived for different purposes. In this optic, scanners have been used to acquire image of an array of colorimetric indicators¹¹. Conventional optical disk drives, such as CD and DVD, were used for quantitative detection of sensor films changes. The process does not alter the properties of the drives, and consequently any disk can be used and they also maintain their original capability of reading, writing and storing digital content¹². We will see other application of common devices for chemical sensors in the next paragraphs.

1.5.1 Reagent-Mediated Optical Sensors

When an analyte does not exhibit a convenient spectroscopic optical response such as absorption or luminescence, sensing can be achieved by monitoring the optical response of an intermediate species or reagent whose response is modulated by the presence of the analyte.

This indirect sensing technique requires the reagent to be immobilized, either in the liquid or in the solid phase, to facilitate interactions with the analyte. Reagent-based optical sensing is based mainly on solid-phase immobilization matrices, where the reagent dye can be adsorbed, covalently or ionically attached, or simply encapsulated in a solid matrix that is permeable to the analyte. If the immobilization matrix has the capability of being coated on a substrate in liquid form, as is the case for sol-gel glasses or polymer coatings, a wide range of sensor configurations is enabled including, for example,

fibre optic, planar waveguide and array-based sensors. Indirect optical sensors are very well developed for pH sensing, that is based on the change in optical absorption of organic pH indicators. They also allow for colorimetric detection of CO₂ by measuring the pH change in response to carbonic acid generated by the acidic CO₂ gas¹³. On the other hand, many analytes, are detected with luminescent probes with the advantage that luminescence is intrinsically more sensitive than absorption as a sensing technique¹⁴.

In those applications that need to study the distribution of the concentration of non-luminescent species over larger areas, the system to be analyzed is exposed to a *paint* that responds to the respective parameter of interest. The term paint refers to a material that consists of a solvent, a polymeric support (sometimes referred to as a binder), and an indicator dye. This mixture can be painted or sprayed onto the surface of the object of interest or can be manufactured as a thin film that, after solvent evaporation, is placed on the system to be studied. The indicator dye in the paint undergoes diffusional equilibration with its environment, and the analyte of interest thereby modulates either the fluorescence or the absorption features of the paint, which is then photographed or imaged (Figure 1.10)¹⁵.

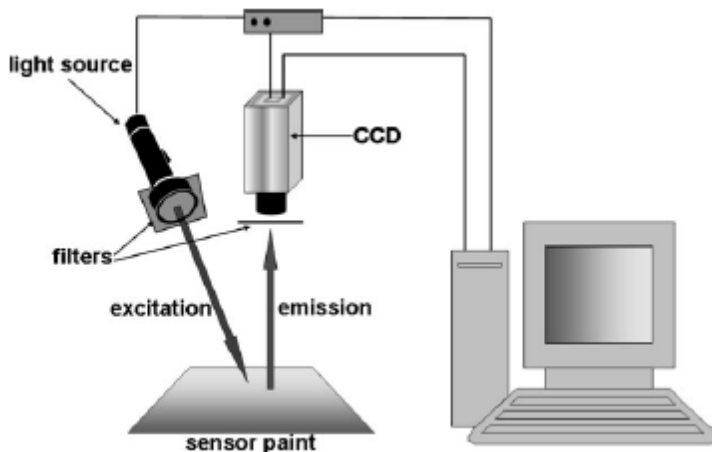


Figure 1.10. General scheme of the setup for imaging of optical sensor paints.

1.5.2 Fibre Optic Chemical Sensors

In a fibre optic chemical sensor the role of the fibre can be either passive or active. The fibre is considered passive if the sensor response is not linked in any way to an intrinsic change in the optical properties of the fibre itself, which acts merely to transport the optical signal to and from the sensing environment. Whereas the fibre is active if it has been modified to own an intrinsic sensitivity to analytes. In this manner, the optical properties of the fibre are modulated by the presence of the analyte. Frequently the cladding of the fibre is replaced with a matrix containing a fluorescent analyte-sensitive indicator. This is the case of the sensing platform proposed by Walt and co-workers, which centres on high density fibre bundles. Fibre bundles are arrays of hundreds to

many thousands of fibres bundled and fused such that they can transmit images. Walt group reported an odour sensing device based on an array of fibres whose distal end was coated with a various combination of polymer and solvatochromic dyes, with the light being both delivered to and collected from the proximal end of the fibre¹⁶. Lately, they also demonstrated the use of chemical etching to transform the distal tip of a fibre into a well, which can be filled with fluorescent solvatochromic material either bound to the surface of microspheres or entrapped within a microsphere. The surface or interior of a microsphere causes the solvatochromic dye to fluoresce at a particular wavelength and with a certain intensity. When a given microsphere is exposed to an organic vapour, the vapour partitions into the microsphere and the polarity of the microsphere is changed such that it is a combination of the intrinsic polarity of the microsphere material and the polarity of the vapour itself¹⁷.

1.5.3 Optical Chemical Noses

Electronic nose have been introduced at the end of the eighties to mimic the main functionalities of human olfaction, in particular the ability to detect a large amount of different odours with a limited number of different receptors¹⁸. The similitude between artificial and natural system is centred on the combinatorial selectivity of olfaction, namely on the fact that each receptor senses more compounds and each compound is sensed by more receptors, in this way a specific receptors

pattern emerges for each odour. This approach has a universal validity and it has been demonstrated that it can be applied to any kind of sensor technology¹⁹.

In spite to the wide development of optical chemical sensors, this technology has been seldom used for electronic nose development.

Walt and Kauer designed an artificial nose based on high-density optical arrays comprised of thousands of microsphere sensors randomly dispersed across the face of an etched optical imaging fibre. In their set-up the tips of a fibre optic bundle were functionalized with fluorescent indicators, and the whole fibre optic was imaged by a CCD giving rise to a continuous sensing surface with several dozens of sensors. The large amount of sensors gave also the opportunity to analyse the produced signals with algorithms directly derived from biological olfactory paradigms²⁰.

A more basic approach was provided by Di Natale et al that developed an artificial nose based on a set of metallo-porphyrins probed by a set of LEDs and measured by a set of photodiodes²¹. The concept was further explored by Di Natale *et al.* replacing the wide band probes and detectors with a spectrophotometer. In this implementation a number of metallo-porphyrins were deposited on a revolving substrate interrogated by a fibre optic spectrophotometer²².

An interesting change of paradigm was introduced by Suslick and his co-workers that shown that simple, inexpensive, and widely diffused equipment such as digital flat-bed scanners are sufficiently sensitive to

capture the colour changes occurring in chemical indicators²³. A further extension of this approach is offered by the computer screen photo-assisted technique that will be introduced in the next section.

1.6 Computer Screen Photo-Assisted Technique

The Computer Screen Photo-Assisted Technique is an optical-sensing interface firstly reported by Lundström and Filippini in 2003, which allows for the analytical investigation of visible absorption features of several kinds of samples²⁴. It consists of easily available, cheap and widespread diffuse computer peripherals. The basic hardware is a computer screen, either a cathode ray tube (CRT) or a liquid crystal display (LCD), that is used as a programmable polychromatic light source and a web camera used as a three bands detector (Figure 1.11). Digital cameras were described in section 1.4.4, while computer screens will be discussed in the next paragraph.

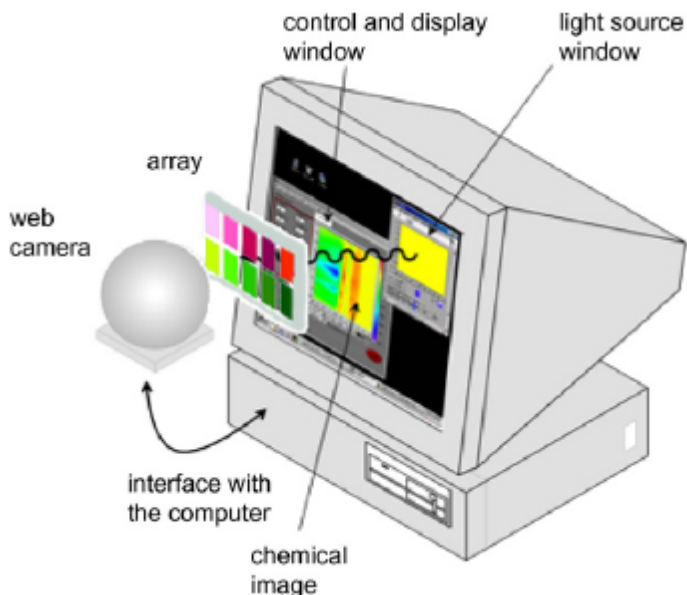


Figure 1.11. Schematic of a possible implementation of the CSPT platform

1.6.1 Computer Screens

Computer screens are capable of displaying confined areas of arbitrary shape, colour, and intensity that can be two-dimensionally scanned on the screen with 200 μm resolution defined by the pixel pitch (distance between two contiguous cells of the same colour)²⁵. In CRT monitors an electron beam scans the inner surface of the screen, exciting a spot of phosphorescent coating. It emits a burst of visible light that decays until it is reached again by the beam in the next scanning cycle. Colour CRT screens use three electron beams exciting blobs of three

different screen coatings. In this case the phosphors are band limited emitters of visible light corresponding to the perception of red, green and blue. The frequency at which the beams reach the same spot is about 85 Hz, and since it is faster than the eye's response it induces the perception of a steady intensity. On the contrary, in LCD screens each cell contains a liquid crystal between two crossed linear polarisers. If a voltage is applied to the cell, the liquid crystals rotate the direction of polarization of the light allowing to regulate the intensity escaping from the second polarizer. A large area white lamp illuminates the rear of the screen. Colour screens are produced by the repetition of groups of cells with red, green and blue filters. LCD screens produce a steady intensity and can refresh images at relatively low frequencies, typically 60 Hz. As far as CSPT measurements are concerned, the main differences between these two types of screens is the pulsed nature of the CRT displays and the linearly polarized light emitted from LCD screens²⁶.

The light emitted from a computer screen is not monochromatic but it is the combination of three polychromatic primary sources. The spectral radiance of these primaries excites the human perception of red, green and blue colours. Any other colour can be generated by the linear combination of these primaries according to²⁷:

$$c_i(\lambda) = r_i R(\lambda) + g_i G(\lambda) + b_i B(\lambda) \quad (1.6)$$

where $R(\lambda)$, $G(\lambda)$ and $B(\lambda)$, are the spectral radiances of the primary colours, r_i , g_i and b_i are numbers within [0 1] that represent the particular modulation of the primaries for a given desired colour, and λ ,

the wavelength, is limited to the visible range (390-800 nm). Conventional true colour systems have a resolution of 8 bits (0–255 values) for each colour channel, yielding a total of 2^{24} colours that can be displayed on the screen.

1.6.2 CSPT Measurements

During a CSPT measure, a colour sequence is displayed in a portion of the screen to illuminate the sample. The light emerging from the assay is simultaneously acquired by the camera operating at a capture rate usually of 1 frame/s. The result of such a measurement is a digital video file (.avi format) of the array under different illuminating colours. The video stream is then decomposed into individual frames and the information from selected regions of interest (ROIs) in the image are extracted. ROIs are marked with white circles in Figure 1.12 and they are located both on the sensing spots and on background areas.

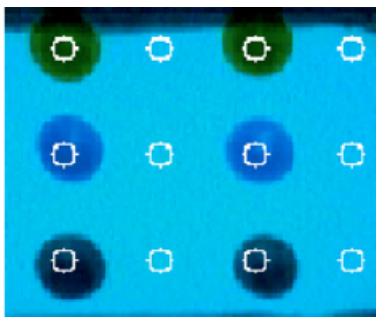


Figure 1.12. Camera image of sensing layers under a bluish illumination. In the picture the regions of interest (ROIs) for each sensitive layer and the corresponding background are also shown

The digital values of each colour level (red, green and blue) of the pixels contained in the ROI are averaged, yielding the intensity per colour channel of each screen colour. As a result, a distinctive spectral signature of the sample is obtained. Usually it is in the form of intensity versus illuminating colours curves and it is often referred to as CSPT fingerprint (Figure 1.13a). The CSPT measurement of any substance transmittance $T(\lambda)$ transforms this illuminating space into a measured space distinctive of the substance. The measured space contains both the spectral signature of the substances and that of the particular CSPT assembly where the measurement is performed. In order to highlight the substance signature, the measured space is subtracted by the measured space without substance, corresponding to the background area (Figure 1.13b).

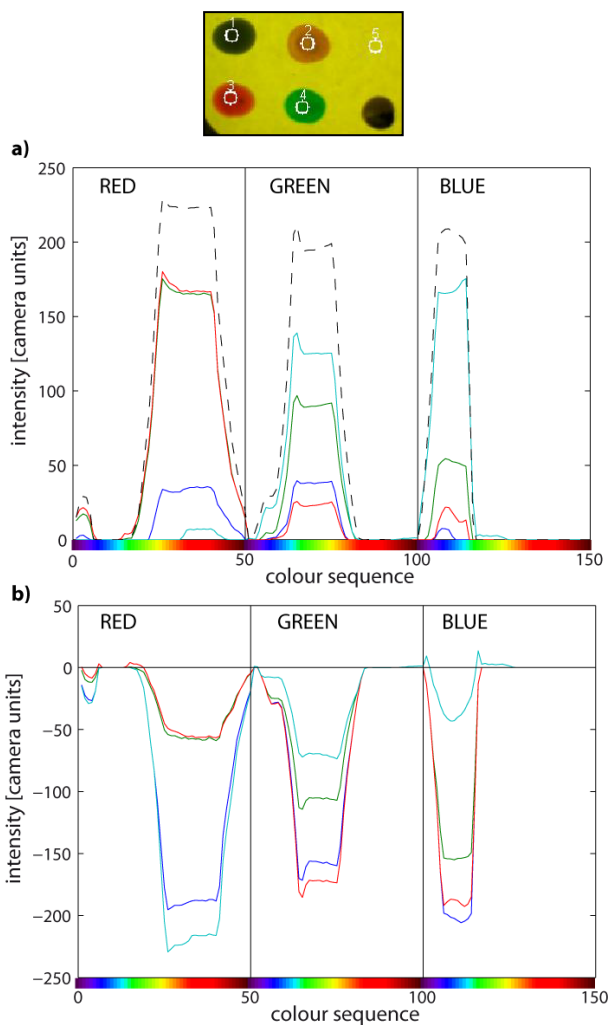


Figure 1.13. **a)** CSPT fingerprints of sensing layers reported in the inset, obtained concatenating the intensity in the three camera channel for a 50 colours illumination sequence. The black dashed line represents the reference light source or background (circle number 5 in the inset). **b)** Difference between the same fingerprint and background intensity. It allows to evaluate the absorption of each spot.

Different substances transform the illuminating space in different measured spaces and emerging light colours become aligned with the respective camera channels. In CSPT measurements, depending on the evaluated substance transmittance, some illuminating colours become clustered in the measured space, which eventually become redundant and reduce the spectral diversity of the fingerprint. Obviously, longer colour sequences have better chances to always incorporate well performing colours. Illuminating sequences homogeneously representing the illuminating space produces diverse distributions of measured values that can be optimized for every particular substance transmittance. However, it is also evident that certain substances will always be represented by a larger volume of the colour space. The larger the volume they occupy in the measured space, the better the chances to find an illuminating sequence that separates all the features creating a distinctive fingerprint. In summary, for substance transmittances with their minima at the centre of the visible spectrum, CSPT is able to retain more spectral features than for substances absorbing at the borders of the spectrum. These better conditions for substances that affect green, yellow, and orange light than for blue or red light can be intuitively associated to the restricted contribution of the later substances on the signals of various channels. So, substances absorbing light in the far red (or blue) only affect the red (or blue) signal of the web camera, whereas a green, yellow or orange absorbing substance gathers distinctive contributions from all the channels, thus enriching the fingerprint²⁸.

Usually, most of the applications are well accomplished with a 50 colour sequence that gradually changes from blue to red colour (Figure 1.14). However, for selected indicators, a shorter and more targeted sequence can be defined, that allows for a continuous imaging of spectral features of the substance. Factors that drove the choice of the colour sequence in this work of thesis will be discussed in the experimental section of next chapters.

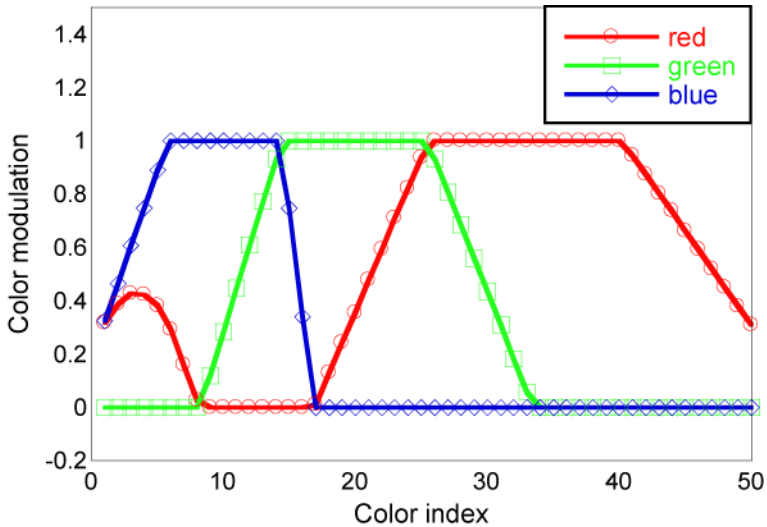


Figure 1.14. Modulation of the colour weight r , g , b in equation (1.6) that produces a colour sequence resembling the human perception of the visible spectrum.

1.6.3 CSPT Model

For a mathematical description of CSPT features, let us consider the whole elements that are involved in a CSPT measure. The spectral

radiances of the screen are given by equation 1.6, and they are specified by (r_i, g_i, b_i) triplets. The next step is constituted of the sample itself that is characterized by its transmittance spectrum. After the samples, the light passes through the three colour filters of the web camera which can be estimated as colour matching functions and that can be described by a matrix F . Finally, the detector of the web camera has also a particular spectral response $D(\lambda)$. For each colour displayed on the screen, a composed spectral radiance is emitted and specifically modulated by the transmittance of the tested substance $T(\lambda)$ ²⁹. The emerging light passes through the camera filters [$F_R(\lambda)$, $F_G(\lambda)$ and $F_B(\lambda)$] exciting the detector, which has a defined spectral response $D(\lambda)$. For non-emitting substances characterized by a certain spectral transmittance, for any colour c_i displayed on the screen, the measured intensities in the web camera are given by:

$$\begin{aligned} I r_i &= \int_{\lambda} c_i(\lambda) \cdot F_r(\lambda) \cdot T(\lambda) \cdot D(\lambda) d\lambda \\ I g_i &= \int_{\lambda} c_i(\lambda) \cdot F_g(\lambda) \cdot T(\lambda) \cdot D(\lambda) d\lambda \\ I b_i &= \int_{\lambda} c_i(\lambda) \cdot F_b(\lambda) \cdot T(\lambda) \cdot D(\lambda) d\lambda \end{aligned} \quad (1.7)$$

Introducing the analytical expression for c_i and rearranging, we obtain:

$$\begin{bmatrix} I r_i \\ I g_i \\ I b_i \end{bmatrix} = \begin{bmatrix} r_R & r_G & r_B \\ g_R & g_G & g_B \\ b_R & b_G & b_B \end{bmatrix} \begin{bmatrix} r_i \\ g_i \\ b_i \end{bmatrix} = \mathbf{S} \begin{bmatrix} r_i \\ g_i \\ b_i \end{bmatrix} \quad (1.8)$$

where the terms of the substance matrix S are functions of $T(\lambda)$. Every illuminating colour produces three intensity equations and if three different light sources are provided, up to nine spectral windows $T(\lambda)$ of any particular substance can be formed. Figure 1.15 shows the nine different primary radiance-filter combinations provided by a LCD screen and a regular web camera based on a CCD³⁰.

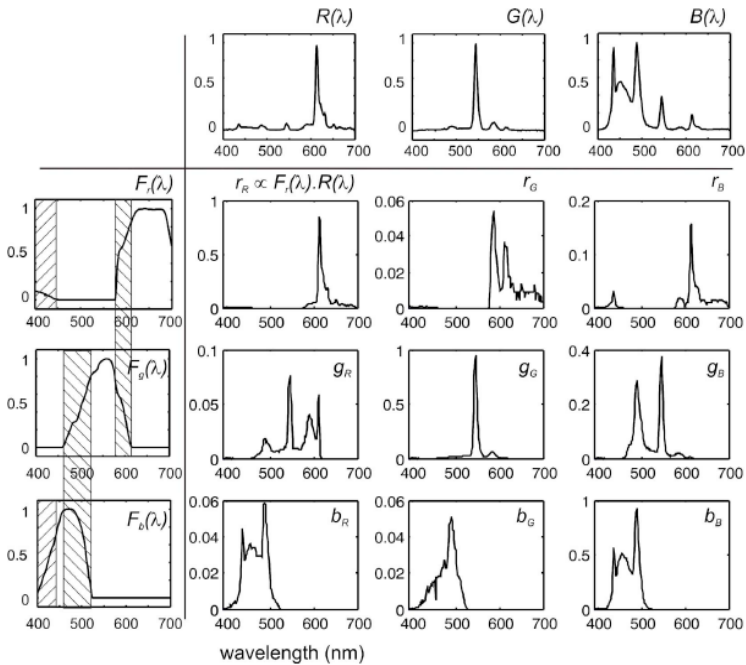


Figure 1.15. Spectral windows formed by the combination of a LCD screen spectral radiances and the three camera filters for a sample transmittance $T(\lambda)=1$.

Sometimes it could be useful to consider a quantity that is related to the spectral absorbance, but that, differently from it, it is a function of the illuminating colour and not of the wavelength. It can be called CSPT absorbance and it is defined as follows:

$$A(\text{color}) = -\log \frac{R_{\text{sample}}(\text{color}) + G_{\text{sample}}(\text{color}) + B_{\text{sample}}(\text{color})}{R_{\text{bg}}(\text{color}) + G_{\text{bg}}(\text{color}) + B_{\text{bg}}(\text{color})} \quad (1.9)$$

where R_{sample} , G_{sample} , and B_{sample} are the intensities recorded in the sample regions, while R_{bg} , G_{bg} , and B_{bg} are the intensities in the background regions that correspond to the reference light source.

1.6.4 Applications

The aim of CSPT is not to unflinchingly reproduce spectroscopic measurements but to detect and classify substances. Retaining spectral features without complete spectral reconstruction is thus sufficient for this purpose. In this optic, CSPT has been demonstrated to probe spectral features in a number of applications and it was used either to evaluate reflectance³¹ and transmittance. By using semitransparent spots of porphyrins or related compounds it was shown that is possible to detect detailed and partially disentangled absorption and emission responses resulting from molecules such as amines, alcohols, CO, and NO_x³². A gas sensor array based on the CSPT transduction platform was used to investigate the global composition of the fish headspace monitoring the evolution from fresh to spoiled products³³. CSPT can also be used as a sort of spectrophotometer to characterize substances

according to their light absorption and emission properties. Also in the case of complex samples, such as red wine, the quantification of integral parameters (colour indicators) and specific compounds (anthocyanins and polyphenols) was possible with the aid of multivariate analysis of spectral fingerprints³⁴. A hyphenated optical-potentiometric platform based on porphyrinoids dispersed in PVC membranes was conceived, using the dyes both as electrodes and as chromophore spots. The sensor array allowed for the evaluation and discrimination among olive and seeds oil samples³⁵. In fluorescent-based applications, CSPT has been used to detect the attachment of complementary DNA strands to a complex of single DNA strands and a polythiophene derivative. The complex is a highly sequence specific indicator, based on non-covalent coupling of DNA to a water-soluble, zwitterionic, electroactive and photoactive polymer able to produce a combined absorption-emission signal readable by this platform³⁶.

An interesting feature of CSPT platform is that it allows for the simultaneous evaluation of both absorption and emission properties. Emission component can be disentangled from transmitted light, making it an easy system for fingerprinting of fluorescent substances³⁷. CSPT displays the different sample contributions of emission and absorption depending on their relative spectral positioning with respect to the camera filters, capturing the sample spectral signature when excited by a controlled colour sequence³⁸.

It is worth to mention that beyond analyze the spectroscopical features of various kinds of samples, other computer screen aided techniques were developed. Back in 2002, a computer screen aided scanning light pulse technique (SLPT) was developed by Lundström and Filippini themselves, to generate chemical images that are spatially resolved responses of field effect devices to chemical stimuli³⁹. The same simple setup, made of a computer screen and a digital camera, was recently demonstrated for angle and spectra resolved surface plasmon resonance (SPR) images of gold and silver thin films coated by protein deposits⁴⁰. Eventually, ellipsometric measurement of thickness with resolution in the nanometre range is also possible⁴¹.

1.6.5 Optical Interrogation of Sensing Layer

An interesting feature of the CSPT measurement platform is that, being based on an image sensor, it decomposes the sensing area in a quantity of individual sensors, i.e. single pixels, whose number is ultimately limited by the camera resolution. It allows to address and access simultaneously up to several thousand virtually independent sensors. Several sensing layers in the form of spots or uniform distribution can be simultaneously analyzed, providing an easy way to prepare arrays of chemical indicators. The signals from sensing layers may be analyzed individually or an average value of pixels belonging to a region of interest may be calculated. Figure 1.16 schematically illustrates this process and identifies single pixel in the image whose

colour variation during a CSPT measurement may be regarded as a sensor signal.

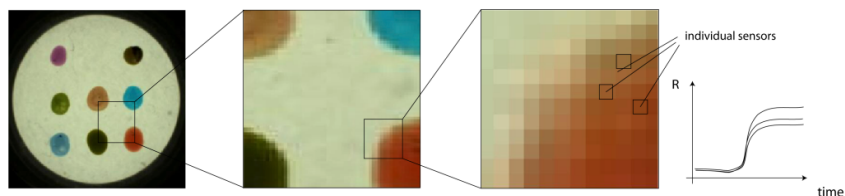


Figure 1.16. Schematic representation of the decomposition of sensing layer into elementary units consisting of camera pixels. During a measure each pixel can be regarded as an independent sensor.

During a CSPT measure, the sample is illuminated through the computer screen with the desired colour sequence and the images are simultaneously acquired by the computer camera. Each frame concerning an illuminating colour can be decomposed into three components relative to three detector bands. This yields a set of three matrices that contains the intensity of individual pixels for each camera filter. Each matrix can be imaged in a colour coded map, as shown in Figure 1.17 for a sequence of primary illuminating colours, namely red [255 0 0], green [0 255 0], and blue [0 0 255]. In this way it is possible to appreciate the colour intensity in the background that represents the light source and the different absorption of light operated by different spots of chromophores in each wavelength band. Usually primary colours are able to capture enough information to probe sensing layers, since every other colour results from a linear combination of these

primaries. Still referring to the case of RGB sequence illustrated in Figure 1.17, it is worth to mention that three of these signals are considered not meaningful (i.e. colour-camera filter: red-green, red-blue, and green-blue), because they correspond to a detection at shorter wavelength than the illuminating source. These signals originate from the partial superposition of camera filters, and even if they can contain partial information about absorption, they are usually not considered in the analysis because the signal to noise ratio is poor. The camera channel corresponding to the illuminating colour (i.e. colour-camera filter: red-red, green-green, and blue-blue) provides information about absorption, whereas the camera channels corresponding to longer wavelengths than the illumination (i.e. colour-camera filter: green-red, blue-green, and blue-red) contain information about emission. Hence, from a RGB colour sequence six meaningful bi-dimensional matrices are extrapolated, but if the sensing layer in use is not luminescent, three of these contributions originate by the superposition of camera filter as well, and they are not to be considered, obtaining only three useful matrices.

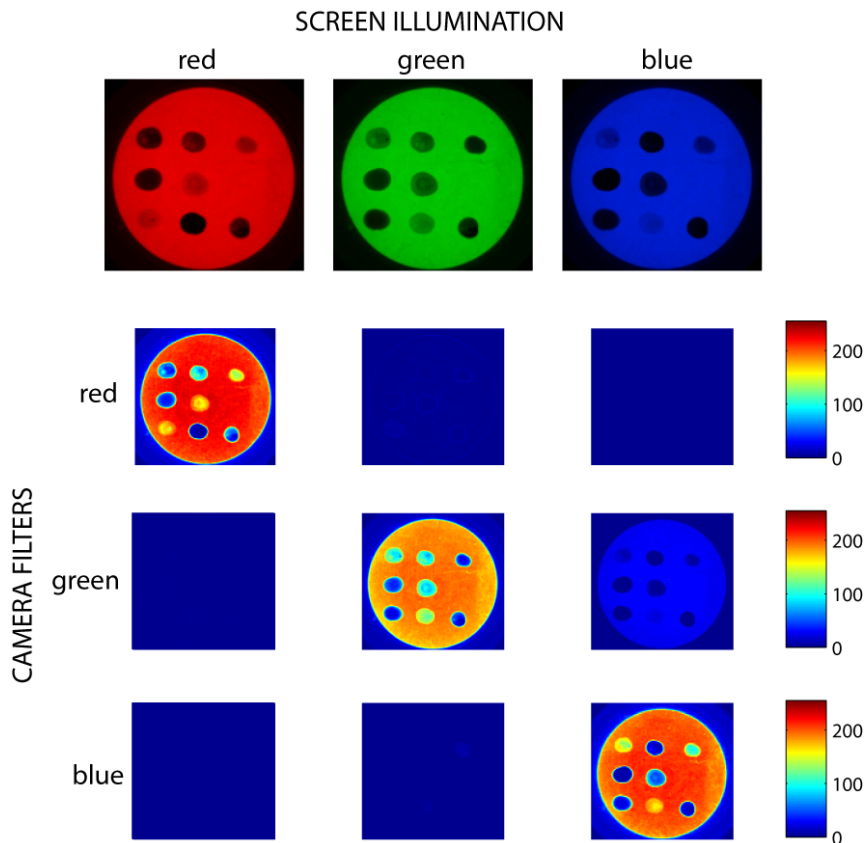


Figure 1.17. Example of an array of sensing layers imaged with a sequence of red, green and blue colours with the CSPT. Each image can be decomposed into three components corresponding to the three spectral regions of camera filters.

To reduce the enormous amount of data that arise from temporal CSPT measurements and to avoid dealing with three-dimensional matrices, a selection of regions of interest that identify the useful area of the image is operated. The average intensity of all pixels contained in

the ROIs is evaluated and usually referenced to zero with respect to the first frame. In this way, each measure provides a number of signals corresponding to the number of ROIs for each camera channel, and it is possible to graphically represent and compare multiple measures.

References

- ¹ McDonagh, C. S. Burke, B. D. MacCraith, Optical Chemical Sensors, *Chem. Rev.* 108 (2008) 400-422
- ² R.G. Mortimer, Physical Chemistry, 3rd edition, Academic Press, 2008
- ³ P. K. Kaiser, R. M. Boynton, Human Color Vision, 2nd ed., Optical Society of America, Washington, D.C., 1996.
- ⁴ G. Sharma (Ed.), Digital Color Imaging Handbook, CRC Press, Boca Raton Florida, 2003
- ⁵ S.M. Sze, Physics of semiconductor devices, 2nd edition, John Wiley & Sons, 1981
- ⁶ B. Bayer, Color imaging array, U.S. Patent No.: 3.971.065, Eastman Kodak Company, 1976
- ⁷ R. Ramanath, W. E. Snyder, G. Bilbro, Demosaicking methods for Bayer color arrays, *Journal of Electronic Imaging* 11(3) (2002) 306-315
- ⁸ R. B. Merrill, Color separation in an active pixel cell imaging array using a triple-well structure, US Patent No 5.965.875, 1999
- ⁹ O. S. Wolfbeis, Fiber-Optic Chemical Sensors and Biosensors, *Anal. Chem.* 80 (2008) 4269–4283
- ¹⁰ C. N. LaFratta, D. R. Walt, Very High Density Sensing Arrays, *Chem. Rev.* 108 (2008) 614-637
- ¹¹ N. A. Rakow, K. S. Suslick. A colorimetric sensor array for odour visualization. *Nature* 406 (2000) 710-713
- ¹² R. A. Potyrailo, W. G. Morris, A. M. Leach, T. M. Sivavec, M. B. Wisnudel, S. Boyette, Analog Signal Acquisition from Computer Optical Disk Drives for Quantitative Chemical Sensing, *Anal. Chem.* 78 (2006) 5893-5899

- ¹³ H. Segawa E. Ohnishi, Y. Arai, K. Yoshida, Sensitivity of fiber-optic carbon dioxide sensors utilizing indicator dye, *Sens. Actuators B* 94 (2003) 276-281
- ¹⁴ O. S. Wolfbeis, Materials for fluorescence-based optical chemical sensors, *J. Mater. Chem.* 15 (2005) 2657–2669
- ¹⁵ O. S. Wolfbeis, Sensor Paints, *Adv. Mater.* 20 (2008) 3759–3763
- ¹⁶ T. A. Dickinson, J. White, J. Kauer, D. R. Walt, A chemical detecting system based on a cross-reactive chemical sensor array, *Nature* 382 (1996) 697-700
- ¹⁷ D.R. Walt, Imaging optical sensor arrays, *Current Opinion in Chemical Biology* 6 (2002) 689–695
- ¹⁸ K. Persaud, G. Dodds, Analysis of discrimination mechanisms in mammalian olfactory system using a model nose, *Nature* 299 (1982) 352-355
- ¹⁹ F. Rock, N. Barsan, U. Weimar, Electronic Nose: current status and future trends, *Chem Rev.* 108 (2008) 705-725
- ²⁰ T.A. Dickinson, K.L. Michael, J.S. Kauer, D.R. Walt, Convergent, self-encoded bead sensor arrays in the design of an artificial nose, *Anal. Chem.* 71 (1999) 2192–2198
- ²¹ C. Di Natale, D. Salimbeni, R. Paolesse, A. Macagnano, A. D’Amico. Porphyrins based opto-electronic nose for the volatile compounds detection, *Sens. Actuators B* 65 (2000) 220-226
- ²² C. Di Natale, A.G. Mignani, R. Paolesse, A. Macagnano, A. Mencaglia, A. D’Amico, Array of opto-chemical sensors based on fiber optic spectroscopy, *IEEE Sens. J.* 5 (2005) 1165-1174
- ²³ N. Rakow, K. Suslick, A colorimeter sensor array for odour visualization, *Nature* 406 (2000) 710-712
- ²⁴ D Filippini, S. P. S. Svensson, I. Lundström, Computer screen as a programmable light source for visible absorption characterization of (bio)chemical assays, *Chem. Commun.* 2 (2003) 240–241

- ²⁵ D. Filippini, A. Alimelli, C. Di Natale, R. Paolesse, A. D'Amico, I. Lundström, Chemical Sensing with Familiar Devices, *Angew. Chemie* 118 (2006) 3884–3887
- ²⁶ E.F. Schubert, J. Kyu Kim, Solid-state light sources getting smart, *Science* 308 (2005) 1274–1278
- ²⁷ R. Jackson, L. Mac Donald, K. Freeman, Computer generated color, Wiley, 1994
- ²⁸ D. Filippini, I. Lundström, Preferential color substances and optimized illuminations for computer screen photo-assisted classification, *Anal. Chim. Acta* 557 (2006) 393–398
- ²⁹ D. Filippini, I. Lundström, Spectroscopic information retained in screen photo-assisted techniques, *Anal. Chim. Acta* 521 (2004) 237–244
- ³⁰ D. Filippini, I. Lundström, Spectral characteristics of computer screen photoassisted classification, *J. Appl. Physics* 99 (2006) 114518
- ³¹ D. Filippini, G. Comina, I. Lundström, Computer screen photo-assisted reflectance fingerprinting, *Sens. Actuators B* 107 (2005) 580–586
- ³² D. Filippini, C. Di Natale, R. Paolesse, A. D'Amico, I. Lundström, Computer screen photo-assisted techniques for global monitoring of environmental and sanitary parameters, *Sens. Actuators B* 121 (2007) 93–102
- ³³ A. Alimelli, G. Pennazza, M. Santonico, R. Paolesse, D. Filippini, A. D'Amico, I. Lundström, C. Di Natale, Fish freshness detection by a computer screen photoassisted based gas sensor array, *Anal. Chim. Acta* 582 (2007) 320–328
- ³⁴ A. Alimelli, D. Filippini, R. Paolesse, S. Moretti, G. Ciolfi, A. D'Amico, I. Lundström, C. Di Natale, Direct quantitative evaluation of complex substances using computer screen photo-assisted technology: The case of red wine, *Anal. Chim. Acta* 597 (2007) 103–112
- ³⁵ L. Tortora, M. Stefanelli, M. Mastroianni, L. Lvova, C. Di Natale, A. D'Amico, D. Filippini, I. Lundström, R. Paolesse, The hyphenated

CSPT-potentiometric analytical system: An application for vegetable oil quality control, *Sens. Actuators B* 142 (2009) 457–463

³⁶ D. Filippini, P. Åsberg, P. Nilsson, O. Inganäs, I. Lundström, Computer screen photo-assisted detection of complementary DNA strands using a luminescent zwitterionic polythiophene derivative, *Sens. Actuators B* 113 (2006) 410–418

³⁷ J.W.P. Bakker, D. Filippini, I. Lundström, Enhancing classification capabilities of computer screen photo-assisted fluorescence fingerprinting, *Sens. Actuators B* 110 (2005) 190–194

³⁸ D. Filippini, J. Bakker, I. Lundström, Fingerprinting of fluorescent substances for diagnostic purposes using computer screen illumination, *Sens. Actuators B* 106 (2005) 302–310

³⁹ D. Filippini, I. Lundström, Chemical imaging by a computer screen aided scanning light pulse technique, *Appl. Phys. Letters* 81(20) (2002) 3891–3893

⁴⁰ D. Filippini, F. Winquist, I. Lundström, Computer screen photo-excited surface plasmon resonance imaging, *Anal. Chim. Acta* 625 (2008) 207–214

⁴¹ J.W.P. Bakker, H. Arwin, I. Lundström, D. Filippini, Computer screen photoassist photoassisted off-null ellipsometry, *Appl. Opt.* 45 (2006) 7795–7799

Chapter 2: Sensing Materials - Porphyrins and Polymers

2.1 Introduction

Porphyrins are a molecular family widely used in chemical sensors. The synthetic chemistry of porphyrins is well developed and it is possible to choose among a wide substituent library to prepare the macrocycle of choice for the particular application¹. All these features would not be sufficient to justify an interest in porphyrins, if we do not consider the richness of properties these macrocycles are endowed with. Photophysical and coordination features are just an example of the potentialities of such a macrocycle.

Nature offers a magnificent example of porphyrin usefulness, whereas with this basic molecular framework Nature is able to activate and transport molecular oxygen in animals and convert sunlight in plant photosynthetic systems. Recently, porphyrin based-sensors have experienced a significant growth. The next sections will deal with a

brief description of their basic features and some example of application.

On the other hand, polymers have gained tremendous recognition in the field of artificial sensors in the goal of mimicking natural sense organs. Polymer materials are now being incorporated into a variety of chemical sensors, since they are applicable to all known types of sensors thanks to their extremely broad range of capabilities². The ubiquitous presence of polymers in current technology is mainly based on the enormous possibilities to tailor their chemical and physical characteristics. These properties involve also the chemical reactivity of polymers that can be prepared to cope with different kinds of chemical interactions and then to bind, with controlled properties, a large number of chemical compounds³. Polymer basic properties and their application in optical chemical sensors will be described in the last paragraph.

2.2 General aspects of porphyrins

Porphyrins are tetrapyrrolic macrocycles with a basic skeleton consisting of four pyrrole units connected through four methine bridges with sp^2 hybridized meso-carbons at the α position of the pyrrole rings⁴. The molecular skeleton has formula $C_{20}H_{14}N_4$. The porphyrin macrocycle is an aromatic system containing 22 π electrons of which 18 are involved in any one delocalization pathway. A metallo-porphyrin is

formed when a transition metal atom replaces the two hydrogen atoms at the central core. Almost all metals present in the periodic table have been coordinated to the porphyrins. Furthermore a wide range of different substituent groups can be introduced at peripheral positions (Figure 2.1). Their peculiar chemical and physical properties made them very attractive candidates for a large number of applications. Their basic structure may undergo several modifications that deeply influence the coordination and the related sensing properties of these compounds.

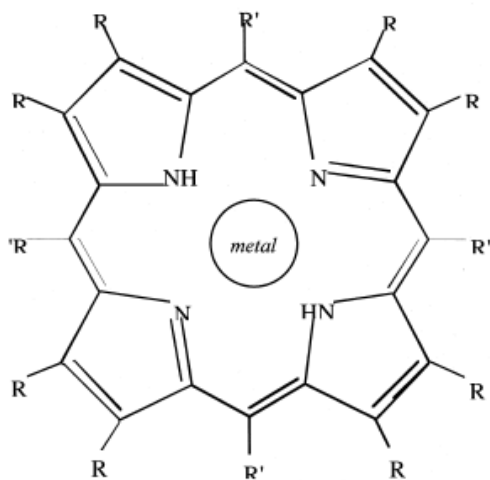


Figure 2.1. Basic structure of a porphyrin. A central coordinated metal and several possible substituent groups are evidenced.

Porphyrins occur widely in nature and play very important roles in various biological processes. For instance heme, the iron(II) protoporphyrin-IX complex, is the prosthetic group in hemoglobin and

myoglobin responsible for oxygen transport in red blood cells, and oxygen storage in living tissues. In plants, porphyrins allow electron transfer (cytochrome c, cytochrome oxidase) and energy conversion (chlorophyll)⁵.

2.2.1 Spectral features

All porphyrins are intensely coloured, with their colour due to absorption processes that involve the excitation of electrons from π to π^* porphyrin ring orbitals. Visible absorption spectrum of porphyrins displays an intense absorption to the second excited state ($S_0 \rightarrow S_2$) usually between 380 and 420 nm, referred to as the Soret band or B-band. This band is characteristic of a highly conjugated macrocycle, and it disappears when the aromatic delocalization pathway is disrupted. Up to four less intense absorption bands appear with lower intensity at longer wavelengths between 500 and 700 nm and are attributable to a weaker transition to the first excited state ($S_0 \rightarrow S_1$). These are called Q bands or, sometimes, satellites bands, and they are marked with roman numbers I-IV with reverse order of magnitude. A typical visible absorption spectrum of a porphyrin is shown in Figure 2.2, with the Soret band and Q bands indicated.

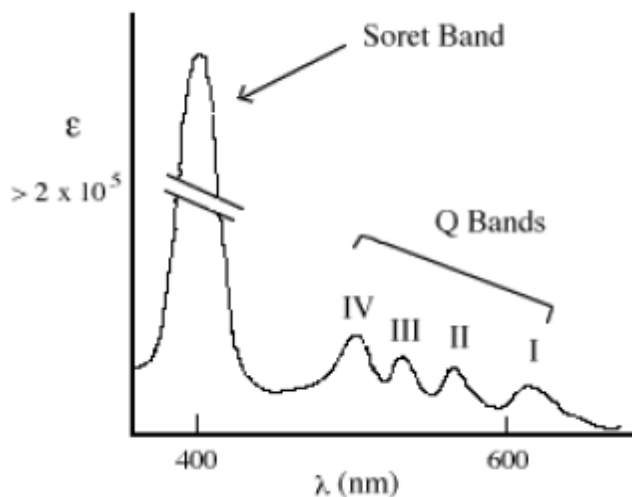


Figure 2.2. Typical absorbance spectrum of a porphyrin

While variations of the peripheral substituents on the porphyrin ring often cause minor changes to the intensity and wavelength of the absorption features, protonation of two of the inner nitrogen atoms or the insertion of metal atoms into the macrocycle usually provoke strong changes to the visible absorption spectrum. Typical spectra of metal complexes of porphyrins will be described in the next section.

2.2.2 Metallo-porphyrin spectra

There are three main classes of metallo-porphyrin electronic spectra. These are called *normal*, *hypso*, and *hyper*, with the *hyper* spectra being further divided into *P*-type and *d*-type.

Normal spectra are observed for metallo-porphyrins with metals from groups 1 to 5 with oxidation states of I to V, respectively, and for other d^0 or d^{10} metals. Characteristically, *normal* spectra have one intense absorbance Soret band between 320 and 450 nm and one or two absorbances (Q bands) between 450 and 700 nm. Normal spectra are alike metal-free porphyrins spectra, although free-base have four peaks between 450 and 700 nm. This larger number of bands is attributed to lowering of the D_{4h} symmetry of the metallo-porphyrin to D_{2h} by protonation of two pyrrole nitrogens in the metal-free porphyrin.

Normal spectra are well explained by Gouterman's four orbital model. In this model, the four orbitals are porphyrin π and π^* orbitals; the two highest occupied molecular orbitals (HOMOs) of a_{1u} and a_{2u} symmetry, and the two lowest unoccupied molecular orbitals (LUMOs) of e_g symmetry. The two major absorbances arise from coupling of the two transitions between the HOMOs and LUMOs ($\pi - \pi^*$) (Figure 2.3).

The Q bands are the result of the transition dipoles nearly cancelling each other out, therefore resulting in a weaker absorbance. The higher energy Soret transition results from a linear combination of the two transitions with reinforcing transition dipoles and is therefore very intense.

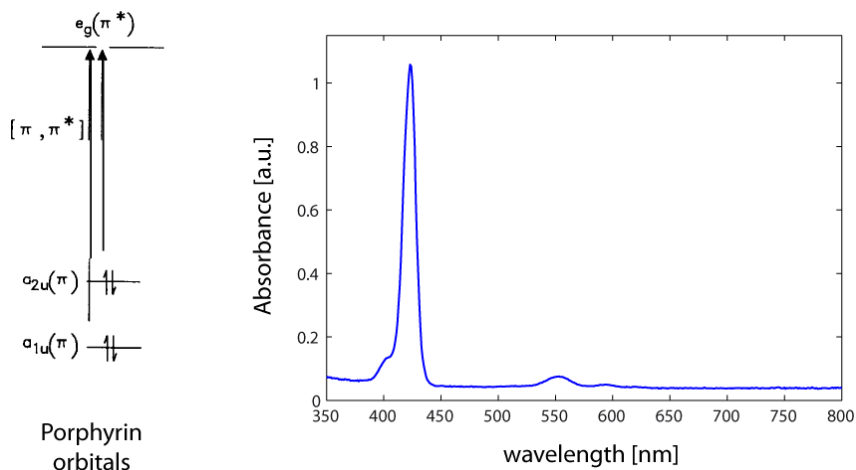


Figure 2.3. a) Molecular orbital diagram for the four-orbital model of normal metallo-porphyrin absorbance. **b)** Example of a normal spectrum (ZnTPP)

The *hypso* spectrum looks very much like the *normal* ones except that the Q-band is blue shifted to wavelengths of less than 570 nm. The *hypso* spectrum is found with transition metal complexes with electron counts of d^6 to d^9 and therefore filled $e_g(d_\pi)$ orbitals. Common examples are Pd^{II} , Pt^{II} , Rh^{II} and Ni^{II} . The blue shift in the Q-band is explained by mixing of the e_g LUMO of the porphyrin ring with the filled $e_g(d_\pi)$ metal orbitals. This interaction pushes the porphyrin LUMO to higher energy as shown in Figure 2.4, thus increasing the π - π^* energy gap of the porphyrin.

The overlap is greater for *4d* and *5d* metals, which show the largest blue-shifts. Within a given row of transition metals, the energy of the d_π electrons decreases with increasing electron count. Thus, as the number

of d-electrons increase, the energy gap between the porphyrin LUMO and the metal increases, and the orbital mixing decreases.

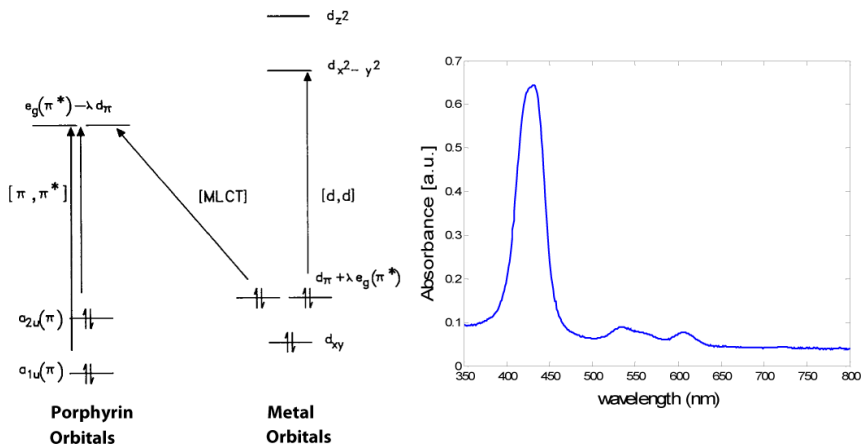


Figure 2.4. a) Molecular orbital diagram for *hypso* metallo-porphyrin. b) Example of a *hypso* spectrum from a NiTPP

The *hyper* spectra show additional absorbance compared to the other varieties. These additional bands are generally due to the blue shift of the Q-band and are of moderate intensity. Main group elements in low oxidation state (e.g., Sn^{II} , Pb^{II} , P^{III} , As^{III}) give p-type *hyper* spectra. In this case the extra bands are due to metal to ligand charge transfer. As shown in Figure 2.5, the charge transfer originates in the metal p_z orbital and is $a_{2u}(np_z)(\text{metal}) \rightarrow e_g(\pi^*)(\text{ring})$.

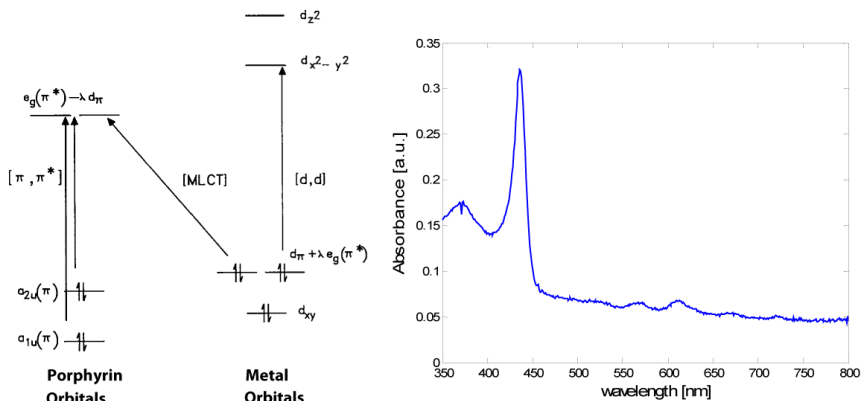


Figure 2.5. a) Molecular orbital diagram for p-type *hyper* metallo-porphyrin. **b)** Example of a p-type hyper spectrum from SnTPP.

D-type *hyper* spectrum is found with d^1 through d^6 metals that have vacancies in the $e_g(d_\pi)$ orbitals. These vacancies make a porphyrin ligand-to metal charge transfer transition possible, as shown in Figure 2.6.

Because the charge transfer results in a change of metal oxidation state, relatively low metal redox potentials are also desirable to make the final product more stable. There is also considerable mixing of the metal d_π orbitals with the LUMO of the porphyrin, since they are of the same symmetry e_g . The extensive mixing then accounts for the complex spectra often observed in d-type *hyper* porphyrins. This mixing occurs more readily when the porphyrin LUMO is close in energy to the metal orbitals. Calculations have shown that Cr^{III} , Mn^{III} , and Fe^{III} metal orbitals are uniquely situated in energy for extensive mixing to occur⁶.

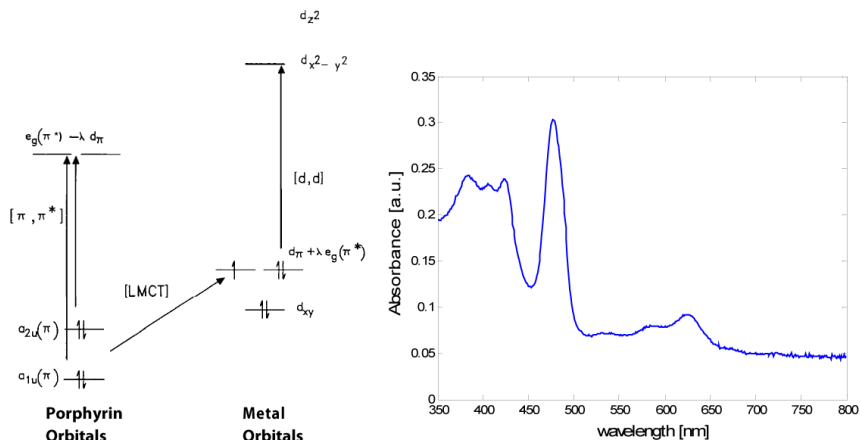


Figure 2.6. a) Molecular orbital diagram for d-type *hyper* metalloporphyrins. b) Example of a d-type *hyper* spectrum from MnTPP

It is worth to be noticed that the spectroscopic features exhibited by porphyrins in solid films are different from those of porphyrins in solution. These differences are often ascribed to electronic interactions between the chromophores in the film environment. The spectra of the monolayer samples are usually characterized by a doubled B (Soret) band with one absorption component shifted toward the red region and the other toward the blue region (≈ 400 nm) compared to the solution's B-state absorption (≈ 420 nm). In contrast, the Q-band spectral features are quite similar for the film and solution sample. In solid state porphyrins another important feature that must be take into account is the presence of π - π^* interactions between macrocycles: the consequence of these aggregation phenomena in the absorption spectra is broadening, splitting and shifts of the bands with respect to the solution spectra⁷.

2.3 Porphyrin aggregates

Porphyrins, as other related chromophores may be arranged in different ways in an aggregate structure, because of the strong electrostatic interactions between the electronic clouds of different macrocycles. The aggregates are usually classified into three types:

- J-aggregates that are “edge-to-edge” structures;
- H-aggregates that are “face-to face” structures;
- non-specific aggregates, with features common to both J and H types.

These species are easily identified by UV-Vis spectroscopy, where the Soret band undergoes either a bathochromic (J-type) or a hypsochromic (H-type) shift in comparison with the non-assembled molecules. From luminescence spectroscopy, aggregation of porphyrins also results in an important decrease in intensity and in a red shift of the fluorescence band. The Soret band for the H-aggregate is blue shifted and weaker with respect to the Soret band of the J-type⁸.

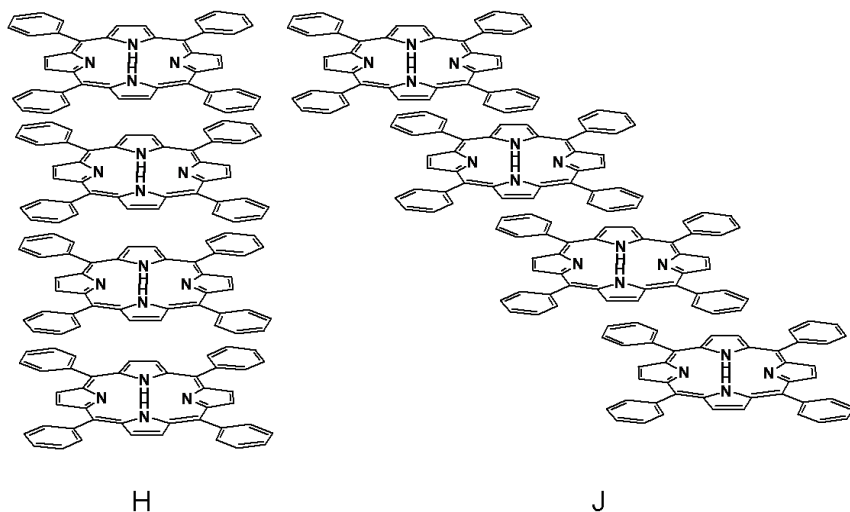


Figure 2.7. J-type and H-type porphyrin aggregate geometries.

These spectral modifications can be explained and visualized considering the interactions between the electrostatic dipole moments of the molecules. For *H-aggregates* with parallel transition dipoles, two types of alignments are possible (Figure 2.8). The *in-phase* orientation (A) determines repulsion because of the summing up of the dipole moments. The E'' level is hence displaced at higher energies. The *out-of-phase* orientation (B) corresponds to a lowering of energy providing a more favourable coupling. So the E' level lies lower than the van der Waals displaced states of the component molecules, but dipole moments cancel each other, resulting in a virtually zero dipole moment vector. Transitions from the ground state to exciton state E' are forbidden, while transitions from the ground state to exciton state E''

are allowed. The ΔE_{tran} is larger for the dimer resulting from the aggregation compared to the monomer, and this leads to a *blue-shift* of the Soret band of the aggregate compared to the one of the monomeric unit.

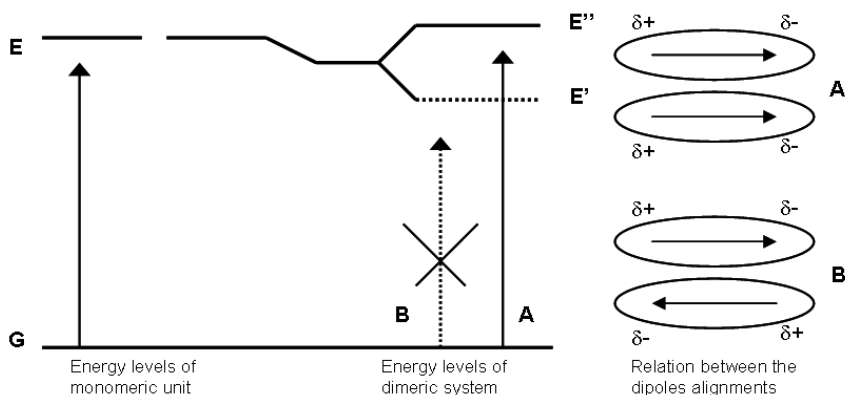


Figure 2.8. Exciton band energy diagram for dimers with parallel dipoles as in H-aggregates.

An opposite situation characterizes J-aggregates whose dipole moments of the monomers are still parallel but shifted. Again, two types of alignments are possible for the transition dipoles (Figure 2.9), an *out-of-phase* alignment (A) and an *in-phase* alignment (B). The *in-phase* arrangement leads to an electrostatic attraction that produces the excited level E', whereas the *out-of-phase* arrangement causes repulsion, producing the state E". However, the transition moments are finite for electric dipole transitions from the ground state to E', and 0 to the state E" from the ground state. Thus, being the ΔE_{tran} smaller for the dimer

resulting, the J-aggregation will result in a *red-shift* of the Soret band of the aggregate compared to the monomeric unit⁹.

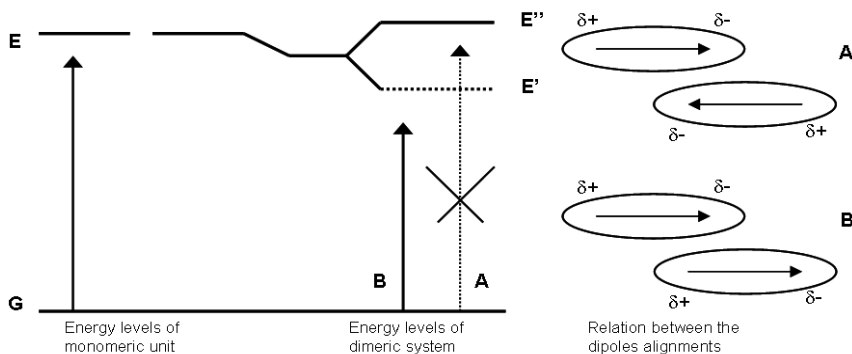


Figure 2.9. Exciton band energy diagram for dimers with dipoles as in J-aggregates.

With respect to intermediate geometries featuring by non-specific aggregates both transitions can be partially allowed so that the electronic spectrum is characterized by the presence of two bands simultaneously, the former at a blue-shifted wavelength and the latter at a red-shifted wavelength in the aggregate relative to the monomer, or a general, less specific, broadening of the starting band resulting from the aggregation.

2.4 Applications in chemical sensors

Porphyrins and metallo-porphyrins represent one of the most intriguing materials for chemical sensors, because of the richness of

their properties, their stability, and the well developed chemistry that allows for a wide modulation of their properties by synthetic modifications or by changing the coordinated metal. Usually, since target analytes are good ligands for metal ions, porphyrins represent a perfect match for the properties required for sensing. Because of this extensive richness of interactions, metallo-porphyrins do not usually behave as receptors for molecular recognition of specific target molecules, but rather as globally selective sensors, whose behaviour is very similar to that found in natural olfactory receptors. Indeed it is argued that olfactory receptors located in the epithelium contain metal ions coordination complexes¹⁰. For this reason, the role of the coordinated metal ion in a metallo-porphyrin is considered of primary importance to determine the sensitivity and selectivity when they are used to identify complex odours in artificial olfactory systems.

A metallo-porphyrin offers a large variety of interaction mechanisms that can be exploited for chemical sensing. Hydrogen bonds, polarization, and polarity interactions are expected to take place between volatile molecules and the porphyrin. The role of metal is of primary importance to determine the sensitivity and selectivity properties of the molecule by axial binding of the volatile molecule since coordination interactions take place at the metal centre in metallo-porphyrin complexes¹¹. From this point of view, since almost all metals may be combined to form metallo-porphyrin complexes, metallo-porphyrins ligand properties enjoy a large versatility. Low energy

mechanisms, such as hydrogen bonding, polarization and polar interactions, may contemporaneously be present and cooperate in the total guest molecule binding¹². Particular molecular arrangement can also be assembled in order to provide metalloporphyrins with more enhanced selectivity^{13,14}.

To exploit porphyrins as sensing materials it is fundamental to couple the sensing layer with a proper transducer capable of translate the interaction with target molecules into a readable signal, usually of electrical nature. The choice is driven by the physical parameter that changes as a consequence of the binding event. A simple and straightforward approach consists in measuring the variation of mass after the adsorption of volatiles on a porphyrin film. Quartz crystal microbalances¹⁵ (QMB) and acoustic wave¹⁶ devices were used to measure sub-ppm quantity of several classes of compounds. Field effect devices¹⁷ and array of capacitive sensors¹⁸ were functionalized with various types of porphyrins to sense volatile compounds. However our main interest lies in the modification of absorption and luminescence properties, triggered by chemical interactions that can be detected with optical set-ups. The next section overviews some of the most representative applications of porphyrin-based optical chemical sensors.

2.4.1 Application in optical chemical sensors

Optical sensors are based on the variation of an optical property, such as absorption or luminescence, of the sensing material as a

consequence of the interaction with target analytes. It has been found that porphyrins and related compounds show significant solvatochromic effects with a broad range of vapours (for example alcohols, amines, phosphines, arenes, and ketones), which induce distinguishable colorimetric effects. This makes metal-phthalocyanine and metal-porphyrins as suitable dyes and pigments because of their easy synthesis, high stability, and the presence of an intense π - π^* transition in the visible range.

One of the firstly reported application of porphyrin based optical sensor dates back to the end of Eighties and it was related to oxygen detection. These devices are based on metal complexes of various substituted porphyrins that undergo to phosphorescence quenching after the interaction with molecular oxygen. The quenching of phosphorescence is linearly dependent on the oxygen concentration, according to the Stern-Volmer relationship. The most widely used metallo-porphyrins for these applications are Platinum and Palladium derivatives, because of their high phosphorescence quantum yields and short lifetimes¹⁹. From then on a huge number of applications with different configurations have been reported²⁰. Depending on the arrangement, the intensity quenching can even be detected either by eye or, more precisely, with a CCD camera²¹.

The coordination of ligands at the axial positions can strongly influence the electronic structure and consequently the electronic spectra. In solid films, the binding with volatile organic compounds

(VOCs) can alter the π - π interactions among macrocycles, leading to additional modifications of the spectra. All these spectra changes are proven to be interesting and useful for applications of optical sensors based on absorption changes. One of the firstly reported applications of an opto-electronic nose made use of a LED in the blue region operating as a light source, coupled with photodetectors to probe the spectroscopic modification of thin film of metallo-porphyrins upon the exposure to VOCs²². This, as previously mentioned, was one of the first reported implementations of an “optical nose”. In other applications, the transduction platform was based on a spectrophotometer. In this case, it is common practice to operate a selection of a number of specific spectral regions taken in the UV–Vis spectral range corresponding to the typical absorption bands of porphyrins. Thin films of metallo-porphyrins are generally prepared by chemical or physical methods, such as vapour deposition, spin coating and Langmuir–Blodgett (LB) deposition techniques. Exposure of a ZnTPP sensing layer to the organic vapours in controlled atmosphere induces variations in the absorption peaks²³. The evidence of these variations can be obtained by the comparison of the responses calculated as the difference $I_n - I_{0n}$, where I is the integral measured in the presence of the VOC vapours and I_{0n} is the integral measured in reference atmosphere. The choice to calculate the responses in terms of the difference in the dynamic integrals is due to the consideration that each absorption peak is proportional to the number of active macromolecules in the sensing process. The sensing

mechanism involves a portion of these complexes by an increase or decrease of the peak area. Consequently, the difference in the integral gives a better evaluation of the sensing phenomenon. In this way, the optical response of the thin film versus different analytes (i.e. isopropanol, ethanol, methanol and acetone) was evaluated²⁴.

2.5 Polymers

It is well known that in order to use a sensitive material in a chemical sensor, it is necessary to couple the sensitive layer with a transducer measuring one physical property changing upon the interaction with analytes. Polymer materials find application with transducers based on a broad range of sensing principles. They are often used with mass transducers, exploiting the mass change upon adsorption of volatiles²⁵. Conducting polymer sensors can be used independently for detection and measurement of individual vapours or jointly in the form of arrays for measurement of complex odours. A particularly natural sensory scheme is found for electrically conducting polymers that display changes in conductivity in response to interaction with analytes. In this case, measurements are performed by connecting two adjacent electrodes with a polymer film and then measuring the conductivity (or resistivity) as a function of analyte^{26,27}. The changes can be correlated

quantitatively to the concentration of the vapours and can be readily reversed when the vapours are removed.

Besides the exploitation of polymers intrinsic properties, their mixture with other molecules was also proposed as a viable method to extend the kinds of physical properties that can be measured to monitor absorption processes. In some cases it is necessary to provide the polymers with some additional properties, for instance doping the polymer including optically active functional groups²⁸ or with powders of carbon black in order to make the electric conductivity measurable. The mixture of polymers with carbon black offers an interesting alternative to transform the amount of absorbed molecules into a shift of electric conductivity. In these materials, the absorption of molecules, and the consequent swelling of the polymer volume, modulates the charge transport through the network of carbon grains dispersed in the volume²⁹.

2.5.1 Sorption and diffusion in polymers

The equilibrium distribution of a vapour between the gas phase and a sorbent polymer phase is characterized by the thermodynamic partition coefficient, K . Let the concentration in the gas phase be C_v and the equilibrated concentration in the sorbent phase be C_s , the partition coefficient is the ratio defined according to:

$$K = \frac{C_s}{C_v} \quad (2.1)$$

Higher values indicate a greater degree of collection and concentration of vapours in the polymer phase, where their presence can be transduced into an analytical signal. These partition coefficients can be deduced in the frame of the linear solvation energy relationship (LSER) as a combination of terms, which express the contribution of every kind of expected interaction to the overall sorption process, according to

$$\log K = c + r \cdot R + s \cdot \pi + a \cdot \alpha + b \cdot \beta + l \cdot \log L^{16} \quad (2.2)$$

These terms describes the contribution of polarity (rR), polarizability ($s\pi$), hydrogen-bond for an acid vapour ($a\alpha$), hydrogen-bond for a basic vapour ($b\beta$) and dispersion interactions ($l \cdot \log L^{16}$). Coefficients R , π , α , β and $\log L^{16}$ describe solubility properties of the solute vapour, while r , s , a , b and l characterize the complementary properties of the polymer^{30,31}.

The permeability of a polymer to a penetrant is:

$$P = \frac{N l}{p_2 - p_1} \quad (2.3)$$

where P is the permeability coefficient, $(p_2 - p_1)$ is the pressure drop, l is the film thickness, and N is the steady-state penetrant flux through the polymer film. The permeation process can be divided into three steps: absorption, diffusion and desorption. When penetrant flux obeys Fick's

law, the permeability coefficient, P , can be expressed as the product of solubility S and diffusivity D :

$$P = S \cdot D \quad (2.4)$$

The solubility of a penetrant in a polymer at constant operating conditions (i.e., temperature, pressure, and composition) is a function of penetrant condensability and polymer–penetrant interactions. The ideal selectivity of a polymer for penetrant A relative to penetrant B is the ratio of the permeability coefficients of the two penetrants:

$$S_{A/B} = \frac{P_A}{P_B} = \frac{S_A}{S_B} \cdot \frac{D}{D_B} \quad (2.5)$$

Diffusion coefficients decrease as penetrant size increases, and diffusivity is often correlated with measures of penetrant size, such as critical volume, van der Waals volume, or kinetic diameter. Diffusivity selectivity increases as the difference in the relative size of two penetrants increases. Typically, larger penetrants are more condensable, and thus more soluble than smaller penetrants³².

2.5.2 Polymers for optical sensors

Polymer materials are frequently used as matrices for the indicator in optical sensors. The indicator needs to be immobilized because due to a hindered diffusion not all the bulk material would interact with the analytes, but only the molecule at the surface. Therefore, the indicator is dissolved in a polymer which allows free diffusion of the analyte to and

from the indicator molecule. The polymer also helps retaining the indicator in place so that no leaching occurs. This can be achieved by covalently immobilizing the dye to the matrix as well as by simply blending the dye in a proper polymer.

The polymer affects the selectivity and sensitivity of the optical sensor and their chemistry can be modified in order to orient the sensitivity to certain classes of airborne compounds. Furthermore, the polymer may show a different permeability towards diverse gases, inducing a selectivity for certain analytes. Finally, the polymer can provide optical isolation against ambient light and thus prevent bleaching and light interference.

Polymer materials have to fulfil several requirements to be suitable components of optical sensors. The indicator dye and possible additives have to dissolve in the polymer and crystallisation or migration of the indicator in the polymer must not occur. The analyte has to be soluble in the polymer and must be able to diffuse within the polymer. The polymer material has to be stable against ambient light, chemicals (acids, bases, oxidants) in order to achieve good operational lifetime and shelf-life. The polymer should not have any intrinsic colour or luminescence, and it should be optically transparent in the spectral range where measurements are being performed. Finally, it is required a good mechanical stability and a proper adhesion to the substrate.

Polymers with high glass transition temperature (T_g) are brittle and have a high density of the chains that hinders the diffusion of gases in

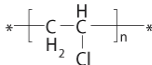
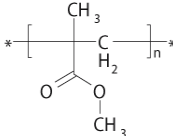
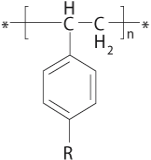
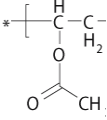
the matrix. Therefore, a plasticizer content of up to 66% is required for the preparation of sensor layers to obtain flexible and permeable films. When a plasticizer is used, the polarity and the lipophilicity of the matrix, and consequently the selectivity and the sensitivity of the layer, can be tailored by using different plasticizers with different physical properties. A significant drawback is an increased instability over time, since the plasticizer may leach out of the membrane or may evaporate on storage. On the contrary, polymers with low glass transition do not require plasticizers and are often unpolar. A brief recapitulation of polymers more frequently used in optical sensors is reported in Table 1.

The preparation of sensor layers is straightforward: the indicator dye, the polymer and the plasticizer (if needed) are dissolved in a solvent, usually tetrahydrofuran. The solutions can be spun, dip-coated or even casted on transparent support materials and fixed in flow-through cells. The same procedure can be followed for optical fibres as well as planar wave guides.

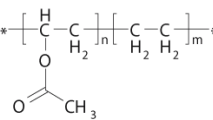
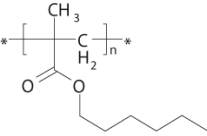
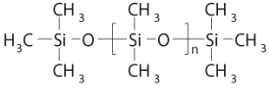

The solid support can be a glass plate mounted in a photometer, or a surface plasmon resonance (SPR) cell, an attenuated total reflection (ATR) crystal. A direct immobilisation on the light source, such as a light emitting diode (LED) is possible as well³³.

Table 1. Chemical structures and physical properties of some polymer used for optical chemical sensors.

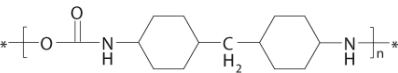
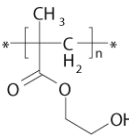
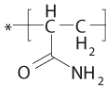
Lipophilic polymers

			
poly(vinyl chloride) (T _g ~90 °C)	poly(methyl methacrylate) (T _g ~100 °C)	polystyrene-derivatives (T _g 100-140 °C)	poly(vinyl acetate) (T _g ~30 °C)

Unpolar polymers

			
poly(ethylene vinyl acetate)	poly(hexylmethacrylate) (T _g -4 °C)	poly(dimethyl siloxane) (ε ~ 3, T _g -80 to -40 °C)	cis-polybutadiene (ε ~ 2, T _g -100°C)

Hydrophilic polymers

		
polyurethane	poly(2-hydroxyethyl methacrylate)	poly(acryl amid)

References

- ¹ S. Horn, K. Dahms, and M. O. Senge, Synthetic transformations of porphyrins—advances 2004–2007, *Journal of Porphyrins and Phthalocyanines* 12 (2008) 1053–1077.
- ² B. Adhikari, S. Majumdar, Polymers in sensor applications, *Prog. Polym. Sci.* 29 (2004) 699–766
- ³ K. Persaud, Polymers for chemical sensing, *Materials Today* 8 (2005) 38-44
- ⁴ K. M. Smith, Porphyrins and Metalloporphyrins, Ed. (Elsevier, Amsterdam, 1975)
- ⁵ K.M. Kadish, K. M. Smith, R. Guilard, Eds., The Porphyrin Handbook, vol. 1, Academic Press, San Diego, Calif, USA, 2000.
- ⁶ K. S. Suslick, R. A. Watson, The Photochemistry of Chromium, Manganese, and Iron Porphyrin Complexes, *New. J. Chem.* 16 (1992) 633-642
- ⁷ G. A. Schick, I. C. Schreiman, R. W. Wagner, J. S. Lindsey, D. F. Bocian, Spectroscopic Characterization of Porphyrin Monolayer Assemblies, *J. Am. Chem. Soc.* 111 (1989) 1344-1350
- ⁸ K.M. Kadish, K. M. Smith, R. Guilard, Eds., The Porphyrin Handbook, vol. 18, Academic Press, San Diego, Calif, USA, 2000
- ⁹ M. Kasha, H. R. Rawls, M. A. El Bayoumi, The Exciton Model In Molecular Spectroscopy, *Pure Appl. Chem.* 11 (1965) 371
- ¹⁰ J. Wang, Z. A. Luthey-Schulten, K. S. Suslick, Is the olfactory receptor a metalloprotein? *PNAS* 100(6) (2003) 3035–3039
- ¹¹ R. Paolesse, F. Mandoj, A. Marini, C. Di Natale, Porphyrin-based chemical sensors, in: H.S. Nalwa (Ed.), *Encyclopedia of Nanosciences and Nanotechnology*, American Scientific Publ., 2003.
- ¹² T. Ohshiro, T. Ito, P. Bühlmann, Y. Umezawa, Scanning Tunneling Microscopy with Chemically Modified Tips: Discrimination

of Porphyrin Centers Based on Metal Coordination and Hydrogen Bond Interactions, *Anal. Chem.* 73 (2001) 878–83

¹³ C. Di Natale, R. Paolesse, A. D'Amico, Metalloporphyrins based artificial olfactory receptors, *Sensors and Actuators B* 121 (2007) 238–246

¹⁴ A. D'Amico, C. Di Natale, R. Paolesse, A. Macagnano, A. Mantini, Metalloporphyrins as basic material for volatile sensitive sensors, *Sens. Actuators B* 65 (2000) 209–215

¹⁵ C. Di Natale, R. Paolesse, A. Macagnano, A. Mantini, P. Mari, A. D'Amico, Qualitative structure–sensitivity relationship in porphyrins based QMB chemical sensors, *Sens. Actuators B* 68 (2000) 319–323

¹⁶ M. Benetti, D. Cannatà, F. Di Pietrantonio, V. Foglietti, E. Verona, Microbalance chemical sensor based on thin-film bulk acoustic wave resonators, *Appl. Phys. Lett.* 87 (2005) 173504–173506

¹⁷ M. Andersson, M. Holmberg, I. Lundstrom, A. Lloyd-Spetz, P. Martensson, R. Paolesse, C. Falconi, E. Proietti, C. Di Natale, A. D'Amico, Development of a ChemFET sensor with molecular films of porphyrins as sensitive layer, *Sens. Actuators B* 77 (2001) 567–571

¹⁸ E. Martinelli, M. Stabile, A. Catini, R. Paolesse, A. D'Amico, C. Di Natale, An array of capacitive sensors based on a commercial fingerprint detectors, *Sens. Actuators B* 130 (2008) 264–268

¹⁹ J. R. Bacon, J.N. Demas, Determination of Oxygen Concentrations by Luminescence Quenching of a Polymer- Immobilized Transition-Metal Complex, *Anal. Chem.* 59 (1987) 2780–2785

²⁰ S. M. Borisov, I. Klimant, Luminescent nanobeads for optical sensing and imaging of dissolved oxygen, *Microchim. Acta* 164 (2009) 7–15

²¹ X. Wang, X. Chen, Z. Xie, X. Wang, Reversible Optical Sensor Strip for Oxygen, *Angew. Chem.* 47 (2008) 7450–7453

²² C. Di Natale, D. Salimbeni, R. Paolesse, A. Macagnano, A. D'Amico, Porphyrins-based opto-electronic nose for volatile compounds detection, *Sens. Actuators B* 65 (2000) 220–226

²³ J. Spadavecchia, R. Rella, P. Siciliano, M. G. Manera, A. Alimelli, R. Paolesse, C. Di Natale, A. D'Amico, Optochemical vapour detection using spin coated thin film of ZnTPP, *Sens. Actuators B* 115 (2006) 12–16

²⁴ J. Spadavecchia, G. Ciccarella, P. Siciliano, S. Capone, R. Rella, Spin-coated thin films of metal porphyrin – phthalocyanine blend for an optochemical sensor of alcohol vapours, *Sens. Actuators B* 100 (2004) 88–93

²⁵ J. Grate, Acoustic wave microsensor arrays for vapor sensing, *Chem. Rev.* 100 (2000) 2627–48

²⁶ D. T. McQuade, A. E. Pullen, T. M. Swager, Conjugated Polymer-Based Chemical Sensors, *Chem. Rev.* 100 (2000) 2537–2574

²⁷ J. Janata, M. Josowicz, Conducting polymers in electronic chemical sensors, *Nature Materials* 2 (2003) 19–24

²⁸ L. Basabe-Desmonts, D. N. Reinhoudt, M. Crego-Calama, Design of fluorescent materials for chemical sensing, *Chem. Soc. Rev.* 36 (2007) 993–1017

²⁹ M. Koscho, R. Grubbs, N. Lewis, Properties of vapor detector arrays formed through plasticization of carbon black-organic polymer composites, *Anal. Chem.* 74 (2002) 1307–15

³⁰ M. H. Abraham, G. S. Whiting, R. M. Doherty, W. J. Shuely, P. Sakellariou, An analysis of polymer-probe interactions in some hydrocarbon polymers using a new solvation equation, *Polymer* 33 (1992) 2162–2167

³¹ M. Abraham, Scales of Solute Hydrogen-bonding: Their Construction and Application to Physicochemical and Biochemical Processes, *Chem. Soc. Rev.* 22 (1993) 73–83

³² K. Ghosal, B. D. Freeman, Gas separation using polymer membranes: an overview, *Polym. Adv. Technol.* 5 (1994) 673–697

³³ F. Baldini, A.N. Chester, J. Homola, S. Martellucci, *Optical Chemical Sensors*, Springer Eds. (2006)

Chapter 3: Chemical Sensitivity of Porphyrin Nano-Aggregates

3.1 Introduction

Functional self-assembled materials with well-defined shapes and dimensions are of great interest especially in chemical sensor applications¹. Since the report of the preparation of carbon nanotubes², we have witnessed the preparation of a wide range of different nanostructured inorganic materials. The inherently small size and unusual optical, magnetic, catalytic, and mechanical properties of nanoparticles not present in bulk materials permit the development of novel devices and applications previously unavailable. One of the earliest applications of nanotechnology that has been realized is the development of improved chemical and biological sensors³.

In the case of organic compounds, the preparation of nanostructures is far less developed. Molecules can interact without forming strong covalent bonds through much weaker and kinetically labile non-covalent interactions, such as electrostatic and van der Waals forces or

hydrophobic effects, π - π stacking interactions, metal coordination, and hydrogen bonding. Cooperative, weak interactions can be used for the spontaneous formation of large aggregates that have well-defined structures (i.e. helicates, grids, molecular containers, capsules, cyclic arrays, and the like), in which the individual components are not connected through covalent but through non-covalent bonds. The concepts developed in supramolecular chemistry are increasingly used in fields like material science, surface science, sensor technology, and nanotechnology to create particular structures and to introduce specific chemical functions in these supramolecules⁴. The methodologies used to create devices on the nanometer scale can be roughly categorized as those using lithography (*top-down*) or self-assembly (*bottom-up*) approaches, with each having advantages and limitations. Certainly, self-assembly is claimed to be an important route toward the manufacture of the next generation of nanoscaled molecular materials⁵.

Among the manifold of structures that can be obtained, the tubular shape has received great attention in the last few years. Tubular architectures, beyond increase the surface to volume ratio, are expected to add the cavity effect that is also particularly important for sensing. Recently tubular arrangements have been demonstrated for assemblies of organic molecules, as in the case of self-assembled polyaniline nanotubes⁶.

Among the huge number of molecular systems suitable for such an approach, porphyrins, thanks to their brilliant chemical properties

described in Chapter 2, represent one of the most promising building blocks for synthetic receptors. A great effort has been devoted to the preparation and characterization of porphyrin nanostructured materials, but quite surprisingly only limited examples of practical applications have been reported. An intriguing architecture obtained by the aggregation of oppositely charged porphyrin units has been recently reported by Shelnutz and co-workers⁷. In this section we want to verify the hypothesis that these nanostructured assemblies may provide additional sensing properties not found in the individual basic constituents. The interactions of porphyrin nanotubes with guest molecules, both in solution and in the solid state, have been investigated following the changes in their UV–Vis spectra. After a short survey of porphyrin-based nanostructure, the results of characterization and the building up a sensing platform will be given.

3.2 Porphyrin-Based Nanostructures

The self-assembly of molecules, by noncovalent bonds is an approach that offers several advantages, including a relatively easy synthesis and purification of monomers, a generation of the most thermodynamically stable structure, and the possibility of self-repair. However, it also requires a precise arrangement of the monomers into a desired structure, which needs a careful design of the building blocks

during the synthesis process, for example, by equipping them with specific molecular-recognition sites.

Porphyrins are one of the most popular building blocks for nanostructured arrangement⁸. They are a versatile, rich and flexible family of compounds, whose properties can be finely tuned by simple modifications of their basic molecular structure. The coordinated metal, the peripheral substituents, the conformations of the macrocyclic skeleton influence the coordination and the related sensing properties of these compounds. All these properties can be transferred in nanostructured materials based on porphyrin derivatives, for the development of new functional materials applicable in different fields⁹. Porphyrin chemical versatility offers also the possibility to drive self-assembled molecular aggregations to ordered geometrical structures that will be briefly described in the following sections.

3.2.1 Porphyrin Nanoparticles

A first class of porphyrin aggregates is represented by porphyrin nanoparticles prepared by mixing solvent technique. It produces a colloidal suspension of porphyrin aggregates having dimension in the order of hundreds of nanometers. Nanoscaled particles composed of porphyrins are expected to have chemical activities significantly different from those of the free porphyrins or of those immobilized onto or into supports. Porphyrin nanoparticles are promising components of advanced materials because of the rich photochemistry, stability, and

proven catalytic activity. The nanoparticles of catalytic porphyrins provide enhanced stability and catalytic rate because of the structure of the aggregate and the greater surface area¹⁰.

The size of the particles strongly depend on the porphyrin structure and on the preparative protocols, where it is usually used a surfactant to stabilize the suspension, avoiding the collapse of the nanoparticles in larger aggregates. The interest in these systems depends on the potential applications in different fields, such as catalysts, or drug delivery. The aim is to develop architectures that can offer a higher stability than monomer in solution, preserving or even increasing the activity of the starting molecular units. The easiness of preparation and the possibility to modulate the size and properties of such nanoparticles represent the promising characteristics of these structures.

3.2.2 Porphyrin Nanosheets

There have been only a few attempts to make well-defined 2-D organic nanostructures. Wang et al. reported the preparation of self-assembly porphyrin nanosheets using a reprecipitation method, simply injecting an ethanol solution of a SnPyTriPP complex into deionized water. The procedure leads to the formation of square porphyrin nanosheets with high aspect ratios. They also readily adsorb onto various metal substrates such as Si, Au, and glassy carbon. The photometallization of nanosheets previously adsorbed on the substrate suggests that the fabrication of nanoelectrodes with ohmic contacts

between the metal and the nanosheets may be possible. The morphology, the photocatalytic properties, and the large surface areas make them suitable for a wide range of applications in electronics, photonics, and catalytic systems. However the formation of 2D aggregates is strongly dependent on the preparation method, because changing the solution temperature led to completely different aggregates¹¹.

3.2.3 Porphyrin Nanorods and Nanorings

5,10,15,20-tetrakis(4-sulfonatophenyl)porphyrin (TPPS₄) self-assembles in acidic aqueous solution into rods that can span over μm lengths¹². TPPS₄ is of particular interest to our aim because it is one of the precursors of porphyrin nanotubes used in this work. Investigations reveal that TPPS₄ aggregates in three-dimensional micrometers rod and wheel like molecular structures. Scanning force microscopy imaging revealed a thickness of two or four molecular layers and a width of tenths of molecule diameter. It has been hypothesized that such structures could be used in a molecular-scale electronic device¹³. In this regard, the TPPS₄ rods show an intriguing photoconductivity with a rapid turn on/off rate. The nanorods are insulating in the dark, but they exhibit a rapid onset of the photocurrent when illuminated with a 488nm light. The nanorods photoconductivity slowly increases upon continuous light exposure and decline by using short duration light pulses and a constant applied voltage. This intriguing behaviour could allow for the

fabrication of novel photoelectronic devices based on self-assembled porphyrins¹⁴.

Nanorods are also obtained from the aggregation of 5,10,15,20-tetrakis(4-carboxyphenyl)porphyrin in acidic aqueous solutions. In this case the structural motif of the aggregate strongly depends on the acid exploited for the aggregation. Nanorods were obtained in HNO₃ solutions, while HCl induced the formation of nanorings¹⁵. Porphyrin nanorings have been also obtained by evaporation of the solvent through a surface dewetting process, with two distinct mechanisms which describe ring formation: “coffee-stain mechanism” and the “pinhole mechanism”. The fabrication yields micrometer-sized porphyrin rings with pronounced polarized optical properties and it constitutes a further step towards the construction of functional nanoscale architectures in the field of catalysis and molecular electronics.

3.2.4 Porphyrin Nanowires and Nanofibers

Butadiyne-linked porphyrin wires, with length exceeding 600 nm, were synthesized by a self-assembly oxidative coupling reaction. The reaction takes place on surfaces of highly oriented pyrolytic graphite and other substrates and it happens because of the strong interaction between the porphyrin wires and the substrate. Long π -conjugated molecular wires are interesting because they can be used as organic conducting materials and nonlinear optical materials¹⁶.

Porphyrin nanofiber bundles can be obtained by the phase-transfer-ionic self-assembly of water-soluble porphyrins with water-insoluble porphyrins. The nanostructures result approximately 70–140 nm wide and 1–2 μm long. The Soret band in the nanofiber bundles is red-shifted compared to the monomeric porphyrins, which might indicate the formation of J-aggregates without strong electronic coupling. Furthermore, porphyrin nanofiber bundles are highly fluorescent, emitting an intense red light when excited with blue light. Thanks to these properties, the nanofiber bundles operate as photocatalysts. An interesting feature is that a range of metalloporphyrins can be incorporated into the nanofiber bundles, which may allow tuning of their physicochemical properties¹⁷.

3.2.5 Porphyrin Nanotubes

Porphyrin nanotubes were also obtained by self-assembly of a Mo(V) complex of the dodecaphenylporphyrin, a saddle distorted metallo-porphyrin. Herein the aggregation process is driven by the π - π interactions of the macrocycle and the molecular structure is reinforced by an internal frame based on metallic oxocluster. The formation unique shape can depend on the assembly of building block with a curved surface of the distorted porphyrin¹⁸ (Figure 3.1).

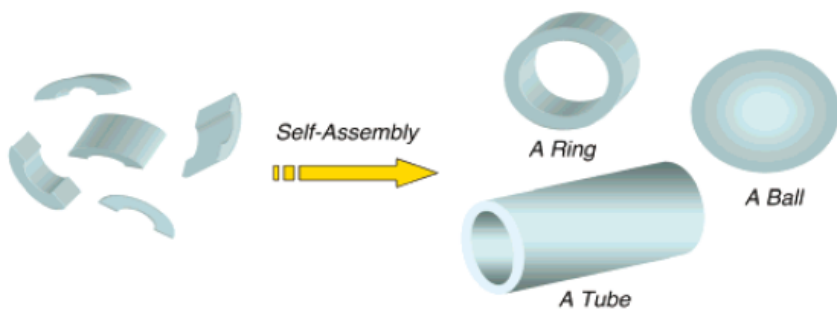


Figure 3.1. Formation of shapes based on self-assembly of building blocks with a curved surface.

Two different solutions for the functionalization with porphyrin molecules of a scaffold with tubular shape have been proposed. In a first case, a metallo-porphyrin was stabilized on a peptide nanotube surfaces with two types of hydrogen bonds¹⁹. The preparation of sapphyrin nanotubes has been reported, and in this case a template of single wall nanotube (SWNT) is needed. The noncovalent functionalization of carbon nanotube materials allow for the development of nanometric constructs with possible application for light harvesting²⁰.

3.3 Self-Assembled Porphyrin Nanotubes

As previously mentioned, Wang et. al. reported a method for the spontaneous formation through ionic self-assembly of porphyrin nanotubes made of two oppositely charged porphyrin units. The ionic self-assembly of two porphyrins bearing opposite ionic charges leads to

the formation of J-aggregates, whose non-planar shape induces the creation of nanotubular structures, reaching free floating aggregates that have lengths of tens of nanometres. Transmission electron microscope (TEM) investigations revealed that the tubes can be micrometers in length and have diameters typically in the range of 50-70 nm with approximately 20-nm thick walls. They have a hollow tubular structure with open ends. The formation of the nanotubes critically depends on the pH because the charge balance of the ionic tectons depends on their protonation state. Tubes are obtained when the Sn(IV) complex is replaced with other potentially six-coordinate metal ions (e.g., Fe^{3+} , Co^{3+} , TiO^{2+} , VO^{2+}). Nanotubes are stable for months when stored in the dark, but irradiation of a suspension with intense incandescent light results in a softening of the tube walls and a collapse of the tube structure. This response to light is reversible, as the tubes reform (self-heal) when left again in the dark.

The nanotubes containing a tin porphyrin are photocatalytic and can reduce metal ions from aqueous solution. The metal is selectively deposited onto the tube surfaces, producing novel composite metal nanostructures. The photocatalytic reduction reaction is mediated by Sn(IV) porphyrins. The metal is deposited within the hollow interior of the nanotubes as a continuous polycrystalline gold nanowire that is of the same diameter as the tube core. At one end, the nanotube is terminated with a gold ball of larger diameter than the tube. These

composites are themselves photocatalytically active and have potential applications as nanodevices²¹.

A photocatalytic application of self-assembled porphyrin nanotubes was recently patented by Shelnutz's group. It claims a method for generating hydrogen gas by decomposition of water using light. Porphyrin nanotubes act as light-harvesting structures to generate free electrons that reduce water molecules of positively charged hydrogen to neutral hydrogen²².

Since chemical sensors could represent one of the most promising application fields for these porphyrin nanostructures, we have been interested in the exploitation of the porphyrin nanotubes as sensing materials. Porphyrin nanotubes are particularly appealing for sensing purposes, because they can potentially show a dramatic increase in sensitivity or selectivity performances relative to the individual subunits. For example, the presence of the inner cavity can give rise to selective endohedral inclusion of different guests, or the interaction with analytes can alter the supramolecular arrangement of the molecular nanostructure. Both interaction pathways lead to dramatic changes of the porphyrin J-aggregate optical properties, which can consequently be used in sensing mechanisms. Hence, even if different transduction methods may be conceived to exploit porphyrin nanotubes sensing properties, the optical transduction seems to be the mechanism of choice for such a nanostructure.

The experiments described in the next section aimed at investigating the sensing properties of porphyrin nanotubes in solution and as thin layers for solid-state gas sensors, in order to develop a sensor platform based on the detection of optical changes. Both UV-Vis spectroscopy and the CSPT optical platform were used to deduce the interactions between nanotubes and guest molecules. The interaction mechanism of porphyrin nanotubes with analytes in aqueous solutions has been firstly investigated; subsequently, the development of solid state chemical sensors through their deposition as thin films has been attempted. We first studied the modification of absorption spectra induced by the addition of different salts to solutions of both precursor porphyrins and formed nanotubes. We noted that porphyrin nanotubes could offer additional features for ions detection, which cannot be possible in the case of isolated porphyrin moieties. With these encouraging results, we have then studied the variations induced by the addition of organic compounds dissolved in solution. This behaviour prompted us to explore the possibility to utilize the chemical sensitivity of porphyrin nanotubes to detect compounds in gaseous phase.

3.4 Experimental

Porphyrin nanotubes were prepared following the procedure described by Shelnutt and co-workers. An acidic aqueous solution (HCl

0.02 mol/l) of 5,10,15,20-tetrakis-(4-sulfonatophenyl)porphyrin [H_2TSPP] with a concentration of 10.5×10^{-5} mol/l was mixed an aqueous solution of the tin complex of 5,10,15,20-tetrakis-(4-pyridyl)-porphyrin [$SnTPyPCL_2$] with a concentration of 3.5×10^{-5} mol/l. Equal volumes of the two solutions were blended, obtaining a final solution with pH 2. The pH of the solution is crucial for the outcome of the procedure because it provides the appropriate level of protonation of the subunits. Solutions were then stored in the dark at room temperature for three days, until a greenish precipitate was formed. Molecular structures of porphyrinoid precursors are shown in Figure 3.2.

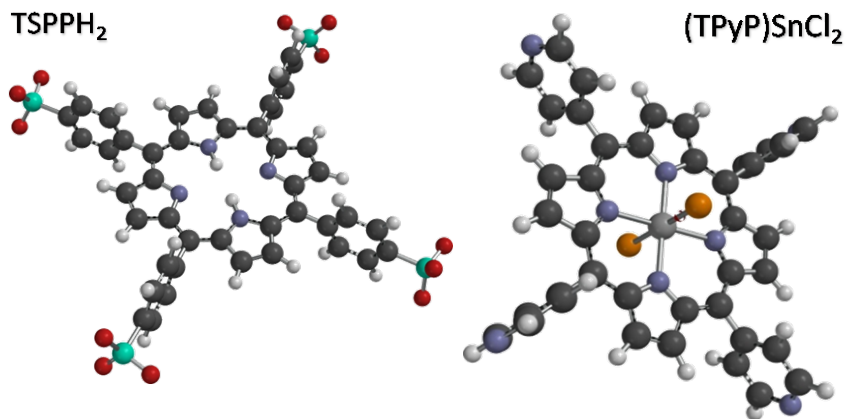


Figure 3.2. Molecular structure of 5,10,15,20-tetrakis-(4-sulfonatophenyl)porphyrin [$TPPSH_2$] and 5,10,15,20-tetrakis-(4-pyridyl)-porphyrin [$(TPyP)SnCl_2$].

For atomic force microscopy (AFM) measurements, 2 μ l of solution containing the porphyrin nanotubes were deposited onto a glass surface previously cleaned with an alkaline solution. AFM measurements were

performed in air (at room temperature), with the microscope working in the weak repulsive regime of non-contact mode.

For optical measurements, in order to reduce the optical density, the suspension was dispersed in a polymeric matrix. The polymeric membrane was prepared by dissolving 33 mg of poly(dimethylsiloxane)bis(12-hydroxystearate) terminated (PDMS) (Sigma Aldrich) in 1 ml of THF. A volume of 10 μ l of the nanotube suspension was then added to the polymer solution and, after vigorous mixing, the solution was deposited onto a 25 mm diameter Thermanox plastic coverslip (from Nunc™). The solvent was evaporated under a gentle stream of N₂ to allow for the formation of an even polymeric film. Polymeric layer of nanotubes were used for both UV-Vis spectroscopy and CSPT measurements.

For CSPT acquisitions, a transparent measurement cell was placed in the optical path between a computer screen and a digital camera. During a measurement, the camera captures the image of the sensing layers under an illuminating a rainbow sequence of 50 colours provided by the screen. From this video stream two regions of interests (ROI) for each sensing layer are selected. One ROI is centred on the layer spot and the other one on a close background. RGB values of the pixel enclosed by a ROI are averaged, and a fingerprint for each sensitive layer of each substance is then calculated, subtracting the RGB sequence of the two ROIs (Figure 3.3). The background subtraction is necessary to take into account non-uniformity of the digital images.

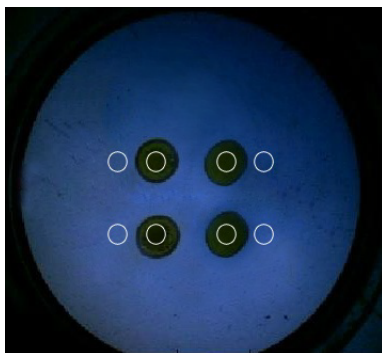


Figure 3.3. Nanotubes sensing layers, as imaged with the CSPT set-up. The regions of interest considered for the analysis are marked with white circles.

Modification of absorbance spectra after the injection of liquid analytes were studied with a Cary Varian 50 spectrophotometer. The liquid solution was prepared in standard disposable cuvettes where different salts were dissolved in the acidic aqueous solution of porphyrin precursors and of nanotubes, namely, $\text{Pb}(\text{NO}_3)_2$, $\text{Cu}(\text{NO}_3)_2$, CdCl_2 , MnCl_2 and SnCl_2 with concentrations of 10^{-4} mol/l and 10^{-2} mol/l. Also organic volatile compounds were dissolved in the sensing solutions: triethylamine, toluene and ethanol.

Gas sensor responses were measured in presence of the following test compounds: NO_x , TEA, ethanol, toluene, and acetic acid. Except for nitrogen oxides, the other compounds are in liquid phase at standard pressure and temperature. Saturated vapours were diluted in pure nitrogen and injected in the measurement cell with a three channel gas delivery system. Dilution factors were controlled with a set of mass flow

controllers (MKS). Saturated vapour concentrations were calculated by Antoine's law; Antoine parameters are provided by the database of National Institute of Standards and Technology (NIST)²³.

For each measurement the nanotubes layers were exposed to the test gas for 15 minutes, where after the test chamber was flushed with a pure nitrogen flow to blow off vapour residuals for 30 minutes.

3.5 Results

3.5.1 Optical properties

UV–visible spectroscopy provides a typical signature of porphyrin nanotube formation. In Figure 3.4 the corresponding UV–Vis spectra are shown for aqueous solutions of the two constituents and for the self-assembled nanotubes. Spectra are consistent with those indicated by Shelnut. The porphyrins in the nanotubes are stacked in a manner that gives absorption bands at 496 and 714 nm, red-shifted from the corresponding bands of the monomeric porphyrins. These bands suggest the formation of J-aggregates similar to those of H₄TPPS₄, but since the bands of the nanotubes are broader, the coherent coupling of the transition dipoles spans fewer molecules⁷.

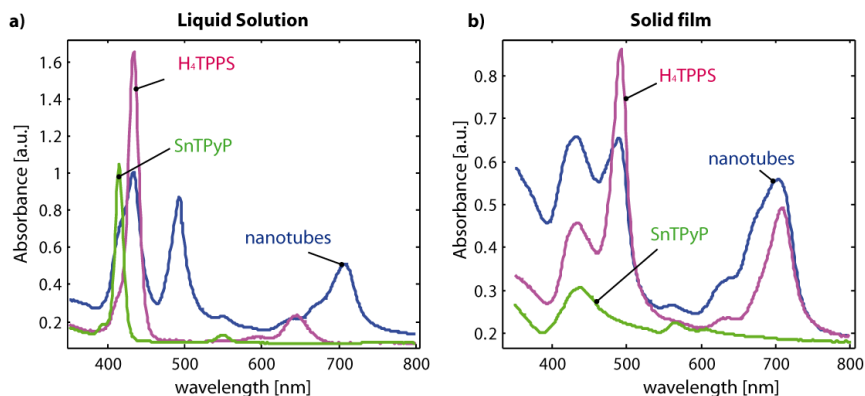


Figure 3.4. Absorbance spectra of the precursor units are compared with the optical spectrum of porphyrin nano-aggregates in liquid solution **(a)** and in the form of solid thin films **(b)**.

3.5.2 Chemical Sensitivity in Liquid Solution

Looking at the potential exploitation of such a nanostructure as sensing material, we first investigated the active role of the porphyrin molecular arrangement in their sensing properties, to understand if the porphyrin nanotubes can offer additional features with respect to those of the single isolated components. To verify this initial conjecture, we studied the modification of absorption spectra induced by the addition of different salts to solutions of precursor porphyrins and nanotubes. In these conditions, indeed, we can safely exclude the influence of analyte coordination interactions with the porphyrin subunits. The porphyrin-free base is protonated in acidic solution (formation of H_4TPPS^{2-}), avoiding the coordination of metal cations, while in the case of anions we used chloride or nitrate salts in order to reduce the influence of axial

ligation equilibria for SnTPyPCL₂. On the other hand, even a small variation in porphyrin J-aggregation, induced by the interaction with analytes, can be amplified by the modification of optical signatures. In all cases absorbance spectra in the visible region of the two precursors show negligible changes, but it is noteworthy that large modifications occur in the case of nanotube solutions.

Figure 3.5 shows the spectra obtained in 10^{-4} and 10^{-2} mol/l of Pb(NO₃)₂ solutions containing two precursors and the assembled structure. Negligible changes are detectable for the single precursors, but an enhanced optical response is found in aggregates solutions. Similar results have been observed after the addition of the same concentration of other salts, as displayed in Figure 3.6.

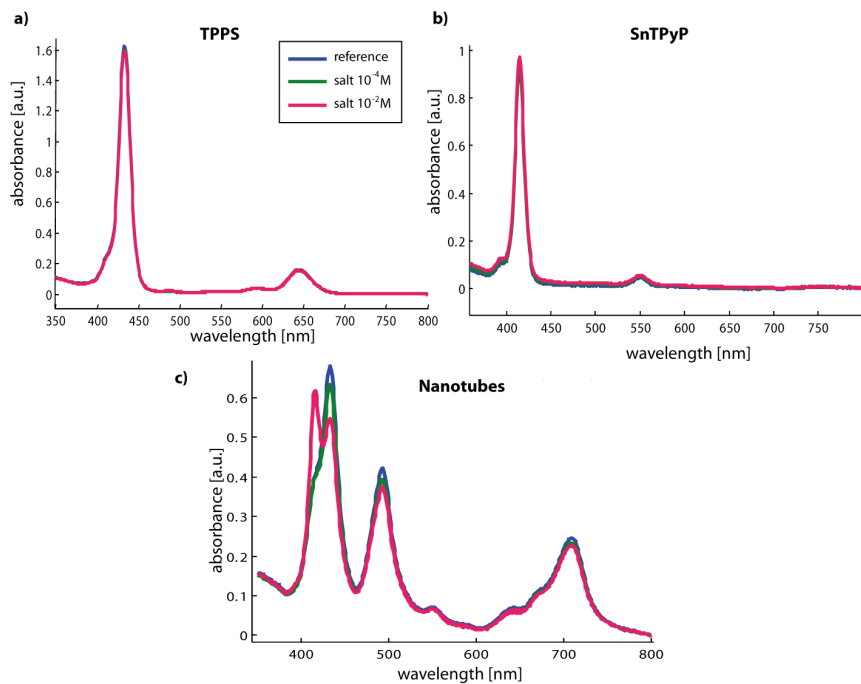


Figure 3.5. Absorbance spectra of H₄TPPS (a) SnTPyP (b) and porphyrin nanotubes (c) before and after the addition of 10⁻² and 10⁻⁴ mol/l of Pb(NO₃)₂.

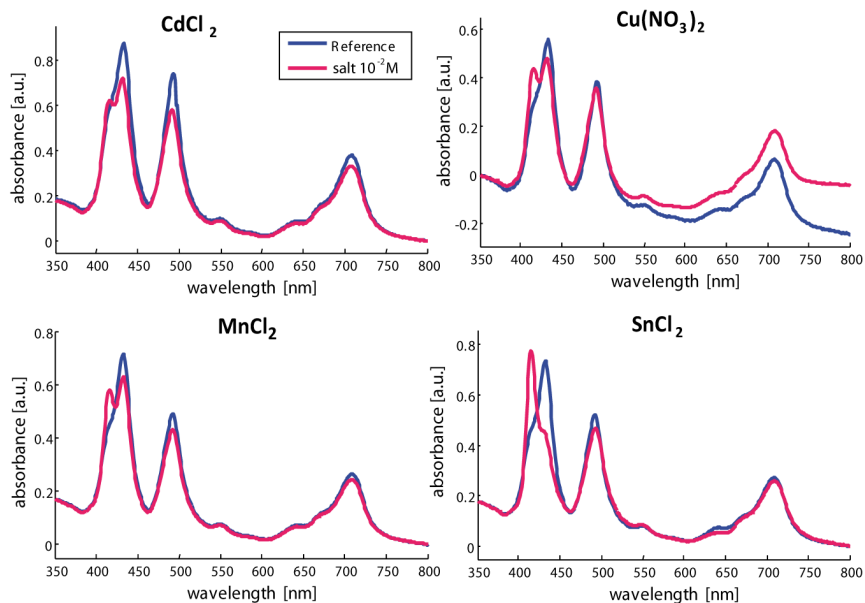


Figure 3.6. Each salt produces a typical variation of the nanotube spectrum, while negligible changes are shown in the precursor units for all the salts (not shown).

This effect may be largely attributed to the sensitivity of the forces holding together the nanotube to the ionic strength of the solution, by the shielding effect of the ionic charges, which induces a partial disassembling of the tubular aggregates. The decrease of interaction between porphyrins is indicated by the fact that the nanotube spectral features tend to disappear, concomitantly evolving into the features of the individual precursors. Nonetheless, beside a non-specific reaction to different metal ions, spectra also evidence a peculiar signature for each ion, showing that the nanotube shows different interactions with respect

to the individual porphyrins (Figure 3.6). This feature results in an enhanced discrimination capability of the particular metal ion.

These encouraging results drove a further study on the variations induced by the addition of organic compounds dissolved in solution, such as triethylamine (Figure 3.7). In this case, it should be noted that other interaction mechanisms, such as acid–base or even coordination for the SnTPyPCl₂ moiety, could be involved. Also in this case the porphyrin nanostructure was more sensitive than the subunits to the analyte addition. While no appreciable modifications were observed in the optical spectra of both H₄TPPS²⁻ and SnTPyPCl₂, triethylamine addition led to a partial disassembling of the nanotube structure, as evidenced by the appearance of SnTPyPCl₂ bands in the UV–Vis spectrum.

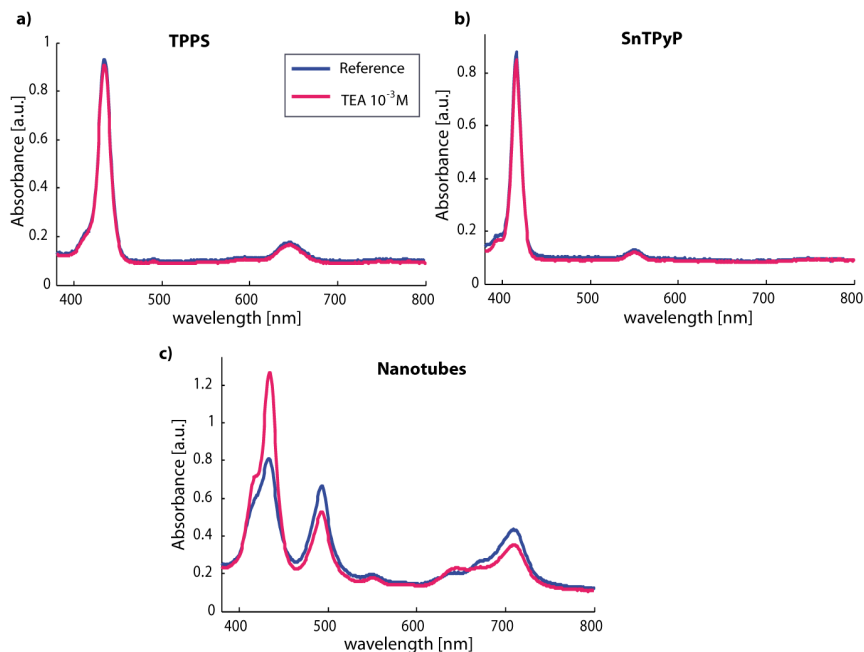


Figure 3.7. Absorbance spectra of H₄TPPS (a) SnTPyP (b) and porphyrin nanotubes (c) before and after the addition of 10⁻³ mol/l of triethylamine (TEA).

3.5.3 Chemical Sensitivity in Gaseous Phase

This behaviour prompted us to explore the possibility of utilizing the chemical sensitivity of porphyrin nanotubes to detect compounds in the gaseous phase which, to the best of our knowledge, has not yet been reported in the literature. To investigate the potential exploitation of this nanostructure in chemical sensors, we used CSPT as the optical sensing platform. For this investigation, nanotubes should be deposited as solid layers and for this reason it was necessary to optimize a deposition

method able of preserving the porphyrin aggregate properties in the thin film. Figure 3.8 shows an atomic force microscopy image of a layer of nanotubes directly deposited from aqueous solution. A tubular structure is retained in the solid state, although the slightly rigid nature of the porphyrin aggregates plausibly leads to their deformation, with the consequent flattening of the nanotubes.

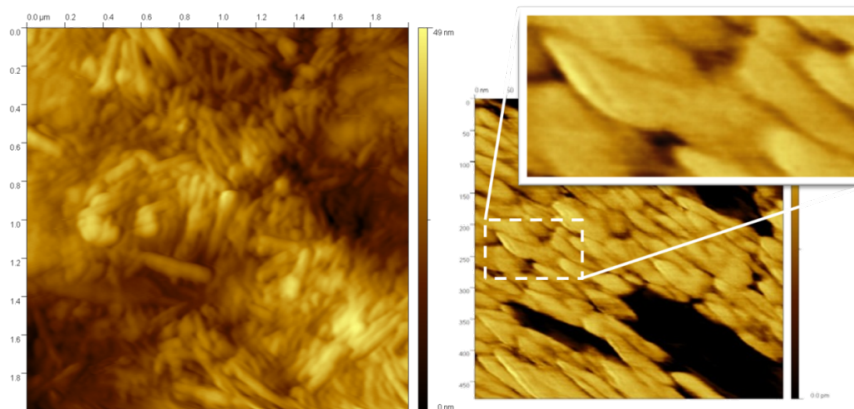


Figure 3.8. AFM topography of a 2 μm area **(a)** and phase contrast image of 500 nm area **(b)** of a solid-state nanotube layer.

However a direct deposition of nanotubes onto a glass substrate resulted in a film characterized by an excessive optical density that was not adequate for measurements with an optical platform. In order to overcome this problem, nanotubes were dispersed in a polymeric matrix transparent and compatible with the formation process of the nanostructures. PDMS was selected and the embedding of nanostructures taking place inside the polymer was confirmed by optical

spectra. Also in this case we cannot exclude a flattening of the porphyrin nanotubes into the polymeric matrix, but the retention of the aggregate features in the resulting optical spectra allowed anyway their exploitation for sensing purposes. In order to study the sensing properties of nanotubes–polymer mixtures PDMS was also requested to not interfere with the sensing process and for this purpose the chosen polymeric matrix showed a good permeability to the investigated compounds²⁴. The response of solid state films of porphyrin aggregates was first transduced with the spectrophotometer, once again comparing it with the response of single precursors. Spectral variations recorded as a consequence of the interaction with vapours of acetic acid are compared for the precursors and the nanotubes in Figure 3.9a, whereas the response of nano-aggregates towards TEA and ethanol is summarized in Figure 3.9b.

This characterization confirmed our hypothesis, hence the testing proceeded with CSPT measurements of sensing layer prepared as described in the experimental section.

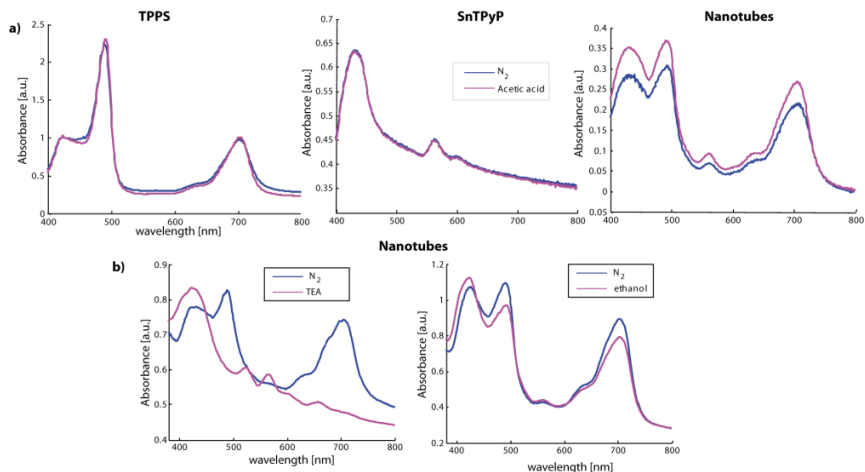


Figure 3.9. (a) Optical spectrum variations of the precursor units and of the aggregates after the injection of acetic acid vapours. (b) Response of porphyrin nanotubes towards triethylamine and ethanol vapours.

CSPT may produce a fingerprint of the optical spectra disassembling the light generated by a computer screen and transmitted by an absorbing layer in the three channels corresponding to red, green and blue filters of the image detector. Herewith, for the sake of simplicity, instead of the extended fingerprints, we consider a CSPT absorbance that follows the usual definition; the light intensity is simply evaluated summing the intensity recorded in the red, green and blue channels²⁵. The absorbance is then defined as follows:

$$A(\text{color}) = -\log \frac{R_{\text{sample}}(\text{color}) + G_{\text{sample}}(\text{color}) + B_{\text{sample}}(\text{color})}{R_{\text{back}}(\text{color}) + G_{\text{back}}(\text{color}) + B_{\text{back}}(\text{color})} \quad (3.1)$$

where *sample* and *back* identify two regions of interest corresponding to the sensitive layer and to the background. Unlike the usual spectroscopy, the quantity A is a function of colours where each colour is a computer-controlled blend of the emission spectra of red, green and blue screen pixels. The response of the sensing layer to the exposure of volatiles was measured by the differential absorbance obtained as the difference between the absorbance measured in pure nitrogen atmosphere and the sample diluted in nitrogen carrier.

Figure 3.10 shows the differential absorbance collected during the experiments. In the inset the sensing layer is shown as imaged by the digital camera and four spots of nanotubes dissolved in PDMS are visible. Each spot defines a sample region of interest for which absorbance can be calculated according to equation 3.1. Each spectrum in the graph is related to a different gas or vapour. Largest absorbance changes are found in the exposure to triethylamine, toluene, NO_x and ethanol and they correspond to green–yellow illuminating colours. As shown from optical spectra, the optical sensitivity is, in large part, likely due to the modulation of the interaction between porphyrins constituting the nanotube. Nonetheless the differences between the changes of CSPT absorbance in the presence of ethanol and triethylamine suggest that a range of interactions are likely to take place.

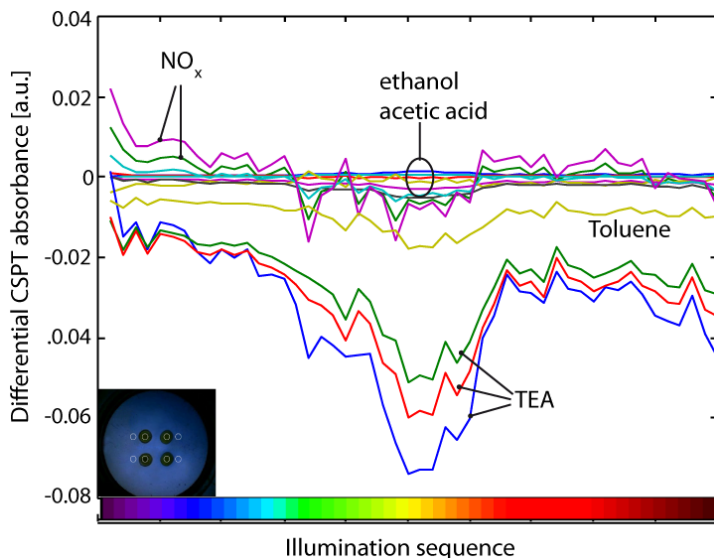


Figure 3.10. CSPT absorbance difference measured exposing the nanotube layers to the several gases. Spectral changes of triethylamine (TEA) and toluene are clearly separated from those elicited by other gases. The 50 colour sequence used during the acquisition is drawn on the x axis.

A simple method to visualize these behaviours may be obtained by calculating the principal components (PC) of the absorbance fingerprints²⁶. Principal Component Analysis (PCA) is a standard method in multivariate analysis to represent, for instance in a bidimensional plot, multivariate data such as spectra. These plots are usually interpreted assuming that the distance between data in the principal component plane is a measure of the dissimilarity among samples, and clusters of data identify similar samples. Figure 3.11 shows the plot of the first two principal components of all collected

fingerprints. A clear separation between triethylamine and other compounds is observed along the first principal component where more than 86% of the total data variance is explained. TEA detection provides the largest CSPT signal, as can be expected for the basic character of this volatile compound. The pH variation induces the partial disassembling of the nanotube, as evidenced by the appearance of $H_4TPPS_2^{-4}$ subunit bands in the UV-Vis spectrum. However, it should be noted that the residual variance displayed along the second principal component (carrying less than 5% of the total variance) can discriminate among the other test compounds. Eventually, even if in different magnitudes, all tested compounds can be satisfactorily distinguished by the CSPT fingerprint of a solid-state porphyrin nanotube layer.

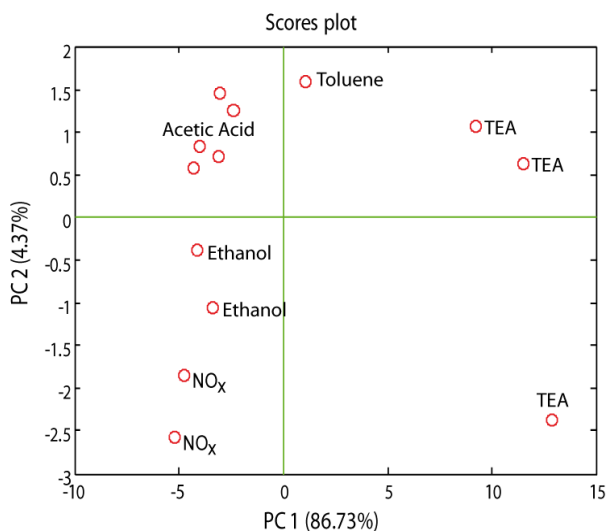


Figure 3.11. Plot of the first two principal components calculated from the differential absorbance. Labelled data points indicate the measured compounds.

3.6 Conclusions

This work demonstrated that ionic self-assembled structures of porphyrins are endowed with peculiar sensitivity properties largely exceeding that of the single precursors. Although the sensing mechanism of the porphyrin nanotubes probably does not involve the inner cavity, the analytes induce a modulation of the interaction between porphyrins, keeping the nanotubular structure in shape. In the case of porphyrin nanotubes this effect is complemented by the peculiar interaction of analytes with the porphyrin macrocycle, resulting in a recognition of individual analyte compounds. These results provide a hint for a methodology, to be properly explored, for chemical sensor design considering not only the molecular modification aimed at direct recognition but also those functionalizations that, promoting the formation of a self-assembly of ordered structures, may also prompt an increase in sensitivity.

References

- ¹ G. M. Whitesides, J.P. Mathias, C. T. Seto, Molecular self-assembly and nanochemistry: a chemical strategy for the synthesis of nanostructures, *Science* 254 (1991) 1312-1319
- ² S. Iijima, Helical microtubules of graphitic carbon, *Nature*, 354:6348 (1991) 56-58
- ³ C. R. Yonzon, D. A. Stuart, X. Zhang, A. D. McFarland, C. L. Haynes, R. P. Van Duyne, Towards advanced chemical and biological nanosensors - An overview, *Talanta* 67 (2005) 438–448
- ⁴ D. N. Reinhoudt, M. Crego-Calama, Synthesis Beyond the Molecule, *Science* 295 (2002) 2403- 2407
- ⁵ T. N. Milic, N. Chi, D. G. Yablon, G. W. Flynn, J. D. Batteas, C. M. Drain, Controlled Hierarchical Self-Assembly and Deposition of Nanoscale Photonic Materials, *Angew. Chem.* 114 (2002) 2221-2223
- ⁶ L. Zhang, H. Peng, C. F. Hsu, P. Kilmartin, J. Travas-Sejdic, Self-assembled polyaniline nanotubes grown from a polymeric acid solution, *Nanotechnology* 18 (2007) 1-6
- ⁷ Z. Wang, C. Medforth, J. Shelnutt, Self-assembly of porphyrin nanotubes. *J. Am. Chem. Soc.* 126 (2004) 15954-15955
- ⁸ J. A. A. W. Elemans, R. Van Hameren, R. J. M. Nolte, A. E. Rowan, Molecular Materials by Self-Assembly of Porphyrins, Phthalocyanines, and Perylenes, *Adv. Mater.* 18 (2006) 1251–1266
- ⁹ D. Monti, S. Nardis, M. Stefanelli, R. Paolesse, C. Di Natale, A. D'Amico, Porphyrin-based Nanostructures for Sensing Applications, *Journal of Sensors* 2009, ID 856053, 10pages.
- ¹⁰ X. Gong, T. Milic, C. Xu, J. D. Batteas, C. M. Drain, Preparation and characterization of porphyrin nanoparticles, *J. Am. Chem. Soc.* 124:48 (2002) 14290–14291

- ¹¹ Z. Wang, Z. Li, C. J. Medforth, J. A. Shelnut, Self-assembly and self-metallization of porphyrin nanosheets, *J. Am. Chem. Soc.* 129:9 (2007) 2440–2441
- ¹² A. D. Schwab, D. E. Smith, C. S. Rich, E. R. Young, W. F. Smith, J. C. de Paula, Porphyrin Nanorods, *J. Phys. Chem. B* 107 (2003) 11339-11345
- ¹³ V. Snitka, M. Rackaitis, R. Rodaite, Assemblies of TPPS₄ porphyrin investigated by TEM, SPM and UV–vis spectroscopy, *Sens. Actuators B* 109 (2005) 159–166
- ¹⁴ A. D. Schwab, D. E. Smith, B. Bond-Watts, D. E. Johnston, J. Hone, A. T. Johnson, J. C. de Paula, W. F. Smith, Photoconductivity of Self-Assembled Porphyrin Nanorods, *Nano Letters* 4 (2004) 1261-1265
- ¹⁵ S. C. Doan, S. Shanmugham, D. E. Aston, J. L. McHale, Counterion dependent dye aggregates: nanorods and nanorings of tetra(p-carboxyphenyl)porphyrin, *J. Am. Chem. Soc.* 127:16 (2005) 5885– 5892
- ¹⁶ M. Kawao, H. Ozawa, H. Tanaka, T. Ogawa, Synthesis and self-assembly of novel porphyrin molecular wires, *Thin Solid Films* 499 (2006) 23–8
- ¹⁷ Z. Wang, K. J. Ho, C. J. Medforth, J. A. Shelnut, Porphyrin nanofiber bundles from phase-transfer ionic self-assembly and their photocatalytic self-metallization, *Advanced Materials* 18:19 (2006) 2557–2560
- ¹⁸ T. Kojima, R. Harada, T. Nakanishi, K. Kaneko, S. Fukuzumi, Porphyrin Nanotubes Based on Self-Assembly of Mo(V)-Dodecaphenylporphyrin Complexes and Inclusion of Mo-Oxo Clusters: Synthesis and Characterization by X-ray Crystallography and Transmission Electron Microscopy, *Chem. Mater.* 19 (2007) 51-58
- ¹⁹ H. Matsui, R. MacCuspie, Metalloporphyrin Nanotube Fabrication Using Peptide Nanotubes as Templates, *NanoLetters* 1 (2001) 671-675

²⁰ P. J. Boul, D. G. Cho, G. M. A. Rahman, M. Marquez, Z. Ou, K. M. Kadish, D. M. Guldi, J. L. Sessler, Sapphyrin-Nanotube Assemblies, *J. Am. Chem. Soc.* 129 (2007) 5683-5687

²¹ Z. Wang, C. J. Medforth, J. A. Shelnut, Self-Metallization of Photocatalytic Porphyrin Nanotubes, *J. Am. Chem. Soc.* 126 (2004) 16720-16721

²² J.A. Shelnut, J. E. Miller, Z. Wang, C. J. Medforth, Water-splitting using photocatalytic porphyrin nanotube composite devices, US Patent 7338590 B1 (2008)

²³ webbook.nist.gov

²⁴ T. Merkel, V. Bondar, K. Nagai, B. Freeman, I.Pinnau, Gas Sorption, Diffusion, and Permeation in Poly(dimethylsiloxane), *J. Polym. Sci. B* 38 (2000) 415-35

²⁵ D. Filippini, I Lundstrom, Spectroscopic information retained in screen photo-assisted techniques, *Anal. Chim. Acta* 521 (2004) 237-44

²⁶ R. Johnson, D. Wichern, Applied multivariate statistical analysis Pearson Education (Englewood Cliffs, NJ: Prentice-Hall), 2002

Chapter 4: Polymer Matrix Effect on Sensitivity and Selectivity

4.1 Introduction

Polymer based sensors are usually non selective, even if large selectivities can be achieved with a suitable chemical functionalization aimed at orient the partition properties towards certain classes of chemicals. This behaviour suggests their use in chemical sensor arrays where selectivity is obtained as a combination of the signals of a number of broadly selective sensors. From the analogy with natural olfaction, the combinatorial selectivity of chemical sensor arrays has been increasingly adopted for the detection of a broad range of analytes¹. As a consequence, a shift of paradigm in the design of sensing material occurred² where, rather than specific material, cross-responsive sensor elements become desirable³.

Polymers impregnated with solvatochromic dyes or fluorophores are a common practice in optical sensors where they are used to sense a large number of different volatile compounds⁴. Nonetheless, in these

applications, the polymeric matrix is limited to retain the indicator in place and to favour the diffusion of analyte molecules to the sensing molecules. However, the polymer properties may affect the characteristics and performances of the sensing layer as well, and, eventually, of the resulting optical chemical sensor.

A variety of polymers have been used in optical sensors which include silicones, plasticized polyvinylchloride (PVC), poly(tetrafluoroethylene) (PTFE), polyurethanes (PU), poly(dimethylsiloxane) (PDMS), Nafion, nylon, agarose, sol-gels. The polymers absorb and concentrate the analyte vapours, thereby influencing the environment surrounding the dye embedded in the polymer. Comparison of the film results with those of dye dissolved in the neat solvents is often favourable⁵. Permeation of analyte molecules through these polymers takes place by different mechanisms. While in some polymers, a mechanism of analyte dissolution is accompanied by diffusion, in others the analyte simply diffuses through the pores of the polymers. Hydrophobic polymers can be permeable to gases, while hydrophilic polymers are permeable to ionic species. Silicone polymers have unique properties exhibiting higher permeability for most gases and vapours. Sol-gel glasses, with certain degree of porosity, have been used in optical gas sensors. Using defined polymerisation conditions one can vary the size of the pore network of this polymer. The thickness of the polymeric film is generally a compromise between sensitivity and response time of the sensor system. The diffusion characteristics of such

materials also make them ideal matrices for gas sensors and can exhibit differential diffusion rates for different gases, allowing selective interaction of gas with the immobilized reagent⁶.

There are some reported works aimed at investigating the influence of the polymeric membrane on the sensitivity and response time, with the ultimate scope of optimize sensor performances⁷. It is also shown that, by the choice of a polymer with a certain lipophilicity and polarity, it is possible to vary the response time and the sensitivity towards amines and humidity of absorbance-based chromoreactand⁸. Other studies focused on whether the polymeric membrane affects the state of aggregation of the reagent molecule. In the case of Zr(IV)-porphyrins the degree of dimer formation can be significantly reduced by the employment of PU instead of PVC⁹.

In this work, our aim is to investigate the influence of polymers in optical gas sensors and to exploit the additional properties of polymers to enhance the possibility to design arrays of dye blended in polymeric matrices. The same optical chemical reporter (a Zinc-TetraPhenylPorphyrin) was dispersed in different polymers with the aim to demonstrate that increasing the number of polymers additional selectivity is obtained.

Herein, the polymers are transparent and optically inactive in the visible range while the indicator undergoes colour changes after the interaction with volatile compounds. The optical sensing properties of ZnTPP dispersed in polymers were investigated in the past evidencing

the different properties of stability of the dye in the polymers¹⁰. In this work, the attention was focused on the dye response alteration induced by the polymers properties.

This set of experiments was prompted by the observation that a particular polymer may enhance the sensitivity of a sensing molecule towards certain compounds, while it may be less permeable towards other compounds. Common approaches aim at identify for each application the polymer that fits better the requirement for target analytes. However, in sensor arrays a selectivity pattern is desirable and a set of polymeric matrices may be introduced to extend the number of sensing layers. Polymer properties determine the permeability and hence the type and the amount of compounds that permeating the polymer matrix can reach and interact with the porphyrin indicator, giving rise to optical transmittance changes.

Colour variations of the chemical indicator were detected with the CSPT transduction platform. The properties of polymers have been tested with vapours of alcohols, amines and their mixtures. Results show that indicator response changes according to the polymer on which it is embedded. Consequently, with different polymers and only a single indicator, the vapours identification was achieved. Results illustrate the possibility of combinatorial design of chemical sensors combining the multitude of available optical indicators with the multitude of optically inert and gas permeable polymers and suggest a novel strategy in the design of opto-chemical sensor arrays. In the next section, a short

overview of polymers used in related sensor applications will be given, in order to clarify the features that drove the choice of polymers used in this work.

4.2 Choice of polymers

Polyvinyl chloride (PVC) is the most commonly used polymeric matrix for ion-selective electrodes and for polymeric membranes in general. PVC is a high molecular weight material suitable for encapsulating reagents. It has good mechanical properties, homogeneity, it is simple to prepare and it is optically transparent. PVC has a very high molecular weight (>100000) and forms a cage-like structure for holding reagents within it. It also allows reproducibility of film production, making it ideal for sensor fabrication. Indeed, not always PVC is the best choice and there has been considerable interest in explore alternate matrices to formulate ion selective electrodes¹¹.

Polyurethanes are a family of block copolymers consisting of alternating hard and soft segment units that have also been attracted particular interest, especially in biomedical applications. They yield adhesive, physically durable, chemically stable, and biocompatible sensing membranes with electrochemical properties comparable to those of PVC-based membranes. Although several reports have demonstrated the usefulness of polyurethane-based membranes for ion sensing and

biosensing devices, there has been little study related to gas sensor applications. The polyurethane exhibits good flexibility even without the use of a plasticizer. The omission of a plasticizer is generally advantageous because plasticizers evaporate at elevated temperatures, thus affecting the shelf lifetime. In addition, the mechanical stability of polyurethane membranes is superior to that of plasticized PVC membranes. Polyurethanes have been successfully employed in a pH-sensitive gas-permeable membrane for $p\text{CO}_2$ ¹².

A commercially available polyurethane, Tecoflex SG-80A (TPU), appears to be an attractive alternative to the conventional PVC matrix due to its better biocompatibility and adhesion properties when compared to analogous cation selective electrodes prepared with PVC-based membranes. TPU is a thermoplastic aliphatic polyurethane which exhibits relatively high hydrophilicity. This is shown in its high water uptake which, depending on the specification, can range from as small as 1% to over 1000%. The material shows higher hydrophilicity than plasticized PVC¹³. Tecoflex is particularly appealing for sensor application because it is biocompatible and it can also be used as coatings on the surface of intravascular electrochemical oxygen sensing catheters. The fact that it is an aliphatic polyurethane implies that there are no carcinogenic by-products¹⁴. Its application is not limited to these but it is also used in gas sensors, for instance, to detect ammonia with functionalized fibre optic sensors¹⁵.

Silicone polymers are useful polymers for optical oxygen sensors because of their excellent gas permeability, high thermal stability, chemical inertness and optical transparency¹⁶. Cross-linked PDMS was for instance used to immobilize different metal phthalocyanines for the detection of amine vapours¹⁷. It swells in non-polar organic solvents and its swelling kinetics differs according to the polarity of the solvent. This consideration led to the fabrication of colloidal crystal-based chemical sensors for the colorimetric detection of VOCs in environmental applications. The swelling of crystal modifies the lattice constant, causing a modification in the optical characteristics that could even be observed with the naked eye¹⁸.

Poly(dimethylsiloxane)bis(12-hydroxystearate) terminated (PDMS) has very low vapour pressure and very high viscosity (paste like consistency) because it is terminated in fatty acid tails. It is not so widespread diffuse as the cross-linked PDMS, but its use was reported in gas sensor application to functionalize surface acoustic wave (SAW) transducers¹⁹.

The chemical structure of the above mentioned polymers, together with a summary of their chemical properties is reported in Table 4.1.

Table 4.1. Chemical structure and properties of the polymers used in these experiments.

Polymers	
PVC	PDMS
$* \left[\begin{array}{c} \text{C} - \text{C} \\ \quad \\ \text{H}_2 \quad \text{H} \\ \quad \\ \text{H}_2 \quad \text{Cl} \end{array} \right]_n *$	$\text{CH}_3(\text{CH}_2)_{15}\text{CH}_2 - \text{C}(=\text{O}) - \text{O} - \left[\begin{array}{c} \text{CH}_3 \\ \\ \text{Si} - \text{O} \\ \\ \text{CH}_3 \end{array} \right]_n - \text{O} - \text{C}(=\text{O}) - \text{CH}_2(\text{CH}_2)_{11}$
Tecoflex PU (TPU SG-80A)	PU
$\left[\text{O} - (\text{CH}_2)_4 - \text{O} - \left[\begin{array}{c} \text{O} \\ \\ \text{N} \\ \\ \text{H} \end{array} \right] - \text{C}_6\text{H}_{10} - \text{CH}_2 - \text{C}_6\text{H}_{10} - \left[\begin{array}{c} \text{O} \\ \\ \text{N} - \text{C} - \text{O} \\ \\ \text{H} \end{array} \right] \right]_n$	$* \left[\text{O} - \text{C}(=\text{O}) - \text{NH} - \text{C}_6\text{H}_{10} - \text{CH}_2 - \text{C}_6\text{H}_{10} - \text{NH} \right]_n *$
Plasticizer (DOS)	
$\text{CH}_3(\text{CH}_2)_3\text{CH}(\text{CH}_2\text{CH}_3)\text{CH}_2 - \text{O} - \text{C}(=\text{O}) - \text{CH}_2(\text{CH}_2)_6 - \text{CH}_2 - \text{C}(=\text{O}) - \text{OCH}_2\text{CH}(\text{CH}_2\text{CH}_3)\text{CH}_3$	

4.3 Experimental

5,10,15,20-tetraphenylporphyrin Zinc [ZnTPP] was the optical indicator used in the experiments here illustrated. ZnTPP was dispersed in four different polymeric matrices based on: poly(vinyl chloride) (PVC) high molecular weight, poly(dimethylsiloxane)bis(12-hydroxystearate) terminated (PDMS), aromatic polyurethane (PU) and a hydrophilic thermoplastic polyurethane (TPU, Tecoflex SG-80A).

PVC and PDMS require the use of a plasticizer; bis(2-ethylhexyl)sebacate (DOS) was the one used in this study. The composition of the membranes is summarized in Table 4.2.

Table 4.2. Composition of the investigated polymeric membranes.

Membrane	Polymer	Plasticizer	Composition wt% (porphyrin:polymer:plasticizer)
1	PVC	DOS	1:33:66
2	PDMS	DOS	1:33:66
3	PU	not used	1:99
4	TPU	not used	1:99

This set of polymers covers a large range of chemical properties and fulfils the experimental requirements. In particular, polymers were considered suitable for this application, since they all share the same solvent of the porphyrin, they form stable thin films on the plastic support, they show gas permeability and allow for gaseous sample diffusion. The sensing membranes were prepared by dissolving the polymer, the plasticizer (if needed) and the porphyrin, with the ratio summarized in Table 4.2 in 1 ml of tetrahydrofuran (THF). 5 μ l of solution were collected with a pipette and spotted by solvent casting onto a 25 mm diameter transparent substrate, a Thermanox plastic coverslip provided by Nunc. At the same time, in order to study the arrangement of porphyrins in the polymeric matrices, the mixed films of

ZnTPP and polymers were deposited on glass substrates and absorbance spectra were measured with a Varian Cary 50 UV-Vis spectrophotometer.

The plastic substrate was placed in a measurement cell with transparent gas-tight windows, endowed with tube connectors for gas delivery through a flow meter. The sample was illuminated with a standard LCD computer monitor (Philips 1704S), and imaged with a webcam (Philips SPC900NC). The experimental arrangement is shown in Figure 4.1, together with an image of the spotted membranes acquired by the webcam under a green illumination.

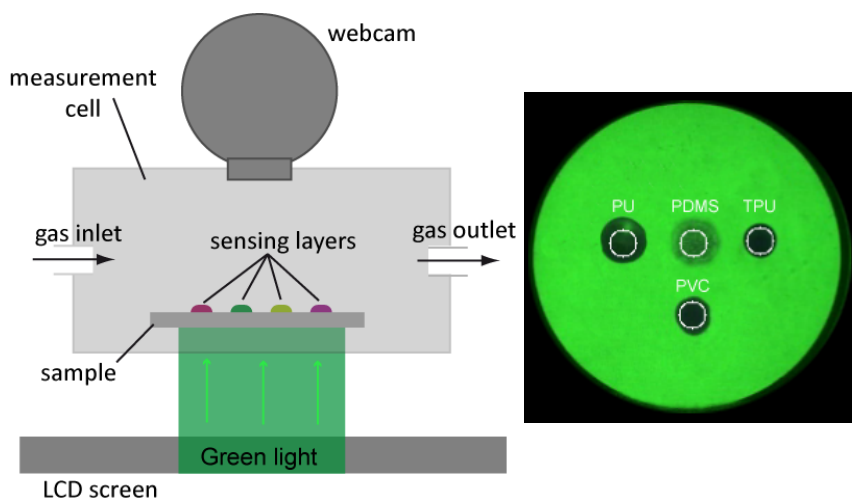


Figure 4.1. (a) Schematic diagram of the experimental arrangement. The sample was inserted in a measurement cell, equipped with tube connection for the gas flow. The sample was illuminated by the computer screen and imaged by the camera through gas-tight windows. (b) Image of the polymeric sensing layer as acquired by the camera with evidenced the ROIs selected for the analysis.

The measurement cell was filled with organic vapours diluted in a nitrogen flow. Two alcohols, butanol and ethanol, three amines, trimethylamine (TMA), triethylamine (TEA) and butylamine, and their mixtures were presented to the sensing layers. Three different dilutions of the saturated vapour were considered for pure compound exposures, while different combinations were produced for mixtures. Concentrations and mixtures are listed in Table 4.3. Every measure was repeated at least three times, yielding a total of 89 measures performed. Dilution factors were kept constant during the measure by a mass flow controller (MKS).

Table 4.3. Vapour concentrations that were tested during the measurements.

Sample	Concentration 1	Concentration 2	Concentration 3
Ethanol	10%	20%	30%
Butanol	10%	20%	30%
TMA	5%	10%	15%
TEA	2%	3%	4%
Butylamine	2%	3%	4%
Ethanol-Butanol	10%-10%	20%-20%	-
Ethanol-TMA	5%-10%	5%-30%	15%-30%
TEA-TMA	2%-5%	2%-15%	-

Saturated vapour pressures were evaluated from Antoine's law using the parameters provided by the NIST library²⁰. Since previous investigations have shown that the optical changes of ZnTPP

consequent to adsorption of volatile compounds occur prevalently in the wavelength range corresponding to the green colour²¹, during the exposure, the substrate was illuminated with a sequence of pure green (0 255 0) colour.

The webcam recorded the image intensity in its three channels with a resolution of 320x240 pixels and a sampling time of 5 seconds. For this reason, optical measurements were carried out illuminating the sensing film with a pure green light and taking only the green channel of the camera as the output signal.

Standard webcams offer a variety of parameters for control the processing of the raw image (such as brightness, contrast, and white balance) and the physical parameters determining the exposure of the detector (such as gain and shutter time). The conditions selected aimed at minimizing the effect of the camera processing, leaving as clean as possible the raw signals. Typical values are: brightness 50%, maximum saturation, gamma = 1, daylight white balance, minimum gain, and shutter speed slowest possible.

For data treatment, a number of circular regions of interest (ROIs) corresponding to each spotted area were defined on the image (Figure 4.1). The average intensity of all pixels in the ROI was calculated and the time evolution of camera signals was referenced to zero by subtracting the first value of each measurement.

4.4 Results and discussion

4.4.1 Preliminary studies on the polymeric matrices

In order to be acquainted with the aggregation status of porphyrin molecules within the polymeric matrix, UV-Vis spectra of ZnTPP embedded in the four polymers were measured in ambient air. As a comparison, a diluted liquid solution of ZnTPP was evaluated. Figure 4.2 shows these absorbance spectra normalized to the maximum value. Porphyrin spectra in polymers have a similar shape and only small deviations from the spectrum of the ZnTPP dissolved in the diluted solution of chloroform are observed. The peak of Soret band is well resolved and the presence of small features different from those found in the chloroform solution indicates that within the polymeric matrix porphyrins molecules aggregation is negligible.

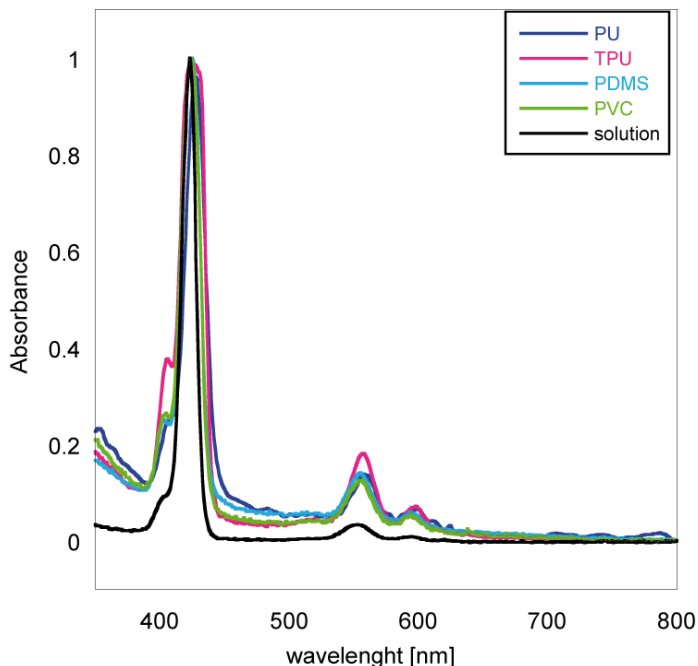


Figure 4.2. UV-Vis absorbance spectra of ZnTPP embedded in polymers, and, as a comparison, of ZnTPP in a dilute chloroform solution. Spectra are normalized to the maximum values.

The exposure to vapours elicits distinct responses by the porphyrin indicators embedded in polymers. Figure 4.3 shows an example of the signals recorded exposing the films to vapours of TMA, butylamine, and ethanol. Each subplot displays for each polymer the time evolution of signals averaged on the number of pixels contained in each ROI, when an abrupt change of concentration is applied. Interestingly, both the saturation value of the response and its dynamics differ in the polymeric

matrices, indicating an involvement of partition and diffusion characteristics of polymers on the response signals.

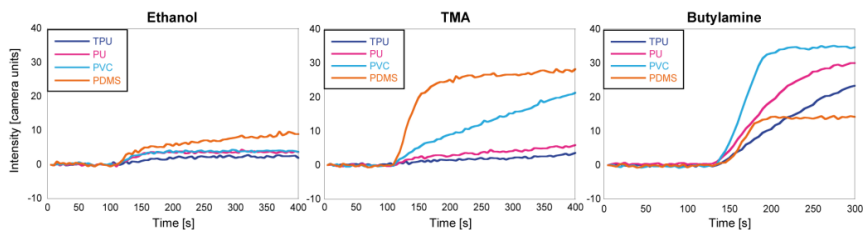


Figure 4.3. Example of the time evolution of signals averaged in the 4 ROIs for vapours of ethanol, TMA, and butylamine.

It is interesting to note that using a ZnTPP without the polymeric matrix (i.e. simply casted into the plastic substrate), a response with far less intensity is recorded. In Figure 4.4 the responses of ZnTPP in the polymeric matrix and the ZnTPP without matrix are plotted as a comparison in the same graph. As expected, the polymeric matrix, reducing the stacking of molecules, favours the diffusion of the analytes within the membrane and it assures a greater number of porphyrin molecules to interact with the airborne compounds.

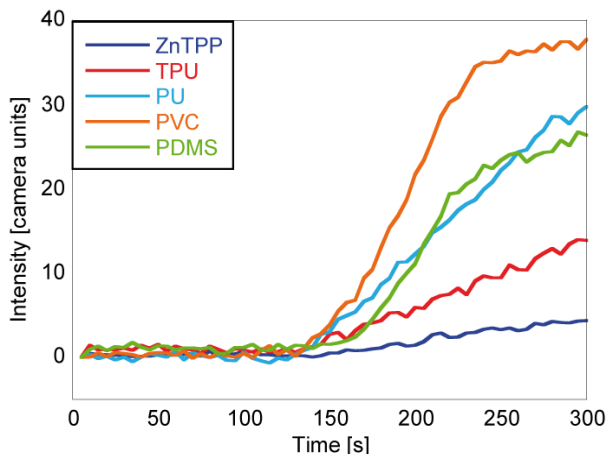


Figure 4.4. Comparison of the response to butylamine vapours of the ZnTPP dispersed in the four analyzed polymeric matrices with the response of ZnTPP without polymers.

This is confirmed by the observation through an optical microscope of a layer of ZnTPP casted onto a plastic surface (Figure 4.5a) and of a ZnTPP dispersed in a PVC matrix, casted onto the same substrate (Figure 4.5b). The size of each spot is about 2mm and the optical magnification is set to 8x. The ZnTPP, even at this low magnification, evidences the formation of crystals and shows a very intense optical density. Also the coffee stain effect is more marked, and it leads to a less uniform sensing surface. When the molecules are dispersed in a polymer, the overall surface results more homogeneous, no crystals are visible at this magnification and the coffee stain effect is negligible. Thanks to the PVC width (evidenced by the shadows of the microscope light), the ZnTPP molecules are more spaced, and the optical density

results lower. Once again, it is demonstrated that the polymer is a crucial part of a sensing layer for an optical platform, assuring a reduced optical density, producing an even surface to image, and favouring the diffusion of airborne compounds towards the sensing molecules.

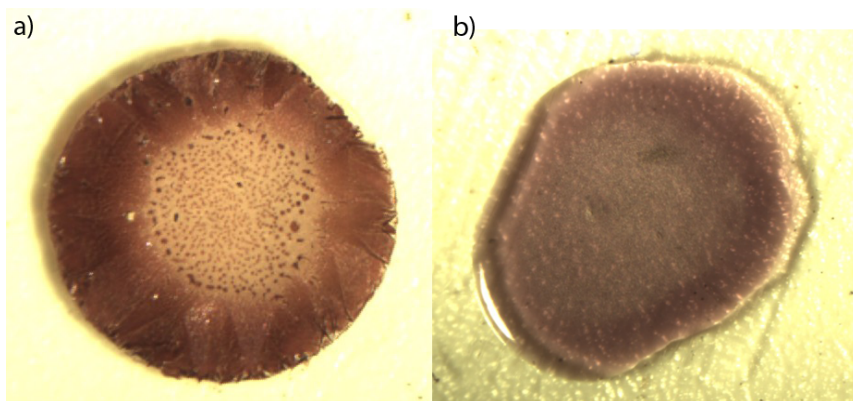


Figure 4.5. Optical microscope magnification (8x) **(a)** of a ZnTPP layer and **(b)** of ZnTPP dispersed in a PVC matrix.

All polymeric layers showed a good reversibility of the responses. Among tested compounds, butylamine is the worst case by the reversibility point of view, since it is supposed to show the strongest interaction bond with the ZnTPP. Figure 4.6 shows a complete measurement cycle of butylamine at the highest tested vapour concentration. In the graph it is shown the absorption, when the measurement cell is filled with the analyte vapour, and the desorption, when the analyte is removed and the sensor is cleaned with a flow of pure nitrogen. Desorption takes roughly twice the time of the whole

absorption process, and allows for a complete restoring of the initial conditions. The polymeric matrices does not differ in the desorption rate and all of them assure a good cleaning even from this aggressive compound.

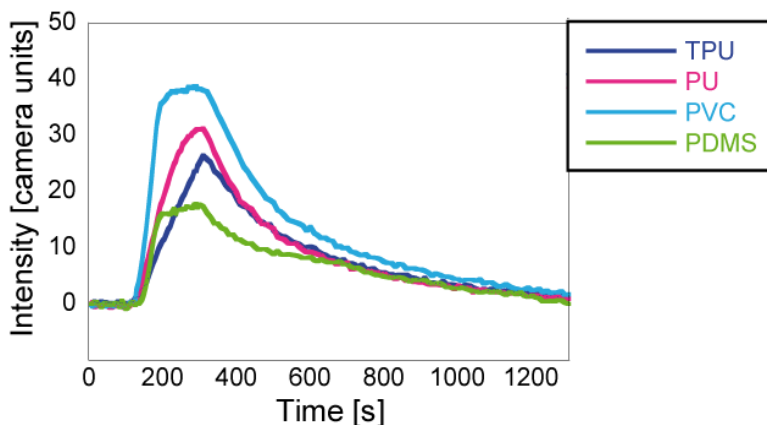


Figure 4.6. Evidence of the reversibility of sensing layers for a measure of butylamine vapours.

4.4.2 Array of polymeric matrices for VOCs discrimination

A rough evaluation of the effects of the polymers can be observed in Figure 4.7 where the response patterns to pure vapours and mixtures, all delivered at the same concentration of 3000 ppm, is shown. In figure, each bar represents the average and the standard deviation of the value of saturation response of each measure. Figure 4.7 shows that, except

for butylamine, in all cases the largest responses occur for the PDMS spot.

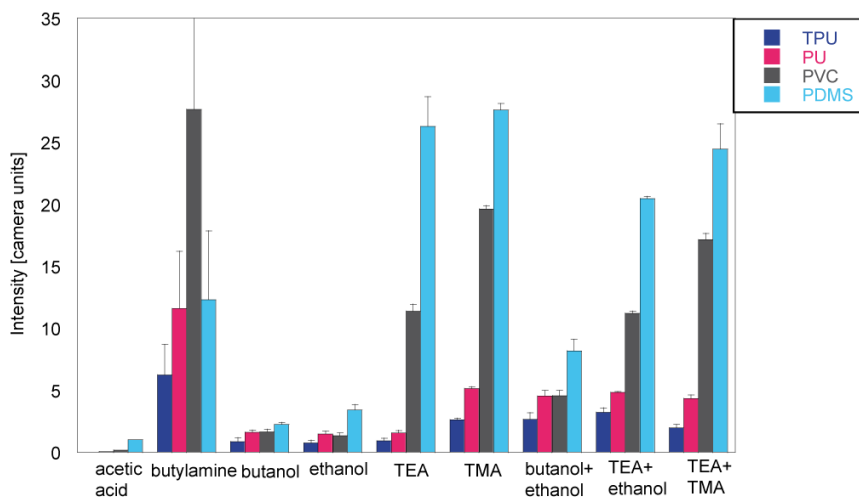


Figure 4.7. Response pattern of ZnTPP in the four polymeric matrices. Each bar represents the average value of response elicited by a concentration of approximately 3000ppm.

The largest increase is then observed for triethylamine (TEA) and trimethylamine (TMA), while in presence of alcohols the effect of PDMS properties is less intense. The different behaviour of butylamine with respect to the other amines is likely triggered by the different polymers permeability that determines the amount of vapour molecules that in each case can reach the indicator molecules. It is important to note the peculiar character of the response to butylamine for which the largest response occurs in the PVC membrane. On the other hand, trimethylamine (TMA) and, most importantly triethylamine (TEA),

show a preferential partition in the PDMS-based matrix. This different behaviour may be explained considering the very different steric structures of these molecules. Indeed, butylamine has a linear structure, contrary to TEA and TMA that are characterized by a branched structure.

In order to correctly interpret these results the role of the ZnTPP indicator cannot be neglected. The interaction mainly responsible for optical properties changes is indeed the coordination of the volatile compound to the Zn ion at the porphyrin inner core. The affinity of coordination with a metal ion can be qualitatively described by the Pearson's principle for which hard acids exhibit a preference for hard bases and soft acids prefer to bind to soft bases²². Zn ion has a moderate hardness and it is known to have higher affinity to nitrogen ligands (amines) than to hard oxygen ligands, such as acetic acid, ethanol, and butanol.

The effect of polymers is expected to influence also the dynamics behaviour of the signals. To the scope of illustrating the response dynamics, the temporal evolution the signals of PDMS and PVC, for which the largest responses are found, have been plotted in Figure 4.8 one versus the other. In this plot, each measure corresponds to a trajectory in the plane. A deviation from the bisector line indicates the prevalence of the response of one polymer with respect to the other, and butylamine is the only gas whose trajectory lies in the PVC side of the plane. It is worth to mention that alcohols trajectories tend to lie closer

to the bisector indicating that responses in the two polymers differ of a small quantity with respect to amines for which the trajectories significantly diverge from the bisector line. The change of slope that characterizes some of these curves means that the response dynamic is different in the two polymers, because of a different diffusion rate through the polymers.

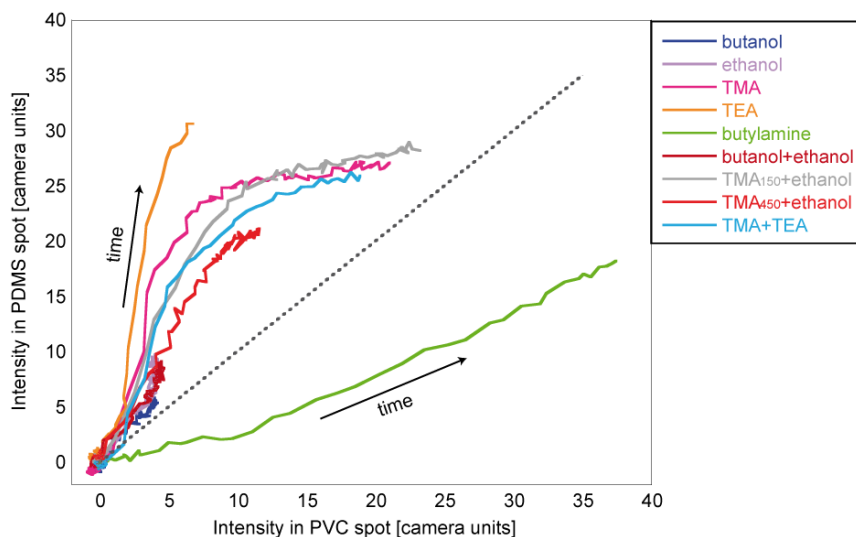


Figure 4.8. Time evolution of the response of spot based on ZnTPP-PDMS plotted against the response of ZnTPP-PVC. This allows to appreciate the different permeability of the polymers.

These results suggest that even if the magnitude of the signals is ruled by the indicator-analytes relationship, the change of responses between polymers can be attributed to the polymer-analytes relationship. Thus, even using a single indicator, a response pattern

arises that depends exclusively on the physicochemical properties of the polymers, such as diffusivity and permeability. The occurrence of response patterns implies that a single indicator dispersed in several polymeric matrices can identify different analytes as a sensor array.

Another interesting aspect of using different polymeric matrices is that the response dynamic is characteristic for each couple polymer-vapour, because of the diffusion rate of the analyte through the matrix (Figure 4.9). Therefore, it becomes another interesting feature that favour vapour discrimination.

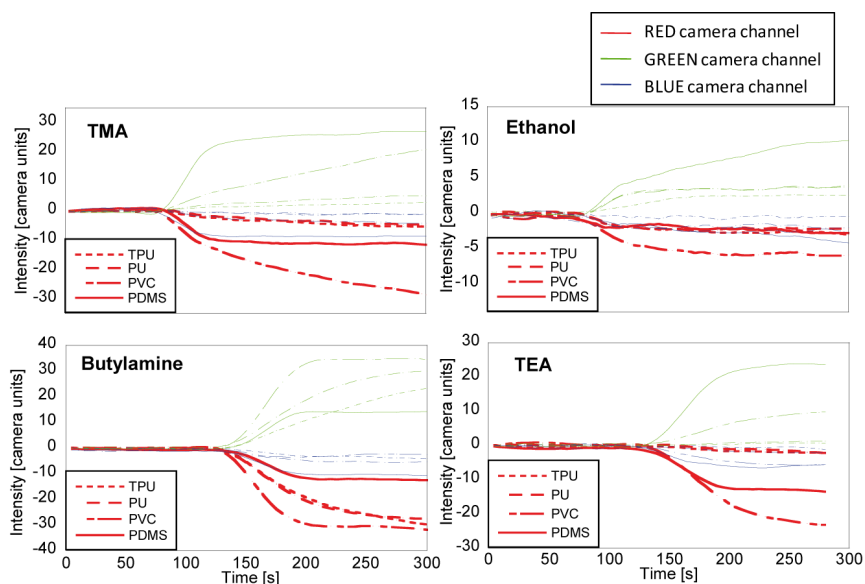


Figure 4.9. Evidences of different response dynamics within the four polymeric matrices for diverse vapours.

A qualitative appraisal of the recognition properties of these patterns can be obtained by means of a chemometric data analysis. For each polymeric spot the response intensity change was calculated, collecting four features per sample exposure. All the measurements were assembled in a data matrix of 89x4 elements, and Principal Component Analysis (PCA) was applied to the data matrix scaled to zero mean and unitary variance²³. In Figure 4.10a, the plot of the first two principal components (PC) is shown, about 98% of the total variance of the data is explained by the first two PCs. A separation between alcohols and amines is observed, although, most scores cluster in the right side of the graph because of the large response to butylamine samples. However, magnifying the area where most of the scores lie, it is possible to visually appreciate the separation between alcohols and amines (Figure 4.10b). Among the amines, TEA and TMA are easily distinguishable and the direction of increasing concentration can also be identified. A further magnification of the area where the scores of alcohols responses are clustered reveals that it is possible to distinguish between ethanol and butanol and to identify the three vapour concentrations (Figure 4.10c). Finally, almost no optical response is observed for acetic acid. As previously discussed, the large separation between alcohols and amine is attributable to the preferential binding of amines, and in particular of butylamine, to ZnTPP.

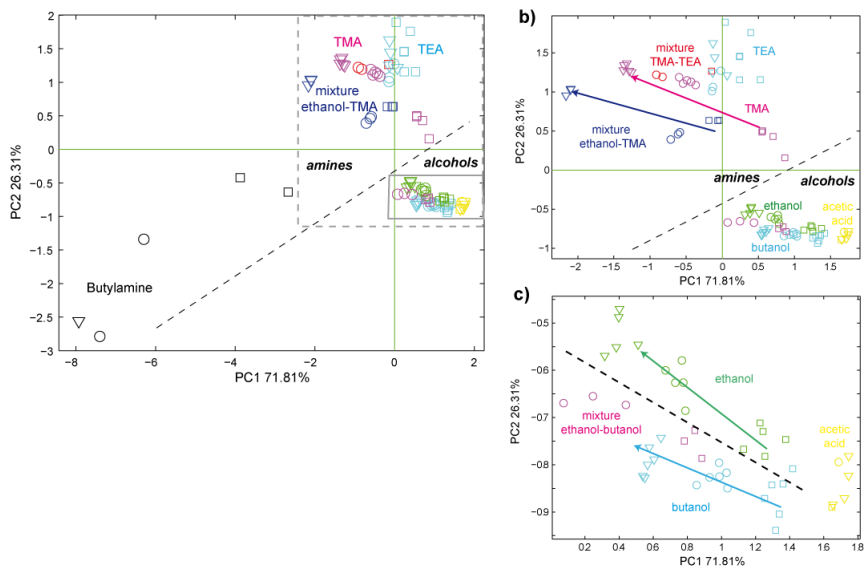


Figure 4.10. (a) Scores plot of the PCA of the data matrix. For each compound, squares indicate the lower value of concentration, circles the intermediate value and triangles the higher value. (b) Magnification of the area marked with a grey dashed rectangle in (a) where the separation among the different compounds is visible. (c) The magnification of the area marked with a grey rectangle in (b) shows the separation between butanol and ethanol. Arrows indicate the directions of increasing concentration.

The analysis of loadings, on the other hand, allows for the evaluation of the contribution of each signal component to the overall discriminating capabilities of the system. In Figure 4.11 a bi-plot reports the superposition of scores and loadings in the first two principal components plane. Each polymer contributes differently to the scores discrimination as the PCs plane is portioned in three region concerning PDMS, PVC and polyurethanes, TPU and PU. These latter, belonging to

the same class and having a similar structure, show a very analogous behaviour and lie close to each other in butylamine direction. PDMS loadings are orthogonal to those of the two polyurethanes and provides a significant contribution to the discrimination between alcohols and amine. Finally, PVC loading contributes mainly to the discrimination among different amines, which primarily occurs along the first principal component.

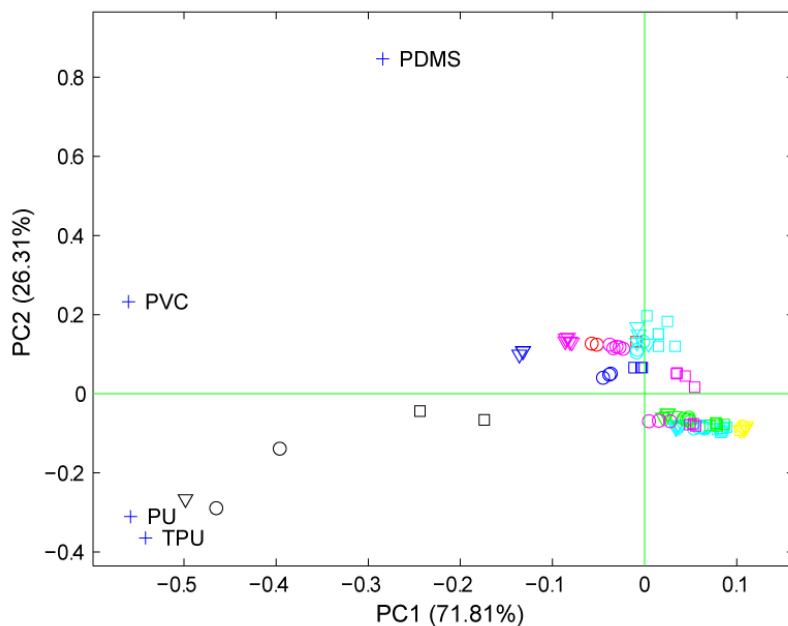


Figure 4.11. Bi-plot of the PCA analysis of the data matrix. In the plane of the first two principal components the scores are normalized and displayed with the same colour code used in Figure 4.10. Loadings are represented with a blue plus mark and a label that indicates the polymer.

Finally, as a demonstration that also a discrimination of concentrations is possible with such a system, the results of the application of a regression model are described. A Partial Least Square (PLS) model was applied to the same set of features to estimate the vapour concentration of samples. The results are shown as a scatter plot of the predicted values of concentration versus the real value. As an example the regression for samples of pure ethanol, pure TMA and their mixture are plotted in Figure 4.12.

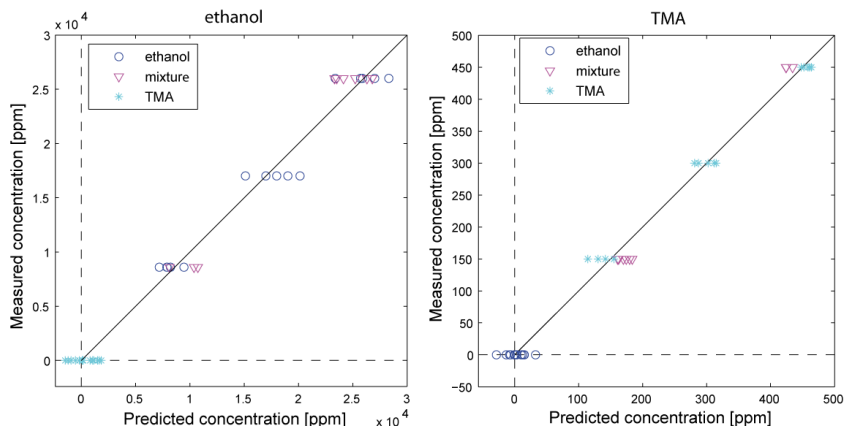


Figure 4.12. Results of the application of a PLS model to the measures. The model predicted concentration is reported against its real value for ethanol (blue circle), TMA (magenta triangle) and their mixtures (cyan star) samples.

4.5 Conclusions

In this study, it was shown that polymers, besides providing a support to retain the chemical indicators, can affect the selectivity and the sensitivity of optical chemical sensors. Beyond a careful design of sensing layer to target molecules, this property can be exploited in order to provide an additional tool in the design of sensing layer arrays where the differentiation of selectivity of individual reporters is a strong requirement. Our findings indicate that the partitioning effect of different polymers extends the range of selectivity of a single colour indicator, providing a simple and efficient methodology to increase the number of sensors maintaining the same number of chemical indicators. Polymers often operate a selection among those volatile compounds that are rather undistinguishable from a pure optical sensing approach. This could be the case of aliphatic alcohols that are expected to elicit the same optical change regardless the aliphatic chain length, on the contrary, a selection among different chain lengths can be operated by a suitable choice of polymers. On the other hand, the selection of further indicators may orient our sensor array toward a greater variety of classes of compounds.

References

- ¹ J. Park, W. Groves, E. Zellers, Vapor recognition with small arrays of polymer-coated microsensors. A comprehensive analysis, *Anal. Chem.* 71 (1999) 3877-3886
- ² J. Lavigne, E. Anslym, Sensing a paradigm shift in the field of molecular recognition: from selective to differential receptors, *Angew. Chem. Int. Ed.* 40 (2001) 3118-3130
- ³ R. A. Potyrailo, Polymeric Sensor Materials: Toward an Alliance of Combinatorial and Rational Design Tools, *Angew. Chem. Int. Ed.* 45 (2006) 702–723
- ⁴ O. Wolfbeis, Sensor paints, *Adv. Mater.* 20 (2008) 3759-63
- ⁵ J. H. Krech, S. L. Rose-Pehrsson, Detection of volatile organic compounds in the vapor phase using solvatochromic dye-doped polymers, *Anal. Chim. Acta* 341 (1997) 53-62
- ⁶ T. E. Brook, R. Narayanaswamy, Polymeric films in optical gas sensors, *Sens. Actuators B* 51 (1998) 77–83
- ⁷ A. Mills, A. Lepre, Controlling the Response Characteristics of Luminescent Porphyrin Plastic Film Sensors for Oxygen, *Anal. Chem.* 69 (1997) 4653–4659
- ⁸ G. J. Mohr, T. Nezel, U. E. Spichiger-Keller, Effect of the polymer matrix on the response of optical sensors for dissolved aliphatic amines based on the chromoreactand ETH^T 4001, *Anal. Chim. Acta* 414 (2000) 181–187
- ⁹ Ł. Gorski, E. Malinowska, Fluoride-selective sensors based on polyurethane membranes doped with Zr(IV)-porphyrins, *Anal. Chim. Acta* 540 (2005) 159–165
- ¹⁰ F. Nwachukwu, M. Baron, Polymeric matrices for immobilising zinc tetraphenylporphyrin in absorbance based gas sensors, *Sens. Actuators B* 90 (2003) 276-285

- ¹¹ B. Adhikari, S. Majumdar, Polymers in sensor applications, *Prog. Polym. Sci.* 29 (2004) 699–766
- ¹² J. H. Shin, J. S. Lee, S. H. Choi, D. K. Lee, H. Nam, G. S. Cha, A planar pCO₂ Sensor with Enhanced Electrochemical Properties, *Anal. Chem.* 72 (2000) 4468–4473
- ¹³ G. J. Mohr, U. E. Spichiger-Keller, Development of an Optical Membrane for Humidity, *Mikrochim. Acta* 130 (1998) 29–34
- ¹⁴ Y. Wu, A. P. Rojas, G. W. Griffith, A. M. Skrzypchak, N. Lafayette, R. H. Bartlett, M. E. Meyerhoff, Improving blood compatibility of intravascular oxygen sensors via catalytic decomposition of S-nitrosothiols to generate nitric oxide in situ, *Sens Actuators B* 121 (2007) 36–46
- ¹⁵ J. Moreno, F. J. Arregui, I. R. Matias, Fiber optic ammonia sensing employing novel thermoplastic polyurethane membranes, *Sensors and Actuators B* 105 (2005) 419–424
- ¹⁶ H. He, R. J. Fraatz, M. J.P. Leiner, M. M. Rehn, J. K. Tusa, Selection of silicone polymer matrix for optical gas sensing, *Sens. Actuators B* 29 (1995) 246–250
- ¹⁷ L. Sutarlie, K. L. Yang, Colorimetric responses of transparent polymers doped with metal phthalocyanine for detecting vaporous amines, *Sens. Actuators B* 134 (2008) 1000–1004
- ¹⁸ T. Endo, Y. Yanagida, T. Hatsuzawa, Colorimetric detection of volatile organic compounds using a colloidal crystal-based chemical sensor for environmental applications, *Sens. Actuators B* 125 (2007) 589–595
- ¹⁹ N. Levit, D. Pestov, G. Tepper, High surface coatings for SAW-based chemical sensor applications, *Sens. Actuators B* 82 (2002) 241–249
- ²⁰ www.nist.gov/webbook
- ²¹ J. Spadavecchia, R. Rella, P. Siciliano, M. Manera, A. Alimelli, R. Paolesse, C. Di Natale, A. D'Amico, Optochemical vapour detection

using spin coated thin film of ZnTPP, *Sens. Actuators B* 115 (2006) 12-16

²² R. Pearson, Hard and soft acids and bases, *J. Am. Chem. Soc.* 85 (1963) 3533-3559

²³ R Johnson, D Wichern, *Applied Multivariate Statistical Analysis*. New York: Upper Saddle River; 2002

Chapter 5: A bio-mimetic Approach to Volatile Detection

5.1 Introduction

In current models of natural olfaction, the identification of odours is barely based on the molecular recognition properties of the single olfactory receptors¹. In this regard, it is known that individual receptors are limited in kinds and broadly selective, and that the recognition of odours is rather achieved considering the collective response of all the receptors^{2,3}. This provides a sort of combinatorial selectivity allowing, with a limited number of different kinds of receptors, the detection of millions of distinct odours.

The principle of combinatorial selectivity was the basis for the development of artificial olfaction systems as arrays of broadly-selective chemical sensors whose signals are processed by some multivariate algorithms in order to enable the identification and the classification of odours⁴. In natural olfaction, the combinatorial selectivity of receptors is complemented by a number of ancillary mechanisms. Among them,

several investigations point out the importance of spatio-temporal patterns arising in the peripheral olfactory system and in the olfactory bulb⁵ to the coding of olfactory information. Patterns arise thanks to the partitioning properties of the thin mucous layer that covers the receptors in the nasal epithelium. The mucosa acts as a sorption layer where the adsorption and desorption of odorant molecules occur, in a way similar to the stationary phase of a gas-chromatographic (GC) column⁶.

In this section, in analogy with gas-chromatography and with the principles of natural olfaction, a polymeric coating is used to partition and delay vapours that diffuse in the layer. Methods for the continuous imaging of gases diffusing through a sensing layer will be illustrated. A layer of chemical optical reporters, uniformly embedded in the polymeric coating, is used to detect the vapour molecules as they diffuse through the polymeric membrane. The colorimetric changes of chemical reporters induced by volatiles are detected with the CSPT optical platform. A continuous monitoring of gas diffusion is possible thanks to the feature of the image sensor that segments the sensing surface in a great number of pixels so that each acquired image actually corresponds to the contemporaneous measure of the optical properties of a quantity of spatially distributed virtual sensors. The gas is forced in a certain path where the chemical indicators are deposited; the response of these distributed sensors allows to image the volatile molecule as they flow through the path.

Several geometries have been considered, herein only two have been reported: a strip and a bi-dimensional layer. The properties of sensitised polymer layers have been tested with vapours of alcohols and amines. Results show that sensors signals are spatially and temporally structured, these structures depend mainly on gas-polymer interaction while the magnitude of the sensor signal depends on the gas-indicator interaction. Different combinations of polymers and indicators are then expected to provide a manifold of different encodings of volatile compounds. Our results mimic thus also the spatio-temporal patterns observed in the olfactory mucosa.

5.2 Chromatographic principles

At the beginning of 1900 M. Tswett separated natural pigments into coloured zones by percolating plant extracts through adsorbent packed columns. These investigations led to the development of a special adsorption technique that permitted the separation of the leaf pigments. In subsequent years, he further refined this technique, which eventually became known as chromatography⁷. Then this technique has evolved, and now chromatography is used for a number of processes in which the substances are separated under equilibrium partitioning between two phases, where one phase is stationary and the other is mobile. When the mobile phase is a gas, the separation process is called gas-

chromatography. In this case, a thin film of the stationary phase, that may be either liquid or solid, is confined to a column, and continuously swept by a stream of a carrier gas (the mobile phase). The column is connected to the inlet of the gas-chromatograph at one end and to a detector to the other. Columns can be either packed or open tubular, and also intermediate solutions can be used. Packed columns are typically 2-5m long with a 1-5mm inner diameter, and they are filled with an inert granular support, each particle of which is coated with the stationary phase. The length of a packed column is limited by the pressure drop generated by the resistance that offers to gas flow. Whereas, in the most widely used open tubular column, the stationary phase is constituted by a uniform thin film affixed to the inner periphery of an open tube. There are also columns where a porous layer, which may serve as a support for a stationary phase or as a stationary phase, coats the inner wall, while the central portion is open.

When a mixture of volatile compounds is introduced at the inlet of the column, each solute in the sample engages a highly dynamic equilibrated partitioning between the stationary phase and the mobile phase in accordance with its distribution constant K_C :

$$K_c = \frac{\text{solute mass per unit volume in stationary phase}}{\text{solute mass per unit volume in mobile phase}} = \frac{C_s}{C_m} \quad (5.1)$$

However, the flow of the carrier gas disrupts the equilibrium distribution at the front and rear of each solute band, causing a continuous evaporation at the rear and a reestablishment at the front as it

flows through the column. Because all solutes are injected simultaneously, separation is contingent on differences between the K_C values of individual solutes. The proportion of a solute that is in the mobile phase at any given time is a function of its net vapour pressure; molecules of those components that exhibit higher vapour pressures partition more in the mobile phase. They are swept toward the detector more rapidly and they are the first solutes eluted from the column. Other solutes exhibit lower vapour pressures, either because they are higher-boiling or because they engage in interactions with the stationary phase that effectively reduce their vapour pressures under the chromatographic condition employed. Individual molecules of these solutes venture in the mobile phase less frequently, their concentration in the mobile phase are lower, and they require longer periods of time to reach the detector (Figure 5.1). At the end of the column molecules are identified by a detector (usually a mass spectrometer), and the result of the analysis is a chromatogram, a graph where the abundance is plotted against the time elapsed after the sample insertion, called elution or retention time.

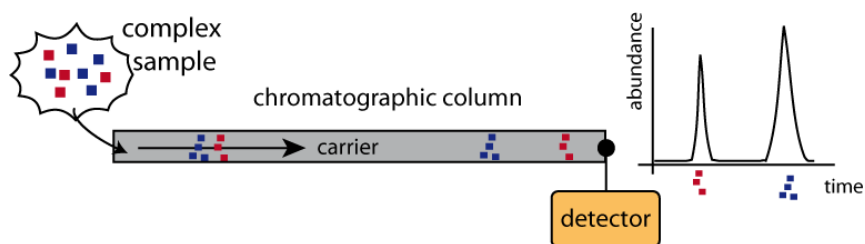


Figure 5.1. Schematic representation of the separation of complex mixtures performed by a chromatographic column.

Summarizing, solutes with high vapour pressures are less retained by the column as they spend a greater percentage of their transit time in the mobile phase, they move through the column more rapidly and emerge to the detector after a time smaller than solutes with lower vapour pressures. Under constant chromatographic conditions, the degree of separation is a function of solute retention factors and concentrations. However, the separation may be modulated by the temperature of the column, that influences solute vapour pressures and by the choice of the stationary phase. A polar stationary phase reduces the vapour pressure of polar solutes by means of additional intermolecular attractions with the stationary phase that may include hydrogen bonding and/or dipole-dipole interactions. Among the members of a homologous series, higher molecular weight homologues have lower vapour pressures and higher K_c values⁸. It is also possible to use multiple columns with different stationary phases. This technique is often referred to as multidimensional chromatography and allows separation of complex mixtures that cannot be separated using a single column. These columns are coupled orthogonally, which means that fractions from the first column can be selectively transferred to other columns for additional separation⁹.

5.3 Chromatographic principles in biological olfaction

Mammals express up to 1000 odorant receptors (about 300 in humans) on the cilia membrane surface of sensory neurons in the olfactory epithelium (OE). In mice, the OE contains more than 2 million sensory neurons. Olfactory sensory neurons express only one type of odorant receptor gene out of a repertoire of up to 1000 genes. It is believed that each sensory neuron responds to a range of odour ligands that preferentially bind to the expressed receptor. Each neuron projects a single axon into the olfactory bulb (OB), a relatively simple cortical structure that contains thousands of signal-processing modules called glomeruli. Glomeruli are spherical neuropils within which axons of olfactory sensory neurons form excitatory synaptic connections on dendrites of mitral and tufted cells, the output neurons of the OB. In mice, each glomerulus receives converging axonal inputs from several thousand olfactory sensory neurons and it is innervated by primary dendrites of about 20 mitral cells¹⁰.

A number of ancillary mechanisms exist to increase the discrimination capabilities of biological olfaction. Early studies suggest that both an inherent pattern, due to a zonal organization of olfactory receptors with similar sensitivities, and an imposed pattern, related to physicochemical properties of odorants, contribute to a spatial distribution of the response in the epithelium¹¹. The inherent pattern

exists because of the classification of odorant receptors into four groups related to their expression patterns in the OE. A given type of odorant receptor is expressed in one of four circumscribed zones arranged from dorsomedial to ventrolateral parts of the OE, which are labelled with roman type numbers from I to IV¹² (Figure 5.2).

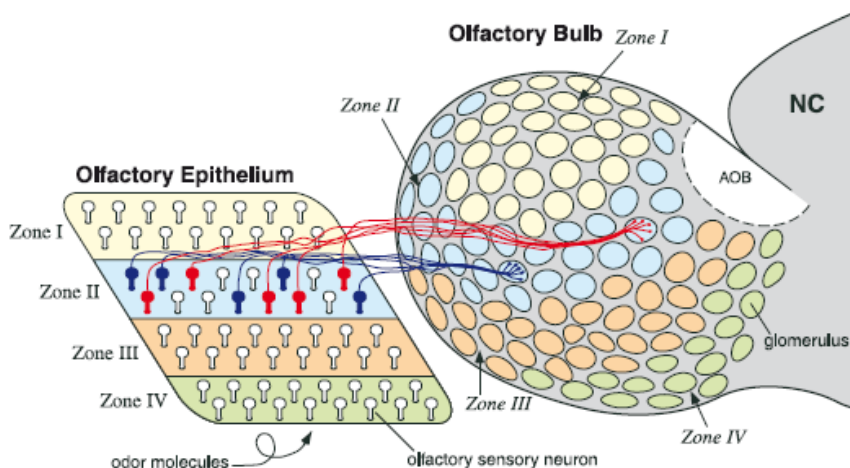


Figure 5.2. Schematic diagram illustrating the axonal connectivity pattern between the olfactory epithelium (OE) and the olfactory bulb. It is evidenced that the OE is divided into four zones (I-IV), defined by the expression of different odorant receptors.

Hence, a distribution of responses is found along longitudinally oriented regions following the olfactory receptor gene expression zones. These response gradients may be produced by the four receptor expression zones described for many of the putative olfactory receptor genes. Structural comparison of various odorant receptors, in relation to

their expression zones, revealed that the odorant receptors with highly homologous amino acid sequences tended to be localized in the same zone of the OE, therefore many of the receptors in each zone may share common properties. However it remains to be determined whether this zonal input is significant in central odour processing¹³.

The second mechanism that engenders spatiotemporal activity patterns in the OE is more interesting for the purpose of our work and will be discussed in more details. The study of differential odorant-dependent spatial patterns developed on the mucosa took its lead from the reports of Adrian^{14,15}. In analogy to chromatography, the separation carried out by the olfactory mucosa might operate as one of the basic mechanisms in olfactory discrimination¹⁶. This happens in the epithelium where a mucous layer, secreted by Bowman glands and supporting cells¹⁷, coats neurons cilia and provides the appropriate molecular and ionic environment for odour detection. The transport of odorants across the mucosa is a complex phenomenon involving chemical and physical processes. An important role is played by the odorant binding proteins. These are a family of proteins endowed with a hydrophobic pocket acting as shuttles for lipophilic molecules that cannot dissolve in the mucosa¹⁸. This mechanism is particularly efficient for pheromones sensing in insects¹⁹. Odorant binding proteins enable and enforce the sensitivity towards a selected number of odorants, while the majority of odorant molecules freely diffuse in the mucosa giving rise to different spatial and temporal patterns according to their diffusion

rates and mucous solubility. To remark the alleged role of olfactory mucosa it is interesting to note that the composition of mucous in contact with the olfactory receptors is very different with respect to the mucus covering the rest of the nasal cavities²⁰.

The molecules of different odorants spread in different spatial and temporal patterns along the mucosa in accordance with their diffusion rates and mucus solubilities. If the molecules of some chemicals are bound less strongly to the olfactory receptors than are the molecules of other chemicals, they will consequently travel farther and faster along the mucosa²¹. While an odour flows along the mucosa, the strongly sorbed odorants accumulate preferentially at the beginning of the path, while the weaker sorbed ones distribute more evenly in the mucosa²². Mozell could measure retention times of several odorants across the olfactory sac of a frog, finding that, in spite of the small size of the mucosa, the odorant molecules migrate at significantly different rates along it. Obviously, as a result of respiration the carrier gas flows through the nose in two directions and is pulsating rather than, as in a standard gas-chromatograph, unidirectional and constant. Consequently, rather than using a measure based upon the time needed for molecules to travel the given distance to the one detector at the end of the column, it is more probable that the nose could measure, with its many receptors spread along its entire column, the distance the molecules travel and the relative number of molecules travelling that distance²³. In addition to the spatial aspect of odour representation, glomerular activation maps

contain reliable, stimulus-specific sequences of onset times. This spatiotemporal pattern contains concentration-invariant information and provides a means of rapid readout. The olfactory system is optimized to take advantage of both space and time, such that for very different odours, the early components of the emerging spatial map are sufficient to discriminate reliably. However, for highly similar stimuli, a more complete map is required and information from later-activated glomeruli is necessary²⁴.

Sniffing behaviour determines the flow rate of air through the nasal passages, and odorant retention and migration vary with flow rate²⁵. Sniffing alters the sorption of odorants onto the lining of the nasal cavity and this may change the spatial distribution of response in the olfactory epithelium and olfactory bulb. Flow rate affects processing since vertebrate noses act to separate odorants by chemical properties in a flow-dependent manner²⁶.

5.4 Spatio-temporal patterns in artificial sensors

The idea of exploiting additional information provided by spatio-temporal response patterns of artificial sensors to enhance gases discrimination has already found few implementations. The main objective is to induce changes in the concentration profile of analytes presented to an array of sensors. A first example of this approach was

implemented by Weimar's group, using a gas chromatographic column to perform a pre-separation of components in a mixture then analyzed with an array of non-specific SnO₂-based Metal Oxide Sensors²⁷. However, in this way a sophisticated set-up is still used, coupled with a more modular sensor system.

Other implementations use catalytic metals to selectively consume components in a mixture in order to produce a stimulus-dependent response pattern²⁸. The catalytic surface coats the entire sensor chamber where discrete chemical sensors are distributed. The change in concentration operated by the catalytical activity of metals modifies the selectivity pattern of the array along the chamber²⁹. The use of metal-oxide-semiconductor in large areas allows to measure the spatial distribution of adsorbed molecules using a laser light to probe the extension of the spatial charge region in the semiconductor³⁰. This system, known as scanning light-pulse technique, allows to generate continuous maps of the gas distributed over the sensor surface providing selective gases fingerprints. In this case, patterns are due not only to the catalytic effect but also to the dynamic properties of the gas flow.

Also the geometry of the measurement chamber is supposed to influence the distribution of analytes to the sensors. In biological olfaction, the conformation of nasal cavities and the odour flow along the turbinates are supposed to play a discriminating role³¹. This evidence was used by Walt and co-workers that placed a number of identical fluorescent indicators in a complex flow environment reproducing a

canine nasal cavity and observing for different molecules distinct distribution patterns inside the cavity³².

A further approach, proposed by Walt, is to form a continuous gradient between two sensing molecules, obtaining gradually changing ratio of concentration of the starting units (Figure 5.3). The signal (in this case the temporal fluorescence) in each region has a characteristic shape and intensity, and different spatial response patterns increase sensor diversity³³.

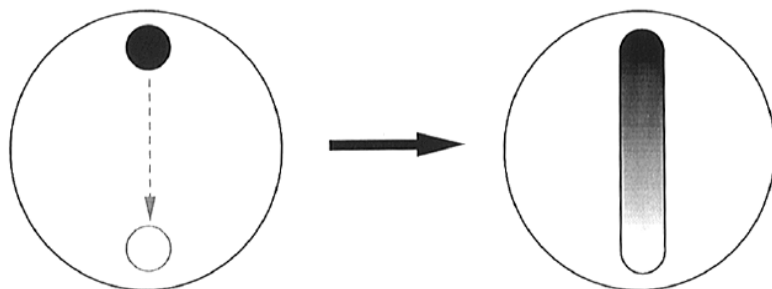


Figure 5.3. Gradient array obtained by a gradually changing concentration of two different sensing materials.

A first implementation of the mucosa properties has been provided by Gardner and co-workers that tried to implement the characteristics of biological chromatographic separation in the sensor system, then referred to as an artificial olfactory mucosa. Its basic concepts will be discussed in the next subsection.

5.4.1 Artificial olfactory mucosa

The artificial olfactory mucosa is conceived as an array of sensors distributed along a channel coated with a polymeric stationary phase that acts as a retentive layer (Figure 5.4)^{34,35}. Compounds that travel along the mucosa are selectively delayed depending on the affinity with the polymeric coating. Spatio-temporal patterns that arise in the mucosa response can then be used to increase the odour discrimination.

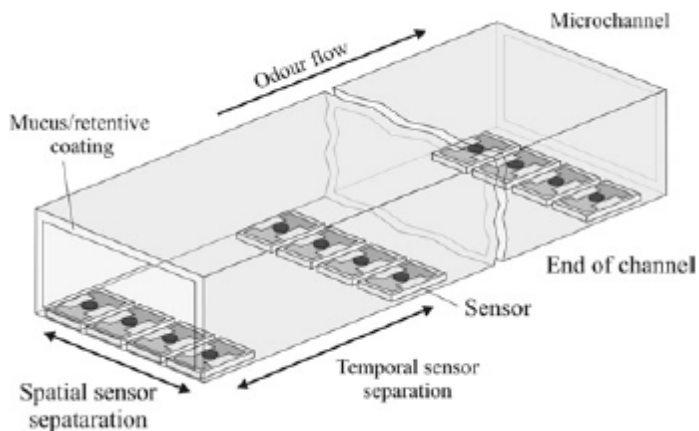


Figure 5.4. Section of the artificial olfactory mucosa developed by Gardner and co-workers.

In a subsequent work, Gardner and co-workers identify the contribution of three different mechanisms to the odour discrimination: one related to the chemosensor array itself, one due to the differential partitioning of components and the last one depending on the sensor

response dynamics³⁶. A further improvement was made within the same research group by adding a further retentive path that integrates a second sensor set. This supplementary column was conceived either uncoated (as a reference) or coated with polymers with different properties³⁷. The development of this artificial mucosa has as ultimate aim not to perform a complete separation of compounds, as in traditional gas-chromatographic system, but to provide an enhancement in discriminations capabilities by means of spatial and temporal information.

5.5 Mono-dimensional separation geometry

In a first set of experiments, the diffusion along two strips, representing a monodimensional track, was studied. These strips aimed at identify a path where the diffusion of volatile compounds could be observed. Two polymers with sufficiently different diffusion properties towards different volatile compounds were used in order to study the influence of the polymeric matrix on the diffusion. A single indicator was dispersed in both the membranes, the ZnTPP to transducer the gas presence. Herein, PVC and PU play the role of the solid phase of a gas-chromatographic column.

5.5.1 Experimental

The strips were simply casted with a pipette on a plastic substrate that was successively covered with a second plastic sheet endowed with a hole for gas inlet at the insertion of the sensing layer, as shown in the schematic cross-section of the system in Figure 5.5a. The image of the sensing layers in the measurement chamber as acquired by the camera under a green screen illumination, is depicted in Figure 5.5b. The sample is placed in a measurement chamber, where the concentration of analytes is settled by means of a mass-flow controller system. Hence, the diffusion of volatiles into the plastic sandwich takes place by simple diffusion, as a consequence of the concentration gradient between the chamber and the inner part of the sample.

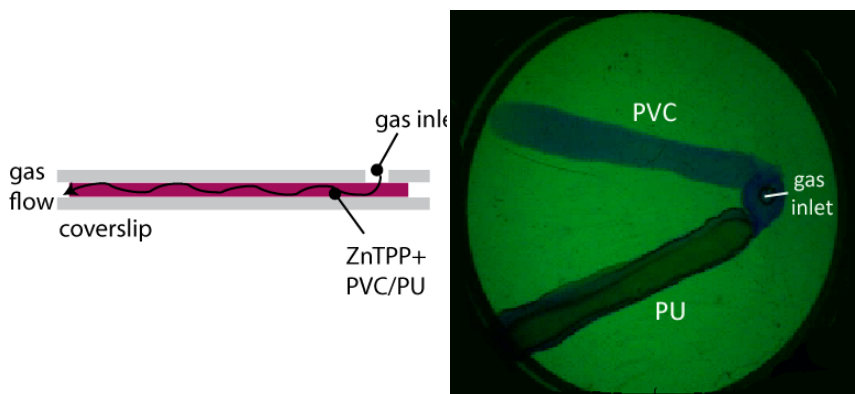


Figure 5.5. a) Schematic representation of the section of the sample. The porphyrin functionalized polymeric membrane is sandwiched between two plastic coverslip, one of which endowed with a hole for gas inlet. b) Frame acquired by the camera of the two strips of ZnTPP dispersed in different polymers.

5.5.2 Results

This preliminary set-up allowed us to get aware that the diffusion of volatiles in a fixed path do depend on the chemical properties of compounds and on the interactions with the polymeric phase. Moreover it evidenced that the diffusion can be easily evaluated with the use of the CSPT platform and a single indicator dispersed in the entire polymeric path, since the presence of the analyte is immediately transduced into a colorimetric change. Since the chemical properties of polymers lead to diverse affinities, the volatiles distribute differently in the two stripes.

To compare the response of different VOCs it is useful to plot the indicator response in the middle point of each path, as shown in the inset of Figure 5.6. In this way it is possible to appraise the different dynamics of compounds along the track. The magnitude and the dynamic of the signals result from the combination of the affinity of the VOC with both the polymer and the ZnTPP. It is interesting to note that also when responses are similar in magnitude they differ in time behaviour and vice versa.

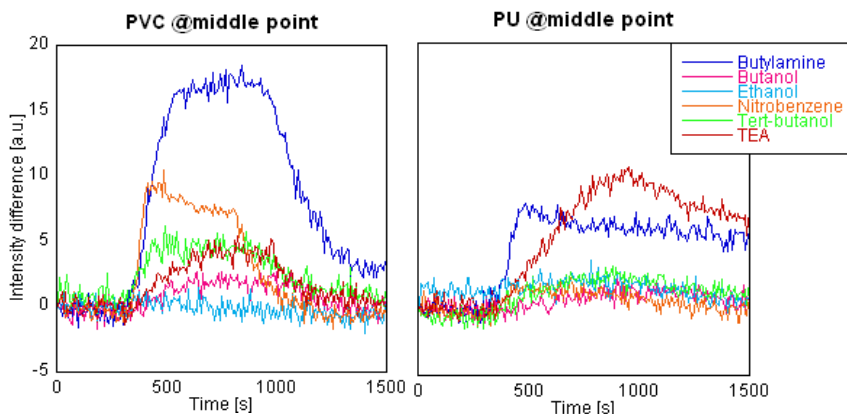


Figure 5.6. Time evolution of the response of the sensitive dye at the central position of PVC (left) and PU (right) strips.

The response of a single indicator in the two polymeric matrices, together with its dynamic trend, provides enough information for a good discrimination among tested compounds.

5.6 Bi-dimensional separation layer

In this set of experiments we implement a system which more closely resembles the olfactory mucosa than earlier attempts. The porphyrin indicator is dispersed in a two-dimensional layer, where one half is covered with PVC and the other with polyurethane. The gas entrance is located in the middle of the layer and a continuous detection of gases diffusing through the sensing layer is possible. The analysis of

the spatio-temporal pattern of responses that allows for the identification of gases will be illustrated.

5.6.1 Experimental

The artificial olfactory epithelium was designed combining onto a substrate a polymer with an optical indicator. A polymer layer was deposited onto the surface of a circular (25 mm diameter) transparent substrate (Thermanox plastic coverslip provided by Nunc). The layer was divided in two semicircles each formed by polymers with different partition properties with respect to the volatile compounds. The first polymer was a plasticized polyvinylchloride (PVC) (membrane composition in weight: 33% PVC, 67% bis(2-ethylhexyl)sebacate) and the second was polyurethane (PU). Both polymers were dissolved in 1 ml of tetrahydrofuran (THF) and 50 μ l of each solution were deposited by solvent casting onto the transparent substrate, thus forming a membrane that coats both the semicircles.

A tetrapyrrolic macrocycle, Zinc(5,10,15,20-tetraphenylporphyrin) [ZnTPP], was chosen as colorimetric indicator. A solution of 1 mg of porphyrin was dissolved in 1 ml of chloroform. The solution was then sprayed onto the polymeric layer in order to assure an even distribution. Chloroform presence is expected to locally dissolve the deposited polymer and to allow the diffusion of the porphyrins through the polymers. The porphyrin functionalized polymers were covered with a

second coverslip endowed with a central hole to allow the diffusion of vapours from the air to the sensing layer.

The substrate was placed in a measurement cell with transparent gas-tight windows. The sensing layer was illuminated by a standard LCD computer monitor (Philips 170S4) and imaged, in transmission mode, by a computer camera (Philips SPC900NC). A schematic diagram of the experimental set-up is shown in Figure 5.7. Since the chosen colour indicator undergoes colour changes mainly in the green spectral range, all measurements were done illuminating the sensing layer with green [0 255 0] light. The camera was used with the resolution of 320*240 pixels and images were captured with a sampling time of 5 s.

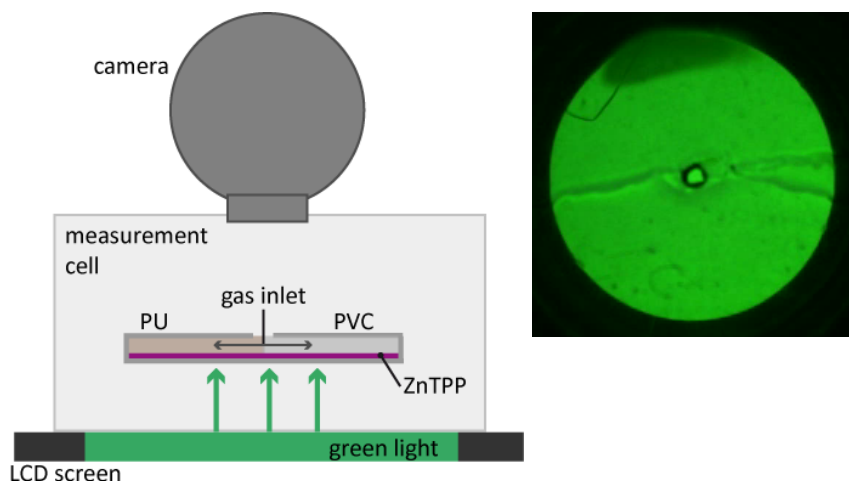


Figure 5.7. a) Schematic diagram of the experimental set-up b) image of the sensing layer with a green illumination.

The sensitive layer was tested under exposures to vapours of alcohols (methanol, ethanol, and butanol) and amines (butylamine, dimethylamine, trimethylamine, and triethylamine). In order to compare the responses, the sensing layer was exposed to 500 ppm in nitrogen of each volatile compound. The concentration was achieved diluting the saturation vapours at room temperature in a nitrogen flow. Dilution factor was kept constant by a mass flow controller (provided by MKS). Saturated vapour pressures were evaluated from Antoine's law using the parameters provided by the NIST library³⁸.

To study the partition properties of porphyrin functionalized polymers, they were also deposited on the surface of a mass sensitive transducer such as the quartz crystal microbalances (QMB)³⁹. QMBs were AT-cut quartz prepared in order to have a fundamental frequency of about 20 MHz. Quartz coating was obtained via casting with a pipette on both side of the quartz. The coating mass corresponded to a total frequency shift of 30KHz. The QMBs were exposed to the same vapour concentration used for optical measurements.

5.6.2 Results

The experiments were aimed at imaging the separation of the volatile compounds while they diffuse through the sensing layer, made of a colour indicator dispersed in two different polymers. The colour indicator (in this case the ZnTPP) transduces the presence and the adsorption of volatile compounds into a variation of its optical

transmittance spectrum. Polymers, on the other hand, are transparent and optically inactive and their role is to select the amount and the species of volatile compounds that interact with the sensing molecule.

A first experiment was designed to investigate how partitioning properties of polymers might separate compounds diffusing through the sensing layer. For this reason, two polymers with substantially different chemical properties were selected to coat the sensing layer. A preliminary analysis of raw data allows to assess the different partitioning in the two polymers. The distribution of volatile molecules was evaluated by the colour changes occurring in individual pixels in the sensing surface. Results are shown in a colour coded map as the difference between the image taken after 500 seconds of exposure and the first frame acquired when the layer was exposed to pure nitrogen. It is possible to observe that the exposure to a homologous series of alcohols with increasing carbon chain length (methanol, ethanol, and butanol) leads to the same partitioning in the two polymers (Figure 5.8a), while each compound evidences a different response intensity and dynamics. On the contrary, considering a set of amines, a different partitioning in the two polymers takes place (Figure 5.8b). In these examples, dimethylamine (DMA) diffusion is similar in both the polymers, while butylamine and triethylamine (TEA) partition with a lower ratio in PU-based membrane and trimethylamine (TMA) diffuses almost exclusively in the PVC-based membrane.

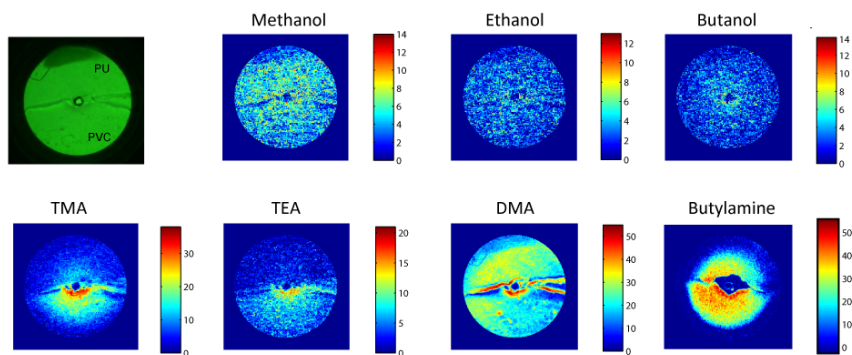


Figure 5.8. On the left top angle, it is shown the image of the layer acquired with the computer camera. The upper part is coated by PU, and the lower part contains the PVC layer membrane. The other figures contain the colour coded map of the layer response, calculated as the difference between the first and the last frame. Alcohols are uniformly distributed while amines are concentrated in the PVC coated side and are characterized by larger signals.

In order to evaluate the response as a function of the position in the sensing layer, 17 half-ring shaped regions of interest (ROIs) with a width of 5 pixels at increasing distance from the centre of the substrate were defined as shown in Figure 5.9. The average intensity of all the pixels contained in the ROI was calculated. The intensity of the first frame was used as a reference and subtracted from the signal time evolution.

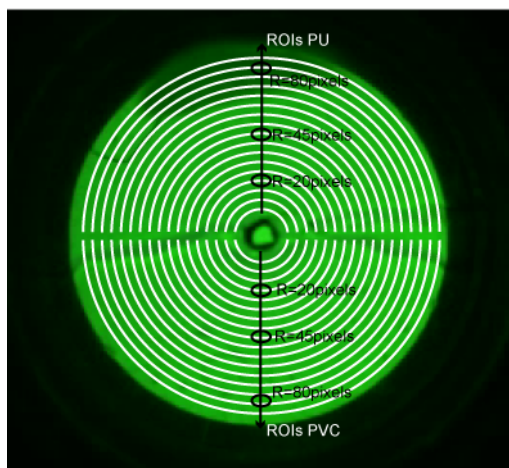


Figure 5.9. The imaged layer has been divided in 34 ROI, 17 per each polymer to study the spatio-temporal response of the sensing layer.

As a demonstration of the separation ability of the polymeric layer, the intensity in three different ROIs, one close to the gas inlet, one in the middle and one at the periphery of the layer (evidenced in Figure 5.9), are compared in Figure 5.10. Indeed, along the path vapours are selectively delayed thanks to the retentive effect carried out by the polymers.

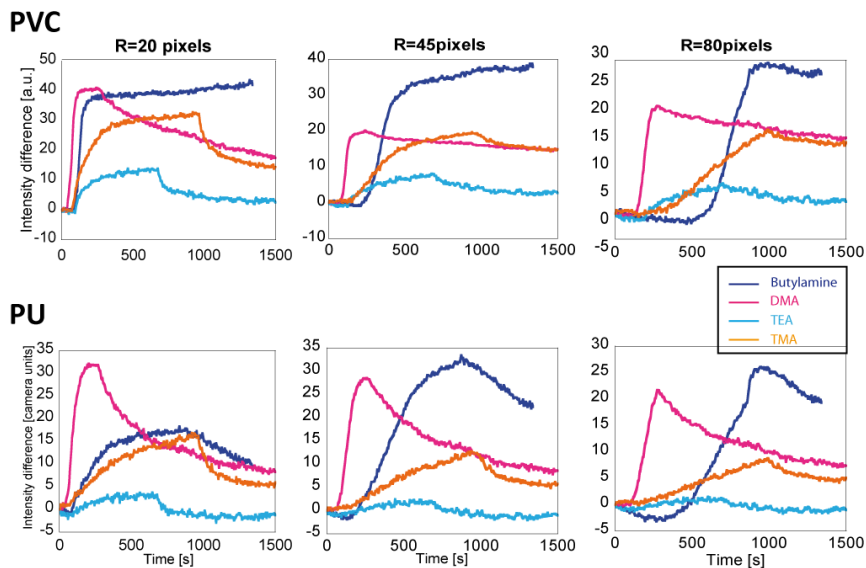


Figure 5.10. Time evolution of the response to the four amines in three ROIs whose position, shown in the inset, are close to the inlet, intermediate and at edge of the layer. Increasing the distance from the inlet, the response curves are separated in intensity and in time delay.

It is worth to observe that in the region close to the gas inlet ($R=20$ pixels), the response time evolution likely depends only on the indicator dynamics. In this regard, the temporal behaviour of the four amines does not show significant differences and no additional information can be extrapolated from the signals time evolution. Increasing the distance from the gas inlet, due to the delaying effect of the polymers, a larger separation of the peak response is observed. At the intermediate region ($R=45$ pixels) the vapours are partially separated, while at the peripheral region ($R=80$ pixels) the temporal

response to the four amines experiences the largest separation. In PVC-based membrane, for instance, the butylamine response is delayed by 920 seconds, while DMA response is delayed only by 270 seconds.

In Figure 5.11 the porphyrin response at the same locations is plotted for three representative substances separately. Spatio-temporal patterns arising in the layer response depend on the different permeability and diffusivity of PVC and PU. In the two semicircles of the layer, different dynamics are observed, confirming different partitioning phenomena and peculiar diffusion rates in the two polymeric membranes. For both the polymers, a first-order dynamics is observed in the region close to the gas inlet, where the change in concentration is nearly instantaneous, and it depends on the coordination of the analyte with the chemical indicator. Increasing the distance from the centre, the latency of the onset transient increases, as a result of the travel time of the stimulus through the layer. Interestingly, since diffusion profile changes according to the stimulus, the onset latency, and hence the response shape, depends on the analyzed compound. Furthermore, the response profile depends on the diffusion through the polymer and hence on its chemical properties, as evidenced by the comparison of Figure 5.11. The increasing onset latency can be mathematically described by the convolution of the first-order indicator response and the dynamics of the chemical compound diffusion through the layer. This latency could be dependent upon the mass distribution constant, while the observed

decreasing steepness of the response might depend upon the effective diffusion coefficient.

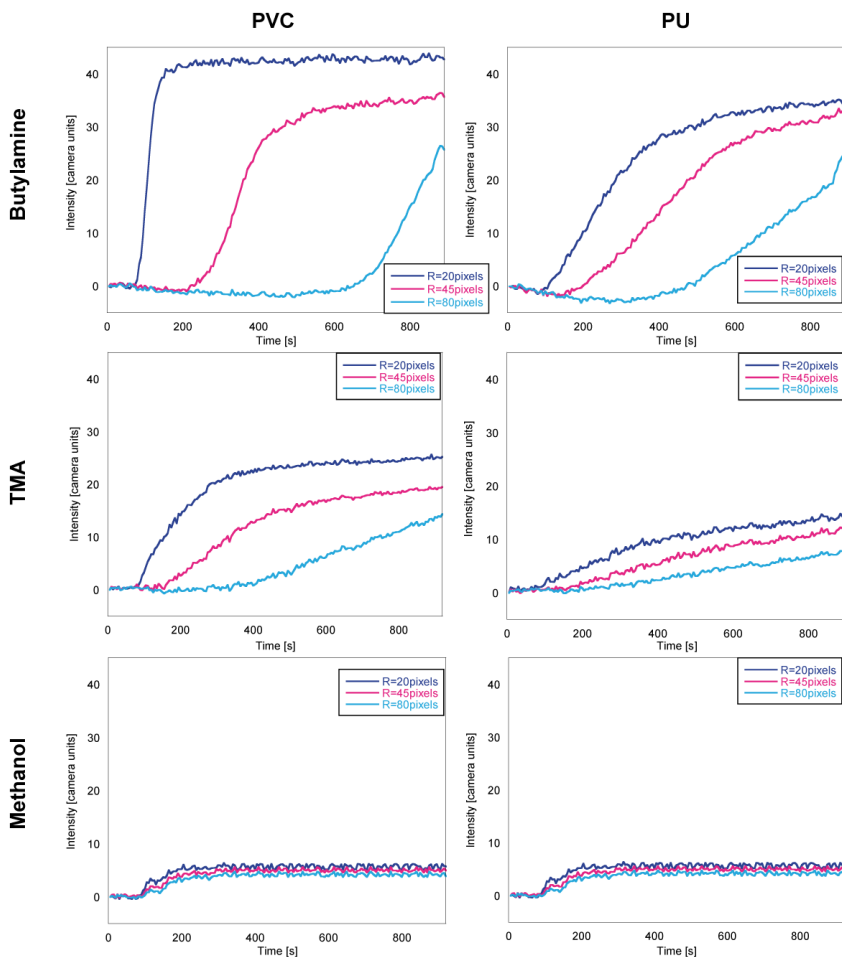


Figure 5.11. Time evolution of the signals in three ROIs in PVC and PU. The difference in the latency of the onset response increases with the distance from the gas inlet and it depends on the characteristics of the substance.

It is also noteworthy to analyze the desorption process that takes place when the chamber is cleaned with a pure nitrogen flow. In Figure 5.12 a complete phase of measure of TMA is shown for three ROIs located in different regions of the layer. It seems that two different phenomena take place when the nitrogen is blown to clean the layer. In the first part, the nitrogen flow cleans the polymer from the analyte molecules and a different dynamics characterize the three ROIs (in the graph between 1000 and 1600s). However, after a certain time (larger than 1600s), the analyte is removed from the polymer but some molecules are still bound to the porphyrin, because the time it takes to cease the binding between analyte and porphyrin is much longer. From this time on, the dynamic of all the ROIs is the same, because it does not depend on the polymer that is analyte-free, but it is exclusively ruled by the time it takes to the porphyrin to get rid of the analyte.

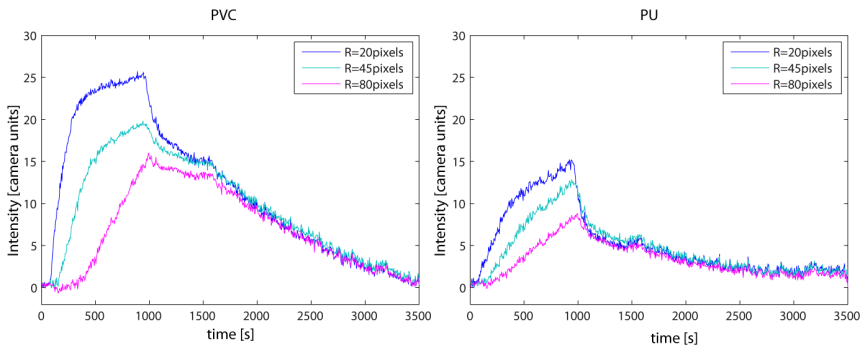


Figure 5.12. A complete measure of TMA for PVC and PU part of the layer, where the adsorption and desorption phases are shown.

A qualitative analysis of spatio-temporal data collected in these experiments was performed by means of a chemometric technique. To compare the behaviour of each polymer, the data have been divided in the PVC and PU part, and analyzed separately. Considering the time evolution of the camera signal for each ROI, the exposure to one gas sample produces, for each part, a data matrix formed by 17 ROI *100 measurements collected in a total of 500 s. The collection of measurements resulted then in two three-dimensional matrices. The matrix was analysed by Multiway Principal Component Analysis (MPCA)⁴⁰. In MPCA, a straight principal component analysis (PCA) is calculated on the unfolded three-dimensional matrix. In this case, for each measurement the operation of unfolding the matrix of ROI's time signals gives rise to a feature vector of 1700 components for each of the two parts.

In Figure 5.13a, the first two scores of MPCA related to PVC part of the sensing layer are plotted. Alcohols are rather clustered at the left hand side of the plot, while the amines are separated from alcohols but largely scattered. The contribution of original variables to the scores is called loadings. The analysis of loadings provides a simple and efficient tool to investigate the role of each variable in a multivariate problem. In the case here analyzed the original variables are the ROIs and the measurement time. In particular, the analysis of loadings is expected to indicate which ROI and at which time play the major role in VOCs

separation. For the scope, the loading vectors are folded back reconstructing the matrix that expresses the ROIs time-evolution.

The reconstructed loadings of the ROIs in the PVC part of the sensing layer are plotted in a colour code in Figure 5.13b. In the first loading the signal evolution is rather similar for all the ROIs, suggesting that the separation along the first principal component (axis x in Figure 5.13a) is mainly due to the different intensity of the response to amines and alcohols. Then, the difference among the test compounds is basically due to the different sensitivity of ZnTPP to the investigated volatile compounds. As expected the largest contribution to the first principal component comes from the initial ROIs close to the gas inlet.

On the contrary, all the ROIs contribute to the second principal component (y axis in Figure 5.13a), and for each ROI the time at which the maximum contribution occurs grows with the distance from the gas inlet. Actually, scores separated along the second principal component are characterized by different diffusion rates, being DMA in the upper part the fastest and butylamine in the lower part, one of the slowest. This behaviour indicates that MPCA splits in the two principal components the contribution of the interaction of the VOCs with the indicator and the contribution due to the diffusion of VOCs through the polymers.

The magnitude of the variance expressed by each principal component, visible in the labels of Figure 5.13a, indicates that about 76% of the total variance is due to the interaction of volatile compounds

with the chemical indicator (ZnTPP) and that 22% is the contribution of the polymers forming the two sensing layers. This result provides practical evidence that most of the recognition capabilities are due to the indicator properties and that the polymer plays an auxiliary function. This resembles the ancillary role of the mucosa in natural olfaction.

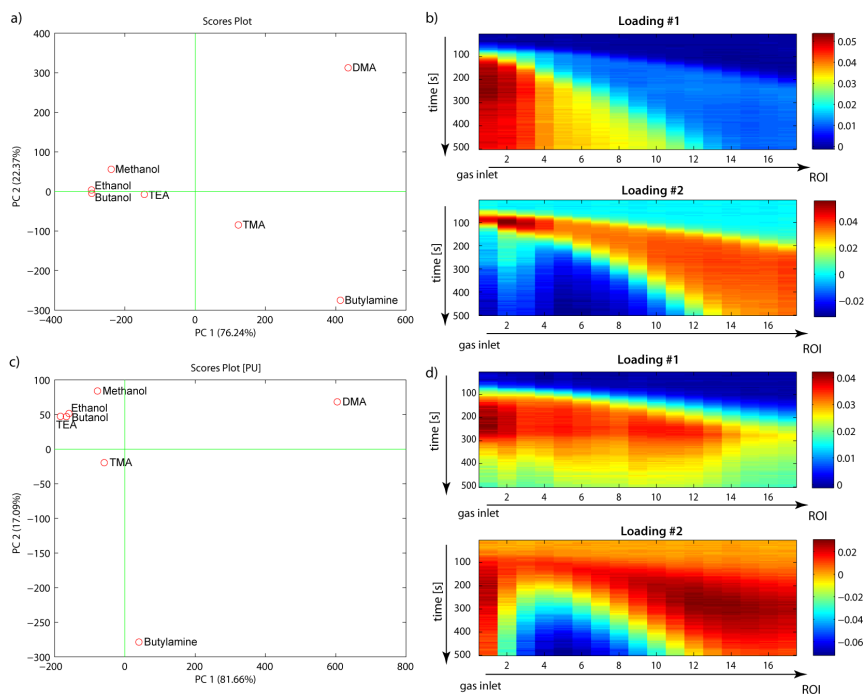


Figure 5.13. Results of the multiway principal component analyses applied to the signals obtained with the PVC and PU layers separately. In both cases the first two principal components are shown. **(a)** and **(b)** show the scores and the loadings of the PVC coated part of the sensing layer, and **(c)** and **(d)** show the scores and loadings of the PU coating part.

Different results are obtained with the ROIs of the PU part. Figure 5.13c shows the scores where, in respect to the PVC data a less sharp separation between alcohols and amines is observed. Larger differences are observed in the reconstructed loadings matrix (Figure 5.13d). PU ROIs do not show a clear separation between indicator and polymer effect suggesting the existence of some competitiveness between the polymer and the indicator modifying the efficiency of the indicator transduction. This result indicates that a sort of optimal coupling between indicator and polymer can be found and that in general both the indicator and the polymer contribute to the overall recognition capabilities.

In both cases, MPCA evidences that colour change signals are dominated by the properties of ZnTPP where the interaction with amines produces larger colour change with respect to alcohols. In order to study the effective distribution of volatile compounds in the sensing layers the properties of polymers and indicator were separately evaluated with a mass transducer. To do so, quartz crystal microbalances (QMB) were coated with layers of the above-mentioned polymers (plasticized PVC and PU including the ZnTPP indicator), and exposed to the test compounds at the same concentrations (500 ppm) in nitrogen gas used in the previously discussed experiments. In both cases the coating corresponded to a frequency shift of about 30kHz. Table 5.1 lists the frequency shifts observed as a consequence of the exposure to 500 ppm of the test compounds. QMB responses confirm the

considerations based on optical analysis. Mixtures of ZnTPP with PVC and PU polymers show about the same response to alcohols while in the case of amines the response of ZnTPP in PVC is more than twice that of ZnTPP in PU. These results indicate that the concentration of amines in PVC is greater than in PU, justifying the larger optical response to amines visible in Figure 5.8.

Table 5.1. Frequency shifts of QMB coated with porphyrins mixed with PVC and PU. Frequency shifts are in Hz, and the uncertainty range is estimated from a series of three repeated measurements.

	ZnTPP-PVC Δf [Hz]	ZnTPP-PU Δf [Hz]
Ethanol	69.7 ± 4.7	91 ± 9.5
Butanol	115.7 ± 3.5	93.5 ± 2.6
Methanol	76 ± 1.5	89.7 ± 3.5
TEA	207 ± 16.7	128 ± 9.2
TMA	162.7 ± 9.1	63.7 ± 4.4
DMA	335.7 ± 14.6	132.3 ± 11.2
Butylamine	749 ± 24	232 ± 12

5.6.3 Discussion

The use of spatial-temporal patterns to increase the discrimination of odours was demonstrated by Gardner and co-workers^{34,35} in a one dimensional system with discrete chemical sensors applied in principle along a chromatographic column. In our approach the chemically

sensitive elements (the colour indicators) are dispersed in the polymer allowing continuous response images to be captured and used for evaluation purposes. Such a system is also close to the arrangement of receptors in the olfactory mucosa.

MPCA of optical measurements shows a clear discrimination between the analyzed compounds and offers the chance for the identification of the mechanisms underlying the recognition of them. First, the magnitude of the indicator spectral changes, due to shifts in the visible absorbance spectrum caused by the coordination of the analyte with the ZnTPP, plays the major role. Moreover, the contribution of spatio-temporal patterns characteristic for the presented platform needs also to be considered. Mechanisms that give rise to spatio-temporal patterns may depend on various factors that cause a stimulus-specific response dynamics. Among these, the intrinsic membrane dynamics takes into account the time necessary to permeate the polymer and interact with the porphyrin molecules. PVC and PU membranes show different permeability and partitioning properties, causing a spatial pattern of response due to a different amount of vapours that is allowed to permeate and interact with the indicator. The gas delivery setup combined with the spatial distribution of the sensing molecule contributes to the manifestation of the spatio-temporal patterns. The retentive effect carried out by the polymeric coatings can be compared to the one performed by the stationary phase in a chromatographic column or by the mucous layer in the olfactory epithelium. Each

molecule is then characterized by a specific time of flight that depends on the strength of the interactions with the polymeric phase and on its intrinsic diffusion coefficient. The combination of these factors can hence increase the information content in collected data, improving the performances of gas detecting systems. In addition, the delaying effect of the polymer favours the detection of those compounds that might be undistinguishable with a pure optical sensing approach. As we have seen in the case of aliphatic alcohols with increasing carbon chain, even if they elicit similar response intensity, identification might be obtained thanks to the different response dynamics along the layer. Moreover, a proper choice of polymer chemical properties allows to modulate the partitioning and delaying effects of the layer, and extends the range of volatile compounds that can be detected and identified. Odour discrimination in the mammalian nose depends both on the intrinsic properties of the olfactory receptors, the zonal nature of the distribution of the receptors in the mucosa as well as the transport of the odorants in the mucosa.

5.7 Conclusions

The development of artificial olfaction systems is based on the emulation of the features of the biological olfaction, such as the large number of non-specific receptors or bio-inspired processing algorithms.

Among these, an interesting feature that may enhance odour discrimination is the spatial distribution of the responses in the mucosa due both to a zonal distribution of receptors and to a chromatographic-like process carried out by the mucous coating. In this paper, a method to incorporate the gas-chromatographic separation principle in a gas identification system has been proposed. The system combines the separation properties of continuous polymeric layers with the sensitivity of chemical colour indicators. Colour changes are measured with the CSPT platform where a computer monitor is used as a programmable light source and a computer camera as a detector.

Optical imaging offers the possibility to simultaneously measure a large amount of sensors, virtually one per image pixel, and to create a map of odour distribution in a continuous sensing layer. In the adopted configuration, odour molecules diffuse through a polymeric layer acting as the stationary phase, delaying volatile compounds on the basis of their physico-chemical properties and diffusion rates. It was demonstrated that, using this strategy, each compound gives rise to a characteristic spatio-temporal distribution of the responses in the layer that depends on the molecule. The layer was tested with different volatile compounds of the families of amines and alcohols. Multiway chemometrics analysis indicates that the identification of the molecular family is largely due to the sensitivity of the colour indicator while the identification inside each class is mainly due to the properties of the polymer layers. As a result, in the proposed system a synergy between

the two effects is obtained in analogy to what found in natural olfaction. Furthermore, by using several different colour indicators with proper distributions in the polymeric layers the zonal nature of natural olfaction may be mimicked, i.e. through a combination of the findings in the present communication and in a previous paper⁴¹ by our group. The intention of the present work was, however, to clearly demonstrate the influence of diffusion on odour discrimination in our experimental system.

Our experimental evidences may be used to implement novel features for advances in artificial olfaction and, under proper design, as a tool to test models of the influence of zonal distribution of receptors in biological olfaction and better understand mechanisms underlying odour discrimination.

References

- ¹ S. Korsching, Olfactory maps and odor images, *Curr. Opin. Neurobiol.* 12 (2002) 387–392
- ² B. Malnic, J. Hirono, T. Sato, L. B. Buck, Combinatorial receptor codes for odors, *Cell* 96 (1999) 713-723
- ³ G. Sicard, A. Holley, Receptor cell responses to odorants: similarities and differences among odorants, *Brain research*, 292 (1984) 283-296
- ⁴ K. Persaud, G. Dodds, Analysis of discrimination mechanisms in the mammalian olfactory system using a model nose, *Nature* 299 (1982) 352–355
- ⁵ H. Spors, A. Grinvald Spatio-Temporal Dynamics of Odor Representations in the Mammalian Olfactory Bulb, *Neuron* 34 (2002) 301–315
- ⁶ P.F. Kent, M.M. Mozell, S.L. Youngentob, P. Yurco, Mucosal activity patterns as a basis for olfactory discrimination: comparing behavior and optical recordings, *Brain Research* 981 (2003) 1–11
- ⁷ M. Tswett, *Ber. Dtsch. Botan. Ges.* 24 (1906) 316–323.
- ⁸ W. Jennings, E. Mittlefehldt, P. Stremple, *Analytical Gas Chromatography*, Second Edition, (1997)
- ⁹ P. Marriott, R. Shellie, Principles and applications of comprehensive two-dimensional gas chromatography, *Trends Anal. Chem.* 21 (2002) 573-583
- ¹⁰ K. Mori, H. Nagao, Y. Yoshihara, The Olfactory Bulb: Coding and Processing of Odor Molecule Information, *Science* 286 (1999) 711-715
- ¹¹ M. M. Mozell, P. R. Sheehe, D. E. Hornung, P. F. Kent, S. L. Youngentob, S. J. Murphy, "Imposed" and "Inherent" Mucosal Activity Patterns - Their Composite Representation of Olfactory Stimuli, *J. Gen. Physiol.* 90 (1987) 625-650

¹² K. J. Ressler, S. L. Sullivan, L. B. Buck, A Zonal Organization of Odorant Receptor Gene Expression in the Olfactory Epithelium, *Cell* 73 (1993) 597-609

¹³ J. W. Scott, D. E. Shannon, J. Charpentier, L. M. Davis, C. Kaplan, Spatially Organized Response Zones in Rat Olfactory Epithelium, *J. Neurophysiol.* 77 (1997) 1950-1962

¹⁴ E .D. Adrian, Sensory discrimination with some recent evidence from the olfactory organ, *Br. Med. Bull.* 6 (1950) 330–331

¹⁵ E .D. Adrian, Olfactory discrimination, *Ann. Psychol.* 50 (1951) 107–130

¹⁶ M. M. Mozell, Evidence for a chromatographic model of olfaction, *J. Gen. Physiol.* 56 (1970) 46-63

¹⁷ M. L. Getchell, T. V. Getchell, Fine structural aspects of secretion and extrinsic innervation in the olfactory mucosa, *Microsc. Res. Tech.* 23 (1992) 111-127

¹⁸ L. Tcatchoff, C. Nespoulous, J. C. Pernollet, L. Briand, A single lysyl residue defines the binding specificity of a human odorant-binding protein for aldehydes, *FEBS Lett.* 580 (2006) 2102-2108

¹⁹ J. Laughlin, T. Soo Ha, D. Jones, D. Smith, Activation of pheromone-sensitive neurons is mediated by conformational activation of pheromone-binding protein, *Cell* 133 (2008) 1255-1265

²⁰ L. Briand, C. Eloit, C. Nespoulous, V. Bezirard, J. Huet, C. Henry, F. Blon, D. Trotier, J. Pernollet, Evidence of an odorant binding protein in the human olfactory mucus: location, structural characterization, and odorant binding properties, *Biochemistry* 41(2002) 7241-7252

²¹ D. G. Moulton, Spatial Patterning of Response to Odors in the Peripheral Olfactory System, *Physiol. Rev.* 56 (1976) 578-593

²² P. F. Kent, M. M. Mozell, S. J. Murphy, D. E. Hornung, The Interaction of Imposed and Inherent Olfactory Mucosal Activity Patterns and their Composite Representation in a Mammalian Species Using Voltage-Sensitive Dye, *J. Neurosci.* 16 (1996) 345-353

- ²³ M. M. Mozell, M. Jagodowicz, Chromatographic Separation of Odorants by the Nose: Retention Times Measured across in vivo Olfactory Mucosa, *Science* 181 (1973) 1247-1249
- ²⁴ A. T. Schaefer, T. W. Margrie, Spatiotemporal representations in the olfactory system, *Trends in Neurosciences* 30 (2007) 92-100
- ²⁵ T. A. Schoenfeld, T. A. Cleland, Anatomical Contributions to Odorant Sampling and Representation in Rodents: Zoning in on Sniffing Behavior, *Chem. Senses* 31 (2006) 131-144
- ²⁶ J. W. Scott, Sniffing and Spatiotemporal Coding in Olfaction, *Chem. Senses* 31 (2006) 119-130
- ²⁷ I. Heberle, A. Liebminger, U. Weimar, W. Göpel, Optimised sensor arrays with chromatographic pre-separation: characterisation of alcoholic beverages, *Sens. Actuators B* 68 (2000) 53-57
- ²⁸ T. Eklöv, I. Lundström, Gas mixture analysis using a distributed chemical sensor system, *Sens. Actuators B* 57 (1999) 274-282
- ²⁹ T. Eklöv, H. Sundgren, I. Lundström. Distributed chemical sensing, *Sens. Actuators B* 45 (1997) 71-77
- ³⁰ I. Lundström, Artificial olfactory images from a chemical sensor using a light-pulse technique, *Nature* 352 (1991) 47-50
- ³¹ K. Zhao, P. W. Scherer, S. A. Hajiloo, P. Dalton, Effect of Anatomy on Human Nasal Air Flow and Odorant Transport Patterns: Implications for Olfaction, *Chem. Senses* 29 (2004) 365-379
- ³² S. E. Stitzel, D. R. Stein, D. R. Walt, Enhancing Vapor Sensor Discrimination by Mimicking a Canine Nasal Cavity Flow Environment, *J. Am. Chem. Soc.* 125 (2003) 3684-3685
- ³³ T. A. Dickinson, D. R. Walt, J. White, J. S. Kauer, Generating Sensor Diversity through Combinatorial Polymer Synthesis, *Anal. Chem.* 69 (1997) 3413-3418

³⁴ J. W. Gardner, J. A. Covington, S. L. Tan, T. C. Pearce, Towards an artificial olfactory mucosa for improved odour classification, *Proc. R. Soc. A* 463 (2007) 1713-1728

³⁵ J.A. Covington, J.W. Gardner, A. Hamilton, T.C. Pearce, S.L. Tan, Towards a truly biomimetic olfactory microsystem: an artificial olfactory mucosa, *IET Nanobiotechnol.* 1 (2007) 15–21

³⁶ M. A. Sánchez-Montañés, J. W. Gardner, T. C. Pearce, Spatio-temporal information in an artificial olfactory mucosa, *Proc. R. Soc. A* 464 (2008) 1057-1077

³⁷ F.K. Che Harun, J.E. Taylor, J.A. Covington, J.W. Gardner, An electronic nose employing dual-channel odour separation columns with large chemosensor arrays for advanced odour discrimination, *Sens. Actuators B* 141 (2009) 134-140

³⁸ www.nist.gov/webbook

³⁹ D.S Ballantine, R.M. White, S.J. Martin, A.J. Ricco, E.T. Zellers, G.C. Frye, H. Wohltjen, Acoustic wave sensors, Academic Press, San Diego, CA, USA (1997)

⁴⁰ Henrion R., N-way principal component analysis theory, algorithms and applications, *Chemometrics and Intell. Lab. Syst.* 25 (1994) 1-23

⁴¹ C. Di Natale, E. Martinelli, R. Paolesse, A. D'Amico, D. Filippini, I. Lundström, An Experimental Biomimetic Platform for Artificial Olfaction, *PLoS ONE* 3 (2008) e3139(10pages)

Chapter 6: Artificial Olfaction Platform

6.1 Introduction

An application that took its lead from previous observations concerns the implementation of a platform for artificial olfaction. Since the pioneering work of Persaud and Dodds¹, a great number of artificial olfaction system (or electronic noses) have been proposed. Later on, progresses in electronic noses were mainly focused on the development of artificial receptors. However, receptor properties are only one of the aspects of the rich structure in biological olfaction, while other important features, such as the large number of olfactory receptor neurons, their hierarchical organization, the odour patterns in the olfactory bulb², and the odour diffusion along the olfactory epithelium³ have been far less considered. An interesting challenge is to extend the similarities among natural and artificial systems by trying to mimic these aspects as well. In this regard, image sensors are extremely interesting to be used for large sensor arrays development⁴.

In this work, an image sensor such as a computer camera is used to acquire a stream of pictures of a sensitive surface coated by a layer of

chemical indicators. The camera provides a segmentation of the whole sensing layer in a number of elementary units corresponding to the image pixels. Each pixel averages the optical properties of a small volume of the sensing layer and can be considered independent. In analogy to the fact that one olfactory receptor neuron (ORN) in the epithelium expresses only one receptor gene⁵, each pixel of the image may be regarded as an artificial receptor neuron and the output signal from such a neuron is the change in the optical properties of the pixel caused by the odour. This approach offers also the possibility to further develop artificial olfactory structures introducing a layer of glomeruli. Glomeruli are one of the most important units in the olfactory system, where signals from receptor neurons of the same kind are elaborated for further coupling to higher levels in the brain⁶.

The idea of our work is to classify each receptor according to its optical properties into a class that defines its characteristics. This approach resembles the association between ORNs carrying the same chemical receptors into the same glomerulus^{7,8,9}. A representation of the analogy between the wiring scheme of our system and the olfactory system is provided in Figure 6.1. Once the sensors are assigned to a class, signals from artificial receptors belonging to the same class are treated altogether in higher processing levels.

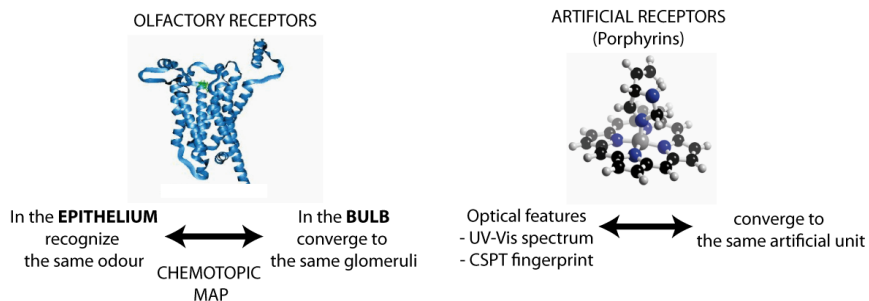


Figure 6.1. Schematic representation of the parallel among natural wiring and artificial wiring proposed in our approach.

Walt and co-workers, dealing with image sensor arrays, proposed a processing unit inspired to the glomeruli layer. Their system uses self-encoded associations between individual artificial receptors, corresponding to the area of fibre tips as detected by the image sensor. Therein, the association is determined according to the similar responses to a test gas and since the receptors are non selective, changes in the kind of test gas may result in a different arrangement¹⁰.

In our approach, even if it is possible to conceive any theoretical description of the glomeruli layer working principle, a simple transfer function is applied so that the glomerulus output is the instantaneous sum of the convergent ORNs signals.

Another important characteristic of natural olfaction is related to the spatial distribution of ORNs where longitudinally oriented zones of genes expressions running along the flow path are found¹¹ that provide a pattern in the epithelium response. To emulate this feature, the available area was divided into sub-regions. Four zones parallel to the gas flow

were prepared where only two indicators were deposited. Moreover, in biological epithelium receptors are embedded in a diffusive media forming the so-called olfactory mucosa. When diffusing through the mucosa, odorant molecules are separated according to a gas-chromatographic principle. To incorporate this property, the sensing molecules are dispersed in a polymer membrane that is sandwiched between two transparent sheets.

In the next paragraphs the steps that allowed for the development of an artificial olfaction platform will be described.

6.2 Experimental

Colour indicators used in these experiments were six metal complexes of the (5,10,15,20 -tetraphenylporphyrin), namely (5,10,15,20 - tetraphenylporphyrin) palladium [PdTPP], (5,10,15,20-tetraphenylporphyrin) rhodium [RhTPP], (5,10,15,20 - tetraphenylporphyrin) zinc [ZnTPP], (5,10,15,20-tetraphenylporphyrin) molybdenum [MoTPP], (5,10,15,20 -tetraphenylporphyrin) iron [FeTPP], (5,10,15,20-tetraphenylporphyrin) manganese [MnTPP], a Silicon (phthalocyanine) [SiPC], and the Nile blue.

Indicators were dispersed in membranes based on plasticized poly(vinyl chloride) [PVC] (membrane composition in weight: 1%indicator, 33% PVC, 66% bis(2-ethylhexyl)sebacate [DOS])

dissolved in a tetrahydrofuran (THF) solution. The artificial epithelium was prepared onto a 25 mm diameter transparent substrate, a Thermanox plastic coverslip provided by Nunc. A membrane made of PVC, (composition in weight 33%PVC, 67% DOS), was pipette casted onto the coverslip to fully coat its surface. This polymeric layer is intended to mimic the function of the mucous coating that covers neuron cilia in the olfactory epithelium and it also provides a continuous connection layer where the gases can diffuse.

Each indicator membrane was randomly spotted onto the PVC layer in few replicas. The available area was divided into four regions parallel to the gas flow where only two indicators were deposited. 5 μ l of membrane solution were collected and several drops were arbitrarily released in the related area. THF present in the drop slightly dissolves the underlying PVC, allowing for a partial merging of the indicator membrane in the polymeric layer. A uniform path for gas diffusion through the artificial epithelium is then formed. The appearance of the epithelium is displayed in Figure 6.2, where the four zones are also evidenced.

Polymeric membranes of the eight chemical reporters were deposited onto a glass slide in order to measure the absorbance spectra with a UV-Vis spectrophotometer (Varian Cary 500). For comparison, spectra of chloroform liquid solutions were also acquired.

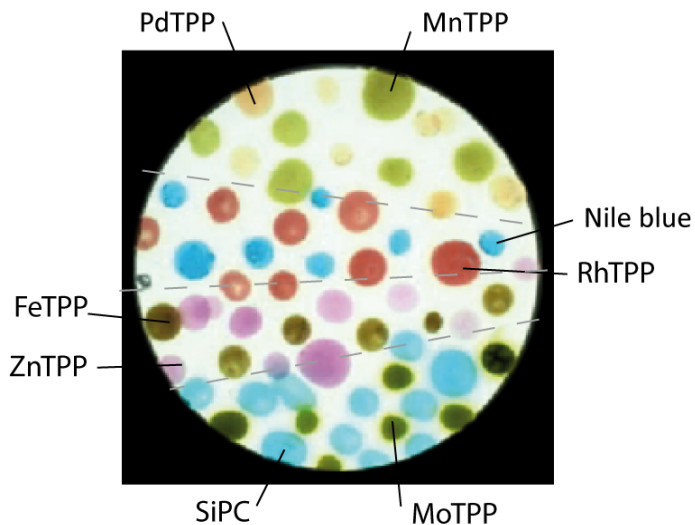


Figure 6.2. Appearance of the artificial epithelium as acquired by the webcam. The sample is ideally divided into four zones where only two indicators are present.

The artificial epithelium was placed in a transparent cell with gas-tight windows equipped with tube connectors to the gas delivery system. The cell was illuminated through transparent openings with a LCD computer monitor (Philips 1704S) and imaged with a digital camera (Philips SPC900NC). A diagram of the experimental arrangement is shown in Figure 6.3. A 50 colours sequence gradually changing from red to blue was used for fingerprinting the optical properties of indicators.

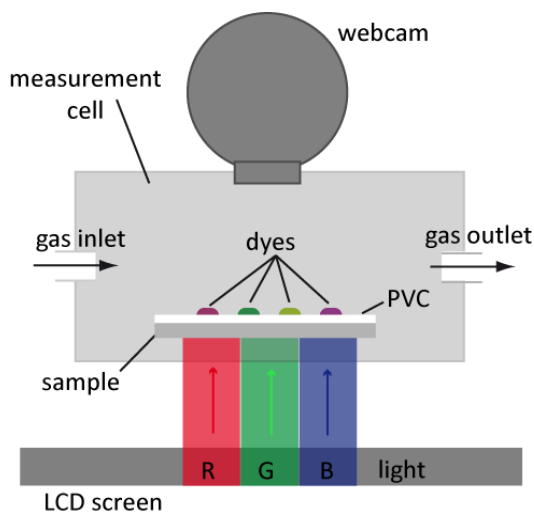


Figure 6.3. Schematic diagram of the experimental arrangement.

For subsequent measures, a sequence of pure red (255 0 0), green (0 255 0), and blue (0 0 255) colours was chosen to illuminate the sample in order to probe optical variations of sensing layers under the exposure to vapours. The response of the epithelium platform was tested exposing the sample to different odours. Vapours were flowed in the measurement cell with a three channels gas delivery system and dilutions were regulated with mass flow controllers (MKS). Vapours of trimethylamine [TMA] (5%), triethylamine [TEA] (5%), butylamine (2%), ethanol (20%), butanol (20%), and mixtures of two alcohols, (butanol 20%-ethanol 20%), two amines (TEA 3% - TMA 5%), an amine and an alcohol, (TMA5% - ethanol 20%) were tested. Each measure cycle lasted 1500 seconds, with the absorption phase consisting

of 400s, and the images were acquired with a sampling time of 5 seconds. The camera was used at a resolution of 320x240 pixels, and frames were then resized to 160x120 averaging four contiguous pixels. A number of 7497 sensors resulted from the useful sensing area and was processed with the following algorithms.

6.3 Results

6.3.1 Considerations on spectral features

As roughly evidenced by the epithelium appearance in Figure 6.2, indicator dyes that were selected are characterized by well separated colours. This observation is confirmed by UV-Vis absorbance spectra of liquid solutions and solid state films, shown in Figure 6.4.

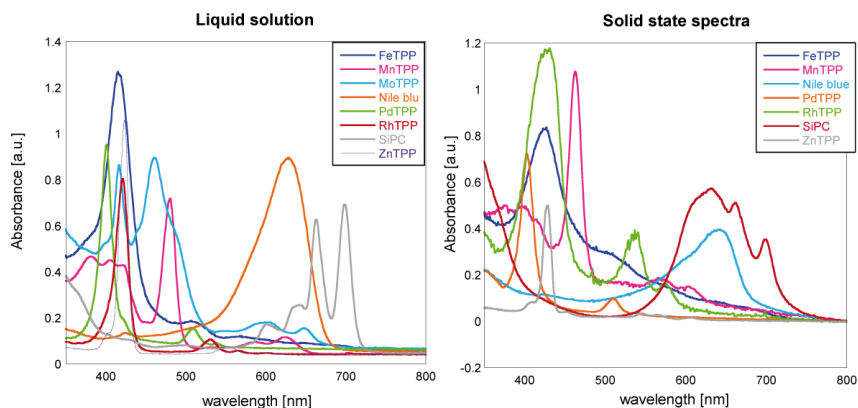


Figure 6.4. UV-Vis spectra of the colorimetric indicators used in liquid solution and in solid state films.

CSPT was used to characterize by an optical point of view the chemical properties of receptors that form the first stage of the sensing process. As described in the experimental section, the substrate was illuminated with a 50 colours sequence, and the images were simultaneously acquired by the webcam. Every image can be decomposed into its three components, corresponding to the red, green and blue camera filters. Each pixel is then described by 50*3 values that reflect its optical features. Figure 6.5 reports the CPST fingerprint of 7497 pixels contained in the useful area of the image. In principle only nine groups of spectra are expected (eight indicators and one for background), but a continuous distribution is found. This is essentially due to density non homogeneity in the spots and to a non uniform background light, attributable to screen imperfections and optical misalignments.

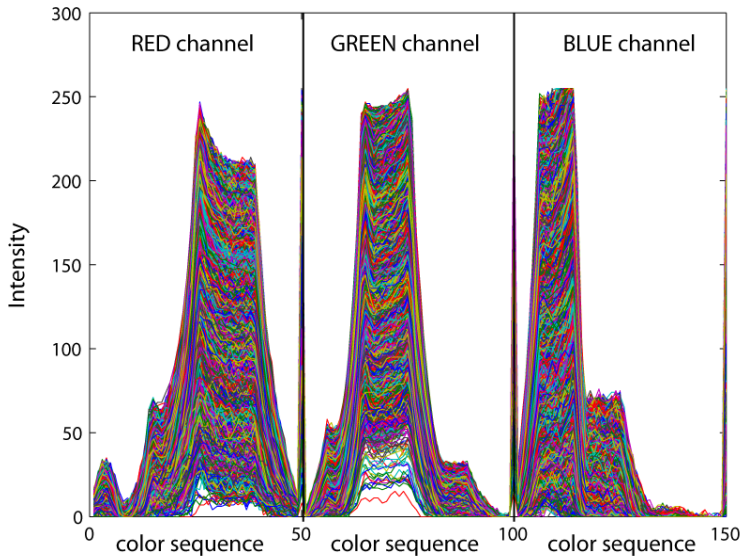


Figure 6.5. CSPT fingerprints of all pixels contained in the useful sensing area.

A Principal Component Analysis of spectral features and CSPT fingerprints reveals a good match among the two techniques (Figure 6.6). Herein, CSPT fingerprints are the average values of pixels containing the eight indicators. Coloured shapes indicate the corresponding visible colour of indicators. Scores, in both cases, are aligned along three directions that divide the principal components plane in equally spaced regions and that correspond to the perception of red, green and blue colours, as evidenced by the coloured shapes.

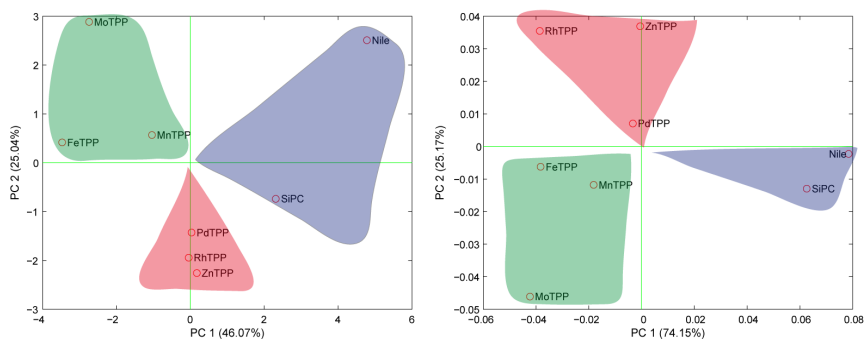


Figure 6.6. Scores plot of the average value of CSPT fingerprint (a) and UV-Vis absorption spectrum (B) for each colorimetric indicator.

6.3.2 Artificial olfactory bulb definition

Image pixels were classified depending on the optical features of chemical indicator contained in the imaged volume, according to the paradigm thoroughly discussed in a previous paper¹². The data matrix of CSPT fingerprints was linearly normalized in order to reduce background non-homogeneities and deposition variability. These heterogeneities can be taken into account with a certain scaling factor that multiplies the “true” intensity. The normalization consists of dividing the measured intensity for each illuminating colour by the sum of the intensities of all colours of the same pixel, so that the scaling factor may disappear.

$$\bar{I}_{ij} = \frac{I_{ij}}{\sum_j I_{ij}} \quad (6.1)$$

Each pixel was assigned to the corresponding class with a neural model: a self organizing map (SOM)¹³. A SOM is based on competitive unsupervised learning algorithms and offers the interesting feature of maintaining the topology of the input space into the output space. In this case a network constituted of $7 \times 7 = 49$ neurons arranged in a hexagonal topology was implemented. Weights were updated so that each neuron new weight vector is the weighted average of the input vector which the neuron and its neighbours responded with a maximum output. During the training phase the neighbourhood is gradually reduced down to one unit. The distance from one neuron is calculated as the number of steps that must be taken to get to the neuron under consideration.

As a result of the classification, every single pixel of the image is attributed to one neuron of the SOM according to the map in Figure 6.7. We regard this convergence as that occurring in natural olfaction between olfactory receptor neurons and glomeruli. SOM neurons are hereafter identified as sub-glomerular units. All pixels belonging to a certain class are then treated as a whole, and their signals are processed within these sub-glomerular units and subsequently they are sent to higher levels for further data analysis. Different processing strategy within the sub-glomerular units can be considered. In this case we chose to average all the signals afferent to the same neuron instead of summing the signals in order to reduce the influence of the number of pixels in each class. A schematic diagram of the artificial olfactory bulb as defined in this context is provided in Figure 6.8.

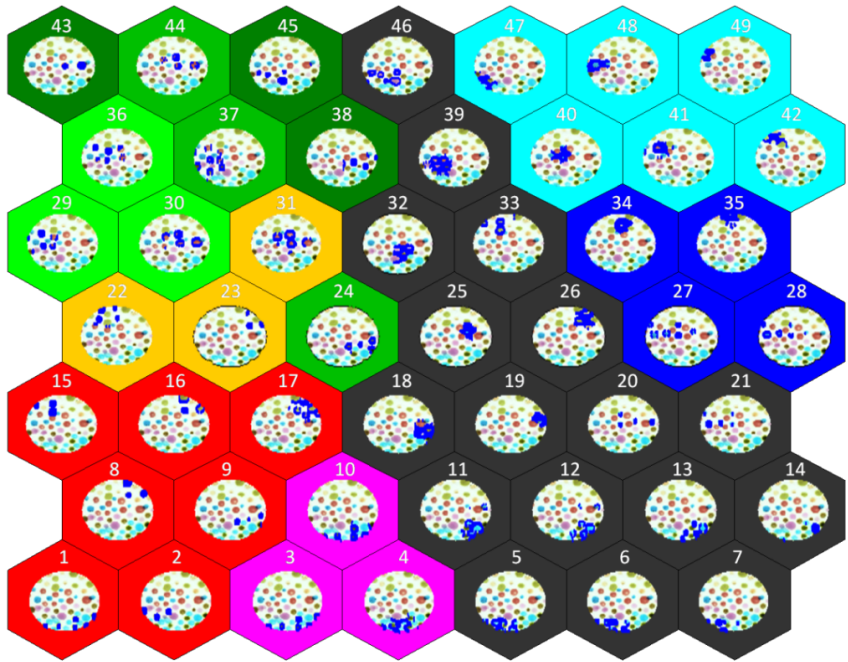


Figure 6.7. Matching between artificial receptors and output neurons in the SOM. Blue areas in the image mark the pixels attributed to the corresponding output neuron. The filling colour of each hexagon identifies the corresponding chemical indicator, whereas a grey filling represents background pixels.

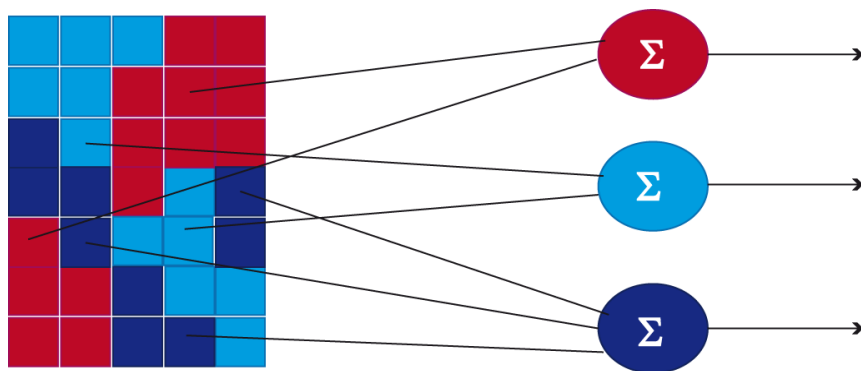


Figure 6.8. Schematic diagram of the matching between pixels and artificial glomeruli according to optical features.

6.3.3 Background removal

A previously proposed algorithm for fluorescence image processing was used to remove background fluctuations from the time trace of measurement data. The algorithm suggested by Schild and co-workers¹⁴ allows to estimate the background of a given region of interest by exploiting the information contained in the intensity dynamics of its individual pixels. Herein a ROI is defined as a subset of image pixels whose intensities may be analyzed as a whole. In our case, ROIs are identified with the classes singled out by the SOM, since all pixels belonging to that region share the same optical properties and follows the same spectral variation when interacting with vapours. However, the intensity time traces of image pixels are not completely identical, but they share a common waveform with amplitude modulated by a certain scaling factor. This scaling factor depends on non-homogeneities of the

deposition, and imperfections in the detection method. Our hypothesis considers a homogeneous background, namely a uniform illuminating colour, within a single ROI. The goal is to calculate the scaling factor characteristic of each pixel and extrapolate the common waveform of the ROI that is supposed to depend exclusively on the optical properties of colour indicators. The measured intensity $y(t)$ of the i^{th} pixel can be expressed in the following form:

$$y_i(t) = u_i f(t) + b + n_i(t) \quad (6.2)$$

where b and $n_i(t)$ denote background and noise contributions. The common waveform $f(t)$ is to be determined. To do so, equation 6.2 can be divided into a time average and a time varying part, reducing the estimation to two separate problems.

$$\bar{y}_i(t) = \bar{f} u_i + b + \bar{n}_i(t) \quad (6.3)$$

$$\tilde{y}_i(t) = u_i \tilde{f}_i(t) + \tilde{n}_i(t) \quad (6.4)$$

The u_i and $f_i(t)$ can be estimated applying the maximum likelihood method to the varying part, from the unit-length eigenvector of the matrix $\sum_{i=1}^q \tilde{y}_i \tilde{y}_i'$ associated to its largest eigenvalue. Consequently b and $n_i(t)$ can be calculated exploiting its linear relationship as the slope and the intercept of the regression line through (y_i, u_i) pairs.

After the application of this algorithm we observed a great reduction of noise and background non homogeneity. The benefits of the application of this algorithm are visible in the next figures. The overall

effect can be better appreciated in Figure 6.9, where the difference between the first frame and the final frame is shown in a colour-coded map. In Figure 6.10 the response of selected pixels shows more accurately the noise reduction performed by the application of the algorithm.

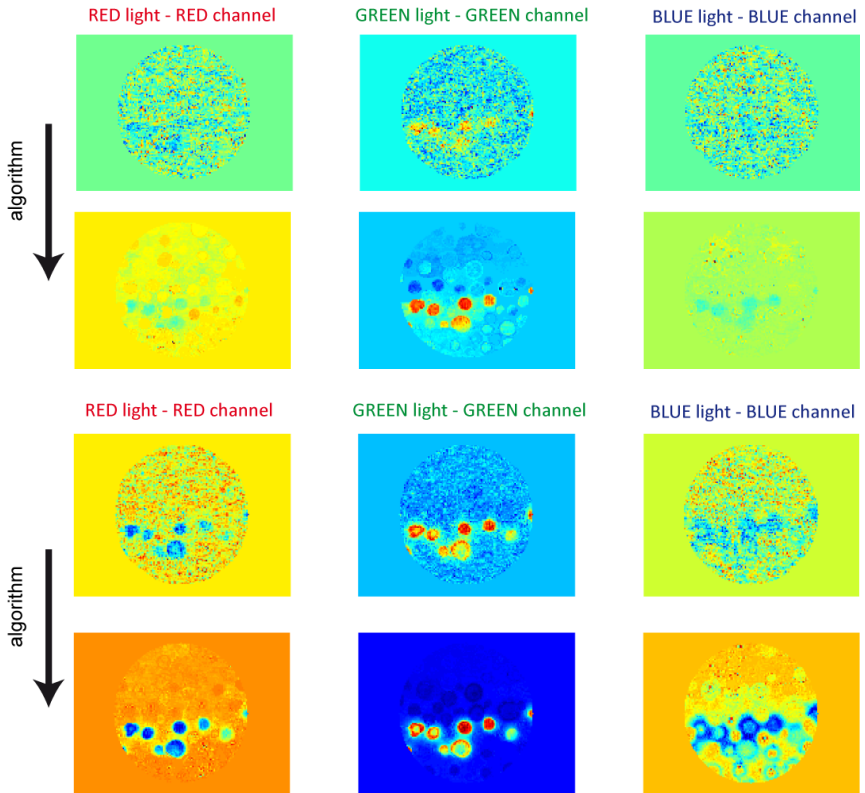


Figure 6.9. Effect of the algorithm for background removal.

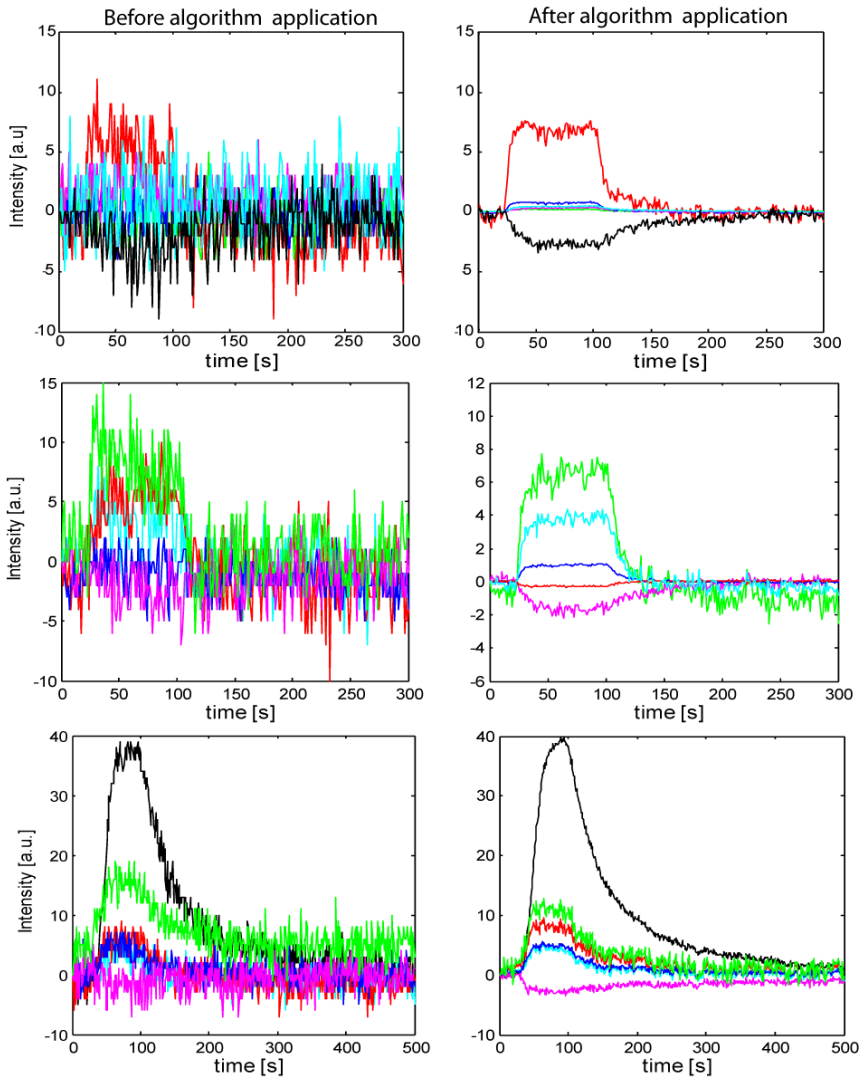


Figure 6.10. Effect of the algorithm for background removal.

6.3.4 Artificial sensors signals

When the sensing layer is exposed to vapours, every pixel of the image undergoes to a change in its optical properties according to the chemical interactions occurring between the vapour and the chemical indicators. Interactions with odours are detected illuminating the screen with the three primary colours and reading the corresponding camera output in the three colour bands, in this way six meaningful signals are formed. In order to simplify the data modelling, the six useful signals were reduced to one considering as pixel output the sum of the absolute values of the six signals.

Each pixel signal is sent to its corresponding sub-glomerular unit and averaged with the signals from other pixels converging to the same unit. From this point on, a reduction of information of about two orders of magnitude is obtained in analogy with biological olfaction.

Different data processing may be conceived for sub-glomerular unit outputs, a simple bio-inspired concept such as the lateral inhibition may be introduced¹⁵. However, the purpose of this work is just to give a demonstration of the potentialities of the introduced artificial system. To do so, glomeruli signals have been analyzed with a Principal Component Analysis. In the resulting scores plot, shown in Figure 6.11, a clear separation of compounds and their mixtures is achieved.

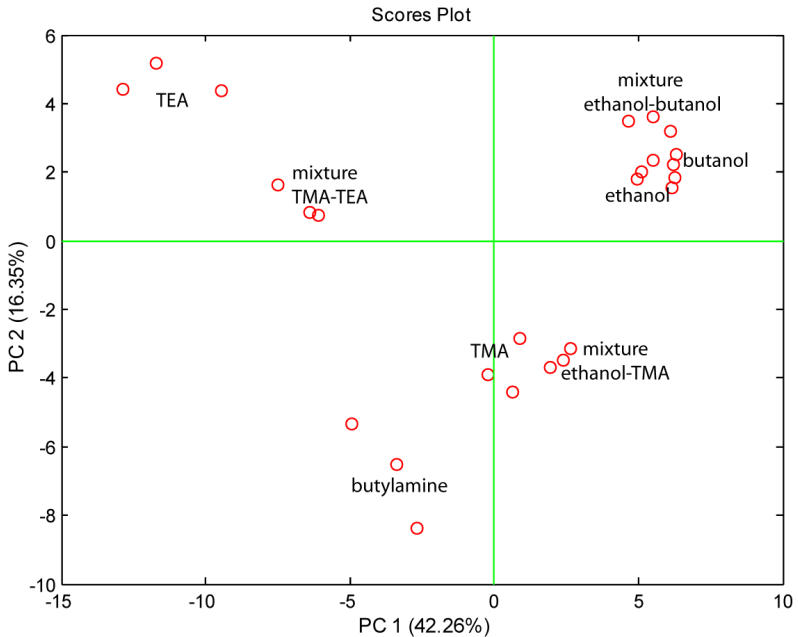


Figure 6.11. Scores plot of the measures. The signal of SOM neurons were considered as features.

6.4 Conclusions

In these experiments, we showed that an artificial olfaction system can be assembled with a layer of distributed chemical indicators acquired with an image detector. In this case, it is possible to take advantage from the large number of artificial receptors that can track the presence of selected gases and vapours changing their spectral properties. The CSPT platform allows to fingerprint the optical

properties of each pixel of the image. The CSPT fingerprint is chosen to characterize the properties of artificial receptors and it is used to define a number of classes whose properties are inspired from those of olfactory glomeruli. The polymeric matrix mimics the olfactory mucosa and provides a support for the diffusion of odorants towards the chemical receptors. Glomeruli signals can be processed with simple bio-inspired data processing. This platform can be used both to model the importance of the distribution of ORNs and of diffusion in olfaction and as a novel approach to electronic noses development.

References

- ¹ K. Persaud, G. Dodds, Analysis of discrimination mechanisms in the mammalian olfactory system using a model nose, *Nature* 299 (1982) 352–355.
- ² H. Spors, A. Grinvald, Spatio-Temporal Dynamics of Odor Representations in the Mammalian Olfactory Bulb, *Neuron* 34 (2002) 301–315
- ³ K. Zhao, P. W. Scherer, S. A. Hajiloo, P. Dalton, Effect of Anatomy on Human Nasal Air Flow and Odorant Transport Patterns: Implications for Olfaction, *Chem. Senses* 29 (2004) 365–379
- ⁴ D. Walt, Imaging optical sensor arrays, *Curr. Opin. Chem. Biol.* 6 (2002) 689–695
- ⁵ P. Mombaerts, Molecular biology of odorant receptors in vertebrates, *Annu. Rev. Neurosci.* 22 (1999) 487–509
- ⁶ S. Korsching, Olfactory maps and odor images. *Curr. Opinion in Neurobiology* 12 (2002) 387–392
- ⁷ S. M. Potter, C. Zheng, D. S. Koos, P. Feinstein, S. E. Fraser, P. Mombaerts, Structure and Emergence of Specific Olfactory Glomeruli in the Mouse, *The Journal of Neuroscience* 21 (2001) 9713–9723
- ⁸ N. Uchida, Y. K. Takahashi, M. Tanifuji, K. Mori, Odor maps in the mammalian olfactory bulb: domain organization and odorant structural features, *Nature neuroscience*, 3 (2000) 1035–1043
- ⁹ F. Wang, A. Nemes, M. Mendelsohn, R. Axel, Odorant Receptors Govern the Formation of a Precise Topographic Map. *Cell* 93 (1998) 47–60
- ¹⁰ T. A. Dickinson, K. L. Michael, J. S. Kauer, D. Walt, Convergent self encoded bead sensor arrays in the design of an artificial nose, *Anal. Chem.* 71 (1999) 2192–2198

¹¹ K. J. Ressler, S. L. Sullivan, L. Buck, A Zonal Organization of Odorant Receptor Gene Expression in the Olfactory Epithelium, *Cell* 73 (1993) 597-609

¹² C. Di Natale, E. Martinelli, R. Paolesse, A. D'Amico, D. Filippini, I. Lundstrom, An Experimental Biomimetic Platform for Artificial Olfaction, *PLoS ONE* 3 (2008) e3139

¹³ T. Kohonen, Self-organizing maps, 3rd edition, Springer-Verlag, Berlin (2001).

¹⁴ T. Chen, B. Lin, E. Brunner, D. Schild, In situ Background estimation in quantitative fluorescence imaging, *Biophysical Journal* 90 (2006) 2534-2547

¹⁵ C. Di Natale, E. Martinelli, R. Paolesse, A. D'Amico, D. Filippini, I. Lundstrom, An artificial olfaction system based on the optical imaging of a large array of chemical reporters, *Sens. Actuators B* 142 (2009) 412-417

Chapter 7: Conclusions

In this thesis, novel strategies for the improvement of chemical sensors have been proposed. The research was focused on the development of sensing layers for chemical sensors based on image detectors. In particular, an innovative transduction platform based on computer peripherals, the Computer Screen Photo-Assisted Technique (CSPT), was used to probe the sensing layers.

During this thesis, the attention was firstly focused on the testing of molecular arrangement of porphyrins that could enhance the sensitivity of chemical interactive materials. It was shown that a tubular arrangement of two differently charged porphyrins is endowed with peculiar sensitivity properties that largely exceed the performances of single precursors. The opportunity to modify the coordinated metal in the precursor units and to explore other nanostructures further enlarges the perspective to improve the performances of sensing layers.

Then, focusing on the other component of a sensing layer, the effect of polymeric matrices was investigated. In this context, it was firstly demonstrated that a set of polymeric matrices with different chemical properties functionalized with a single colorimetric indicator, allows for

the discrimination of several organic vapours. The principle of recognition is based on the diverse affinity of polymers towards analyzed compounds and on the different partitioning operated by the matrices. The matrices affect sensitivity and selectivity of the system, opening a wider range of tools for the design of arrays of sensing materials for image sensors. In a second set of experiments, it was reported a bio-mimetic approach for the separation and detection of volatiles. Therein, a polymeric layer functionalized with a single optically responsive dye was used. The polymer mimics the function of the mucous coating in the biological epithelium and operates a chromatographic-like separation of odours that favours the discrimination. In the same way, the polymer, interacting differently with vapours introduces a spatio-temporal pattern in the layer response, bring a synergy with receptors response that improves information content and volatiles recognition.

Eventually, an application was reported that rises from the combining of previous observations together with an innovative approach for data processing. It deals with the development of a bio-inspired artificial olfaction platform that combines different sensing molecules, acting as receptors, and a polymeric coating that introduces additional information about odours.

The strategies proposed in this thesis are shown to affect the sensitivity and selectivity of image sensors, and can be considered for the development of novel optical chemical sensors.

List of Publications

Peer Reviewed Papers

- F. Dini, E. Martinelli, G. Pomarico, R. Paolesse, D. Monti, D. Filippini, A. D'Amico, I. Lundström, C. Di Natale "Chemical sensitivity of self-assembled porphyrins nano-aggregates" *Nanotechnology* 20, 055502 (8pages), 2009.
- F. Dini, D. Filippini, R. Paolesse, A. D'Amico, I. Lundström, C. Di Natale. "Polymers with Embedded Chemical Indicators as an Artificial Olfactory Mucosa", accepted to *The Analyst*.
- F. Dini, E. Martinelli, R. Paolesse, D. Filippini, A. D'Amico, I. Lundström, C. Di Natale "Polymer matrices effects on the sensitivity and the selectivity of optical chemical sensors" submitted to *Sensors and Actuators B*.
- E. Martinelli, F. Dini, G. Pennazza, M. Canosa, A. D'Amico, and C. Di Natale "A Novel Bio-inspired Digital Signal Processing Method for Chemical Sensor Arrays" A. Gutiérrez and S. Marco (Eds.): *Biologically Inspired Signal Processing*, SCI 188, pp. 109–120, Springer-Verlag Berlin Heidelberg 2009.
- L. Lvova, E. Martinelli, F. Dini, A. Bergamini, R. Paolesse, C. Di Natale, A. D'Amico, "Clinical analysis of human urine by means of potentiometric Electronic tongue", *Talanta* 77, 1097-1104 0039-9140, 2009.

International Conferences

- F. Dini, E. Martinelli, A. D'Amico, R. Paolesse, D. Filippini, D. Schild, I. Lundström, C. Di Natale, "Enhanced Resolution in Optical Image based Chemical Sensors", accepted to the 13th International Meeting on Chemical Sensors (IMCS).
- F. Dini, D. Filippini, R. Paolesse, A. D'Amico, I. Lundström, C. Di Natale, "One-way ANOVA test for volatiles discrimination in a bio-mimetic two-dimensional layer" accepted to the 13th International Meeting on Chemical Sensors (IMCS).
- E. Martinelli, D. Polese, F. Dini, R. Paolesse, D. Filippini, A. D'Amico, D. Schild, I. Lundstrom, C. Di Natale, "Testing Olfactory Models with an Artificial Experimental Platform" accepted to IEEE World Congress on Computational Intelligence (WCCI) 2010.
- F. Dini, E. Martinelli, R. Paolesse, D. Filippini, I. Lundström, A. D'Amico, C. Di Natale, "Optical Sensor Response Modulation Using Different Polymeric Matrices", Eurosensors 2009, Lausanne, Switzerland, September 06-09, 2009.
- F. Dini, R. Paolesse, D. Filippini, E. Martinelli, A. D'Amico, I. Lundström, C. Di Natale, "Bringing Chromatography Back to Colour". International Symposium on Olfaction and Electronic Nose (ISOEN) 2009, Brescia, Italy, April 15-17, 2009.
- F. Dini, M. Santonico, M.C. Basile, E. Martinelli, R. Paolesse, D. Filippini, A. D'Amico, I. Lundström, C. Di Natale, "A Gas Sensor based on Time Resolved Multidimensional Gas-Chromatography", IMCS, Columbus, Ohio, USA, July 13-16, 2008.
- E. Martinelli, F. Dini, D. Monti, R. Paolesse, D. Filippini, A. D'Amico, I. Lundstrom, C. Di Natale "Optical transduction of

chemical sensitivity of porphyrin nanotubes by CSPT platform” IEEE SENSORS 2007, Atlanta, USA, 28-31 October 2007.

- E. Martinelli, F. Dini, I. Iannaccone, D. Monti, G. Pomarico, R. Generosi, M. Luce, A. D’Amico, R. Paolesse, C. Di Natale, “Chemical sensitivity of porphyrin nanotubes” TRANSDUCERS ’07, Lion, France, 10-14 June 2007.
- C. Di Natale, A. D’Amico, R. Paolesse, F. Dini, E. Martinelli, D. Filippini, A. Lloyd-Spetz, I. Lundström. “Multiparametric light-assisted silicon device transduction of molecular recognition events” The 15th International Conference on Solid-State Sensors, Actuators and Microsystems (Transducer 2009), Denver, Colorado, USA, June 21 - 25, 2009.
- C. Di Natale, A. D’Amico, F. Dini, D. Filippini, E. Martinelli, R. Paolesse, I. Lundström, “A gas sensor system implementing time-resolved gas-chromatography and optical sensors” International Conference on Porphyrins and Phthalocyanines (ICPP-5), Moscow, Russia, July 6-11, 2008.
- F. Dini, L. Lvova, A. Bergamini, E. Martinelli, R. Paolesse, C. Di Natale, A. D’Amico, “Clinical analysis of human urine by means of electronic tongue based on an array of metallic potentiometric sensors” EUROSENSORS XX, Göteborg, Sweden, September 17-20, 2006.

National Conferences

- F. Dini, A. Catini, A. Nisti, L. Falasca, R. Paolesse, C. Di Natale, A. D’Amico, “Oxygen distribution monitoring in gas and liquid”, AISEM 2010 Messina, February 8-10, 2010.

- R. Paolesse, L. Tortora, C. Di Natale, F. Dini, A. D'Amico, "Chemical sensors integrated in furniture for indoor atmosphere monitoring", AISEM 2010 Messina, February 8-10, 2010.
- A. Catini, F. Dini, D. Polese, S. Petrocco, R. Paolesse, M. De Luca, C. Di Natale, A. D'Amico, "Fluorescence detection of hydrocarbons in harbour water", AISEM 2010 Messina, February 8-10, 2010.
- C. Di Natale, E. Martinelli, F. Dini, A. D'Amico, D. Filippini, I. Lundström. "Artificial Olfactory Epithelium and Bulb by Optical Imaging of Large Areas of Chemical Reporters" AISEM 2009 Pavia, February 24-26, 2009.
- F. Dini, E. Martinelli, F. Cainero, G. Pomarico, D. Monti, R. Paolesse, A. D'Amico and C. Di Natale. "Porphyrin nanotubes characterization as chemical sensors", AISEM 2008 Rome, February 19-21, 2008.
- E. Martinelli, F. Dini, M. Martellucci, G. Pennazza, C. Di Natale, A. D'Amico, "A bio-inspired architecture for chemical sensor array", XII Annual Conference AISEM 2007, Naples, 12-14 February 2007.

Acknowledgments

I wish to express with these words all the love I feel and the gratefulness I owe to all the special people that were by my side in these years. You made me grow (even if someone says that I am younger now), you taught me a lot of life and science, you made me laugh, you amazed me and supported me in this beautiful path.

So, firstly I want to thank the people that share my days at University, you know me the most and you always show me trust and esteem. This is all that counts for me.

Thanks Corrado, for being always available, stimulating, open to discussion, thanks for having my mind opened and introducing me in what is research, thanks for all the opportunities you gave me and for giving me trust.

Thanks Prof. D'Amico for giving me the possibility to run this path and for your precious and expert teachings.

Thanks Roberto, for being there to talk, to advice, and to teach me about chemistry (and more) and also for sharing other fragment of life.

Thanks Eugenio, for your stimulating conversations, being stuck in your office always meant to come off with new ideas.

Thanks Alex, for your help, for your friendship, for your guidance; you always supported me, you made me laugh, you made me think, thanks for all you did for me and for what you are always ready to do. Thanks Rosa, for understanding me that much, for supporting me and

for sharing moments of difficulty, it has been a real luck that you showed up in our lab. Thanks Davide, for torturing me with your stimulating questions, for your contagious laughter, and for being always ready to help. Thanks Giulia, for your nice support, constant since the beginning of this experience. Thanks Marco for being always ready to help with your expert approach. Thanks Silvia for the breath of fresh you brought in our lab and for your funny initiatives.

A warm thanks goes to all the friends in the chemistry lab, beside helping me with all the chemical stuff, you always welcomed me when I needed you, you sensed my state of mind and often relieved me; thanks for your joyfulness that always cheered me up.

Thanks Manuela, you was always ready to listen me and understand me and you became a good friends too. Thanks Marco, for your friendship, your support and for our talks on facts and people. Both of you were a real push for me and my life. Thanks Federica for your sweet and kind presence, always comforting for me. Thanks Giuseppe, for all your support, for your relentless help and for sharing with me the Swedish experience. Thanks Larisa, you was the first to learn me a lot about lab practice and maybe from there it all began. Thanks Sara, for your expert support and your strict touch that is always stimulating to me. Thanks Luca for all the funny moments we shared, including travels and lab experiences. Thanks Antonella, it has been nice to work with you; I learned al lot from your professionalism.

Thanks to all the diploma students that worked with me, I cannot hide my shameless predilection to Francesco and Daniela, and the new-come Alberto and Lorenzo.

A special and loving thought goes to all the people that made my stay in Linköping a wonder, a soul and life experience that changed my minds, my feelings, my thoughts, I hope they can go on and on. Thanks Ingemar, that is one of the wisest and most prepared professor I've ever met, thanks for being always kind and friendly to me. Thanks Daniel and Anke, for welcoming me in those months, for your help with everything and for the beautiful chance you offered me. Thanks Stephen and Pakorn for your patient help and for introducing me in the LiU labs. Thanks Martin for your friendship and for the nice welcome you offered me when I was there. And finally thanks to all the good friends and wonderful people I met in Sweden, thanks Sharon, Alberto, and Giacomo.

Thanks to all the friends that shared with me the University path, thanks Sergio, Federica and Angelo because you know what is like.

Thanks to my friends, the ones that were with me during this whole period, and the ones that I recently found again. You are always close to me, lightning up everything, you always show me all your love and trust; thanks Barbara and your beautiful crazy children, thanks Sabrina and Selma.

Thanks to all the people I forgot to mention, but that I am sure that there is still someone I bothered that gave me help to get here.

Finally, I owe a special thank to my family, my dad and my mum, thanks for always pushing me, and believing me, you gave me everything, I know that I got here because of you.

And thanks Luca, with your wisdom and brilliant thoughts you stabilize my mind, with your enthusiasm you fill me and complete me. You was always close to me, when I was away, when I came back (and you patiently fixed me), now and ever be with me.